UCRL-10928

University of California

Ernest O. Lawrence Radiation Laboratory

LONGITUDINAL DISPERSION IN PACKED EXTRACTION COLUMNS WITH AND WITHOUT PULSATION

DISCLAIMER

UCRL-10928
UC-4 Chemistry
TID-4500 (24th Ed.)

Research and Development

UNIVERSITY OF CALIFORNIA

Lawrence Radiation Laboratory
Berkeley, California

AEC Contract No. W-7405-eng-48

LONGITUDINAL DISPERSION IN PACKED EXTRACTION COLUMNS WITH AND WITHOUT PULSATION

Joon S. Moon, Alphonse Hennico, and Theodore Vermeulen

October 23, 1963

Printed in USA. Price $2.50. Available from the
Office of Technical Services
U. S. Department of Commerce
Washington 25, D.C.

LONGITUDINAL DISPERSION IN PACKED EXTRACTION COLUMNS WITH AND WITHOUT PULSATION

Contents

Abstract vi

General Introduction 1

References for General Introduction 7

Part I. Single-Liquid Flow Through Pulsed Packed Columns

A. Introduction 8

B. Theoretical Models for Longitudinal Dispersion . . 9

1. Bounded-Diffusion Model 11

2. Random-Walk Model 12

3. Interpretation of Experimental Data 17

C. Apparatus 17

1. Column Assembly 17

2. Column Packing 17

3. Conductivity Probes 21

4. Injection Nozzles 21

5. Column Heads 22

6. Pulsing Units 24

7. Circuitry 27

8. Layout and Accessories 27

D. Procedure 29

E. Results and Discussion. 30

1. Effects of Viscosity and Velocity 30

2. Effects of Packing-Particle Characteristics . . 32

3. Effects of Pulse Frequency and Amplitude . . 32

F. Conclusion 39

G. Notation for Part I 40

References for Part I 41

Appendix I 43

I-1. Table 43

I-2. Sample Calculation 44

Part II. Countercurrent Liquid Flow Through Pulsed Packed Columns

A. Introduction 47
B. Interpretation of Experimental Results 49
C. Apparatus and Procedure 49
1. Columns 49
2. Conductivity Cells 49
3. Feed Nozzle 51
4. Liquid-Interface Level Control 51
5. Piping Arrangement 51
6. Conductivity Measurements 51
7. Holdup Measurements 52
8. Flooding or Emulsification Limits 52
D. Results and Discussion 53
1. Continuous Phase 53
2. Dispersed Phase 55
3. Holdup 56
E. Conclusions 58
F. Notation for Part II 59
References for Part II 60
Appendix II 64

Part III. Concentration-Profile Measurements in a Pulsed Packed Extraction Column

A. Introduction 65
B. Previous Studies 67
C. Experimental Objectives 69
D. Materials, Apparatus, and Procedure 69
1. Extraction System Studied 69
2. Column 69
3. Sampling Probes 69
4. Start-Up 73
5. Method of Analysis 76
6. Calculation of Data 76

E. Results and Discussion 77
1. Experimental Results 77
2. Comparison with Theoretical Profiles 77
3. Effect of Pulsing on H_{ox} 84
F. Conclusions 85
G. Notation for Part III 86
References for Part III 88
Appendix III 89
Part IV. Longitudinal Dispersion in Unpulsed Packed Columns
A. Introduction 91
1. Single-Phase Flow 91
2. Two-Phase Flow 92
B. Apparatus and Procedure 92
1. Columns 92
2. Conductivity Cells 93
3. System Studied 93
4. Procedure 93
C. Results and Discussion 95
1. Single-Phase Flow 95
2. Continuous Phase in a Two-Phase System . . . 95
3. Dispersed Phase 95
D. Conclusions 99
E. Notation for Part IV 101
References for Part IV 102
Appendix IV 103
Part V. Concentration-Profile Measurements in an Unpulsed Packed Extraction Column
A. Introduction 106
B. Materials, Apparatus, and Procedure 106
1. Extraction Systems Studied 106
2. Apparatus and Procedure 106
C. Experimental Results 106
1. Mass Transfer from Aqueous to Organic Phase . 108
2. Mass Transfer from Organic to Aqueous Phase . 108
D. Conclusions 118
Acknowledgments 119

LONGITUDINAL DISPERSION IN PACKED EXTRACTION COLUMNS WITH AND WITHOUT PULSATION

Joon S. Moon, Alphonse Hennico, and Theodore Vermeulen

Lawrence Radiation Laboratory and
Department of Chemical Engineering
University of California
Berkeley, California

October 23, 1963

ABSTRACT

This research was conducted to develop design information that will take longitudinal dispersion into account for packed-column extraction.

Single-phase Péclet numbers were measured by an unsteady-state step-input method. For pulsed columns, the use of pulsation serves to decrease the Péclet numbers as the amplitude increases, and to a lesser extent as the frequency increases. The effect is somewhat more pronounced in beds of Raschig rings and Berl saddles than in beds of uniform spheres. The Péclet-number decrease diminishes with increasing fluid viscosity and also with increasing flow rate; our results indicate a rise in Péclet number for viscous fluids. For unpulsed columns, Péclet numbers in the low-Reynolds-number regime down to a Reynolds number of 0.04 were obtained, using 0.0058-in.-diameter glass beads as a packing material. The modified Péclet number P remained constant at 0.205±0.020.

Péclet numbers for counterflowing liquid-liquid systems were measured for both continuous and dispersed phases, with the behavior of the latter depending upon whether it does or does not wet the packing material. For both pulsed and unpulsed columns, the axial Péclet number of one phase decreases as the flowrate of the other phase increases. The effect is much greater for the continuous than for the dispersed phase, and also for the dispersed-phase wetting rather than nonwetting. A correlation was developed for dispersed-phase Péclet number without pulsation, which includes the physical properties for the dispersed phase.

The measurement of both dispersed- and continuous-phase concentration profiles was undertaken to determine the applicability of the Miyauchi model to steady-state mass transfer, using the Péclet numbers obtained from unsteady-state conditions. Experimental profiles inside the packed bed were compared with the theoretical profiles, and the agreement between these two profiles was quite satisfactory.

From this work, we can conclude that the one-dimensional diffusion model adequately represents the fluid behavior in packed-bed extraction columns with and without pulsation. With appropriate Péclet numbers for both phases, this model should be very useful for accurate and economical design of packed columns. The Péclet numbers determined by the unsteady-state tracer-injection method appear to represent closely the longitudinal-dispersion behavior during steady-state extraction.

GENERAL INTRODUCTION

It has already been recognized that the concentration driving potential for mass transfer is reduced by longitudinal dispersion (or axial mixing) in fixed-bed extraction columns,[6,7] absorption columns,[1] adsorption columns,[2] and chemical reactors.[3,4] Consequently it has been necessary to develop rational design methods for these columns that include the effect of the longitudinal dispersion.

A diffusion model for describing the influence of longitudinal dispersion in countercurrent systems undergoing mass transfer between the phases was given by Miyauchi[6,7] and Sleicher.[8] The dispersion effect for each phase is described by an effective superficial longitudinal diffusivity E_i. The basic equations obtained by material balance in a differential slice of the column, for the X phase and Y phase, respectively, are

$$d^2C_x/dZ^2 - P_xB\, dC_x/dZ - N_{ox}P_xB(C_x - mC_y) = 0 \qquad (1)$$

and

$$d^2C_y/dZ^2 + P_yB\, dC_y/dZ + N_{oy}P_yB(C_x - mC_y) = 0, \qquad (2)$$

with the boundary conditions, at $Z = 0$,

$$dC_x/dZ = P_xB(1 - C_{x0})$$

and

$$dC_y/dZ = 0;$$

at $Z = 1$,

$$dC_x/dZ = 0$$

and

$$dC_y/dZ = P_yB(C_{y1} - C_y^1),$$

where

$P_i = U_i d_p/E_i$, Péclet number of ith phase,

$B = h/d_p$ = dimensionless length,

h = column height,

d_p = particle diameter,

Z = dimensionless length variable, ranging from zero at the X-feed end to unity at the Y-feed end of the column,

C_i = dimensionless concentration in the i phase measured at a point Z expressed relative to X-feed concentration. The number accompanying C, if a subscript, is the Z value inside the column; if it is a superscript (0 or 1), it is the Z value in the feed or product stream outside the column,

m = slope of equilibrium curve, dC_x^*/dC_y ,

N_{oi} = true overall number of transfer units (NTU) for the ith phase,

$N_{oy} = \Lambda N_{ox}$,

$\Lambda = \dfrac{mU_{x0}}{U_{y0}}$ = extraction factor,

U_i = mean linear velocity of the ith phase,

and

U_{i0} = superficial velocity of the ith phase.

Equations (1) and (2) are differential equations of the second order with constant coefficients. Their solution, obtained by differentiation and subsequent integration of a single fourth-order equation, gives the concentration of any point inside the column.[6] Figure 1 shows representative behavior of the concentration profiles in an extractor, for piston flow (broken lines) and for axial dispersion (solid lines); in it, C represents an actual concentration, with $C_x = C_x/C_x^0$, and $C_y = mC_y/C_x^0$. The decrease in driving force due to axial mixing is shown by the arrows. Graphical and tabular results corresponding to the solution of Eqs. (1) and (2) have been provided by McMullen, Miyauchi, and Vermeulen.[5] The solutions are obtained in the form

$$X = X(N_{ox}, \Lambda, P_xB, P_yB, Z) \tag{3}$$

and

$$Y = Y(N_{ox}, \Lambda, P_xB, P_yB, Z) . \tag{4}$$

The outlet concentrations are, at Z = 1,

$$X_1 = \frac{C_{x1} - (Q + mC_y^1)}{1 - (Q + mC_y^1)} , \tag{5}$$

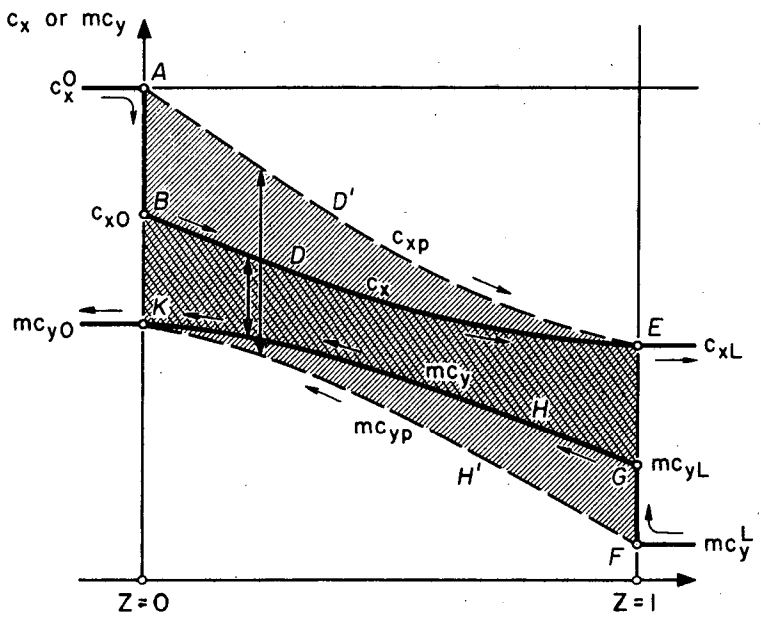

MU-14083

Fig. 1. Concentration profile in a typical extraction.

and, at $Z = 0$,

$$Y_0 = \frac{m(C_{y\theta} - C_y^1)}{1 - (Q+mC_y^1)} \quad . \tag{6}$$

Here Q is the intercept of a linear-equilibrium plot,

$$C_x^* = Q + mC_y \quad . \tag{7}$$

Ideally one should be able to establish the value of any one parameter from a knowledge of the other parameters. The practical use of Eqs. (3) and (4) has been facilitated by the derivation of several empirical relations between the different parameters.[7] An apparent NTU, as given from Underwood's result,[9] has been defined as

$$N_{oxP} = \frac{1}{1 - \Lambda} \ln \left[\frac{1 - \Lambda(1-X_1)}{X_1} \right] \quad . \tag{8}$$

The subscript P indicates that the definition stems from a "piston-flow" model. The true NTU can be related to the apparent NTU by a difference in reciprocals:

$$\frac{1}{N_{oxP}} - \frac{1}{N_{ox}} = \frac{1}{N_{oxD}} \quad . \tag{9}$$

Here N_{oxD} is related to P_xB and P_yB by an approximate empirical equation

$$N_{oxD} = \frac{\ln\Lambda}{\Lambda - 1} \phi + (PB)_y \quad , \tag{10}$$

with

$$(PB)_y = \left(\frac{\Lambda}{f_x P_x B} + \frac{1}{f_y P_y B} \right)^{-1} \quad , \tag{11}$$

where f_x and f_y, the weighting factors, are functions of N_{ox} and Λ; and ϕ may be a function of P_xB, P_yB, N_{ox}, and Λ.

Miyauchi and Vermeulen[7] obtained empirical equations for these weighting factors:

$$f_x = \frac{N_{ox} + 6.8\,\Lambda^{-0.5}}{N_{ox} + 6.8\,\Lambda^{-1.5}}, \tag{12}$$

$$f_y = \frac{N_{ox} + 6.8\,\Lambda^{-0.5}}{N_{ox} + 6.8\,\Lambda^{0.5}}, \tag{13}$$

and

$$\phi = 1 - \frac{0.05}{\Lambda^{0.5}\,N_{ox}^{0.5}\,(PB)_y^{0.25}}. \tag{14}$$

These empirical relations have proved applicable over a wide range of variables. In our investigation these functions have proved very useful for rapid estimation of N_{ox}.

By the use of the foregoing exact and empirical relations, it should be possible to carry out any of the following calculations:

(a) From an experimental X_1, and experimental P_xB and P_yB, to determine the true N_{ox}.

(b) From an experimental X_1, and a correlational N_{ox}, to determine an experimental N_{oxD}.

(c) From experimental or correlational P_xB and P_yB, and correlational N_{ox} values, to predict the X_1 value for a column to be designed or operated.

(d) From experimental concentration profiles inside the column, and a correlational N_{ox}, to determine P_xB and P_yB. A useful procedure is suggested by Miyauchi and Vermeulen.[6]

Among these procedures, (a) has proved the most useful in the work to be reported here. Verification has been provided by obtaining an exact solution to Eqs. (3) and (4) for the parameters chosen.

In Part I, experimental data on longitudinal dispersion in pulsed packed beds with single-phase flow are given, with interpretation and correlation of these results.

In Part II, experimental Péclet numbers of both phases in pulsed packed beds undergoing two-phase flow are presented. As dispersed phase, liquids which were either wetting or nonwetting relative to the packing material were studied.

In Part III, the internal concentration profiles for liquid-liquid extraction in a pulsed packed column are reported, and are compared with profiles calculated from the theoretical model discussed above. Péclet numbers for the individual phases, as reported in Part II, were used for the evaluation of N_{ox} and concurrent calculation of the profiles.

In Part IV, experimental results on longitudinal dispersion in packed beds (without pulsing) are shown. Both single-phase and two-phase flows have been studied. The results are interpreted and are compared with the results of other investigators, and a new correlation for the dispersed-phase Péclet number is proposed.

In Part V, the experimental concentration profiles for liquid-liquid extraction in packed columns (without pulsing) are reported, and are interpreted in terms of the individual-phase Péclet numbers for two-phase flow reported in Part IV. Mass transfer at the column "entrance" (between the distributor and the packed section) appears to occur and has been taken into account in the calculations.

REFERENCES FOR GENERAL INTRODUCTION

1. W. E. Dunn, T. Vermeulen, C. R. Wilke, and T. T. Word, Lawrence Radiation Laboratory Report UCRL-10394, 1962.
2. G. Houghton, J. Phys. Chem. 67, 84 (1963).
3. H. M. Hulburt, ibid. 36, 1019 (1944).
4. O. Levenspiel and K. B. Bischoff, Ind. Eng. Chem. 51, 1431 (1959).
5. A. K. McMullen, T. Miyauchi, and T. Vermeulen, University of California Radiation Laboratory Report UCRL-3911-Suppl., 1958.
6. T. Miyauchi, University of California Radiation Laboratory Report UCRL-3911, 1957.
7. T. Miyauchi and T. Vermeulen, Ind. Eng. Chem. Fundamentals 2, 113 (1963).
8. C. A. Sleicher, Am. Inst. Chem. Engr. J. 5, 145 (1959).
9. A. J. W. Underwood, Ind. Chemist 10, 129 (1934).

PART I. SINGLE-LIQUID FLOW THROUGH PULSED PACKED COLUMNS

A. Introduction

It is widely recognized that in continuous countercurrent solvent-extraction columns, the effective coefficient of mass transfer is lowered by longitudinal dispersion (or axial mixing) in either phase. Although studies have been made of the effect of such mixing in nonpulsed packed columns[3, 16, 24] and of pulsed sieve-plate columns,[22, 29] almost no work has been done on longitudinal dispersion in pulsed packed columns. Columns of the latter type have been constructed, by Von Berg and Wiegandt among others,[7,13,32] to improve the extraction efficiency as compared with gravity-powered equipment.

Longitudinal dispersion is caused by eddies (which result from both the normal flow and the incremental flow due to pulsing) in the void spaces between the packing particles, and also by nonuniformity in the velocities of the individual fluid filaments. The effects of such dispersion can be expressed in terms of an empirical "dispersion coefficient" E, which has the dimensions of a diffusivity. This coefficient can most easily be measured independently of mass transfer, by tracer-injection techniques: a tracer amount of a component is injected in a pattern approaching one of several kinds of idealized disturbance, and the concentration history (or "breakthrough curve") of the tracer is measured at a fixed distance downstream from the injection points.

The characteristics of the experimental breakthrough or response curve may be compared with the forms predicted by a mathematical model for the mixing process. The calculated mixing-parameter value that gives the best fit to the experimental curve is then considered to describe quantitatively the experimental system.

Many different methods of analysis have been used to measure the breakthrough or response curve. These include ionization-current counting of radioactive tracers, electrical conductivity or electrode potential, heat conductivity (for gases), and absorption of ultraviolet or visible light.

The method used in this study involves the response to an inlet step-function. This can be carried out by flowing a solute-free liquid (usually water) and a tracer solution successively through a fixed bed, and determining the exit concentration as a function of time. Special care must be taken to obtain a sharp uniform step-function at the inlet. As the tracer, it is convenient to use an aqueous solution of $NaNO_3$, with the breakthrough curve measured by electrical conductivity.

Previous experimental studies on packed-bed longitudinal dispersion, for liquids in single-phase flow without pulsation, are summarized in Fig. I-1; this shows Péclet number as a function of Reynolds number. The curves represent the data of Cairns and Prausnitz,[3] Carberry and Bretton,[5] Ebach and White,[11] Jacques and Vermeulen,[17] and Strang and Geankoplis.[30] Some of the data for the present investigation have already been reported by Hennico, Jacques, and Vermeulen.[16] A marked transition is observed between the Péclet-number values at low Reynolds number and those at high Reynolds number; the latter correspond more closely to the values observed for gas flow.[24]

B. Theoretical Models for Longitudinal Dispersion

Several different one-dimensional models are available for deriving the theoretical shapes of breakthrough curves: the diffusion model with boundaries at infinite distances,[10] the more exact diffusion model as solved for beds of finite length,[1,33] the perfect-mixing-cell model,[4,20] the unidirectional random-walk[3,12,17] and other statistical models,[19,27] and the segmented-laminar-flow model.[16] As shown by Hennico, Jacques, and Vermeulen,[16] the random-walk model and diffusion model with finite boundaries give similar results. These two models show a close correspondence with experimental breakthrough curves, hence the random-walk model is used in this investigation for theoretical interpretation of the measured curves.

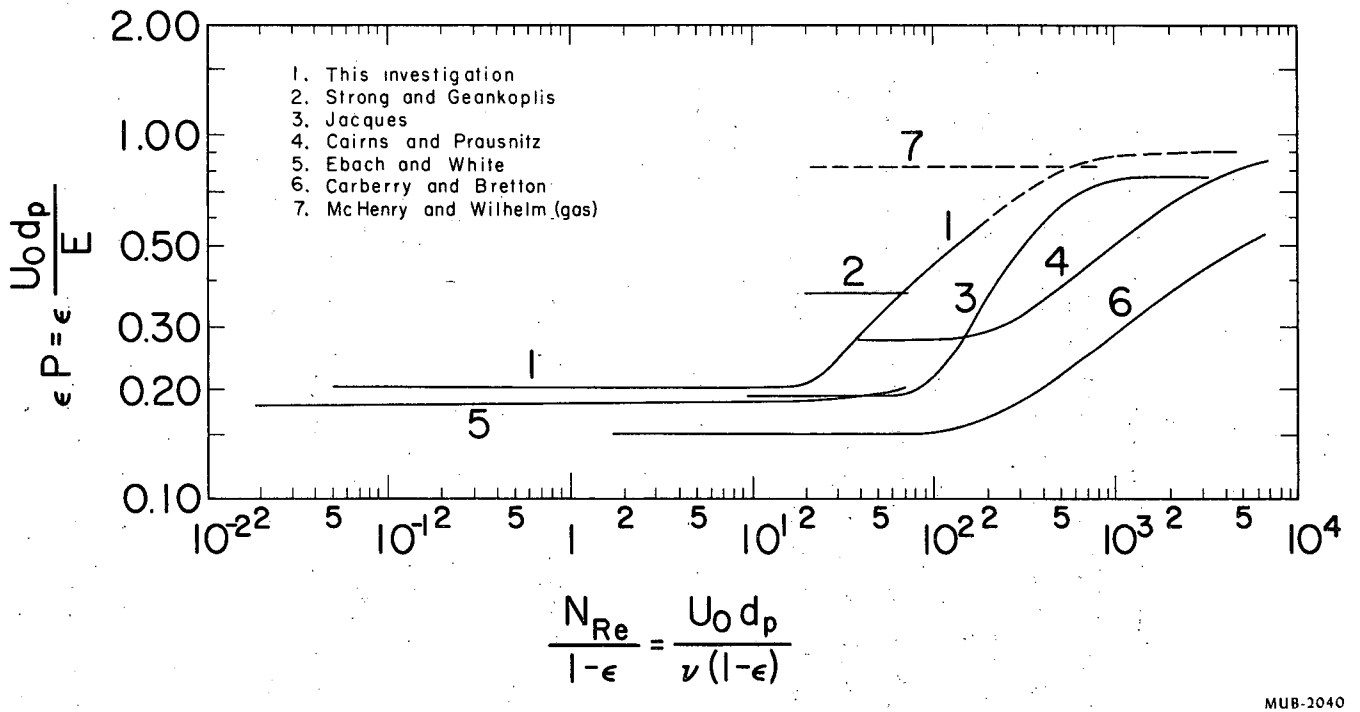

Fig. I-1. Péclet-number values for packed beds without pulsing.

1. Bounded-Diffusion Model

In this model it is assumed that equations of exactly the same form apply as those describing the molecular-diffusion process. The basic equation is

$$\frac{E}{\epsilon}\frac{\partial^2 c}{\partial z^2} - \frac{U_0}{\epsilon}\frac{\partial c}{\partial z} = \frac{\partial c}{\partial t}, \qquad (1)$$

with the following boundary conditions:

for $z = 0$, at $t < 0$, $c = 0$

and at $t \geqslant 0$, $c = c_0$

at $z = 0$, for all $t > 0$,

$$E\frac{dc(0+)}{dz} - U_0 c(0+) = -U_0 c(0-)$$

and at $z = h$, for all $t > 0$,

$$dc/dz = 0,$$

where

c = solute concentration,

E = superficial axial-dispersion,

h = column length,

t = time,

U_0 = superficial velocity,

z = axial distance,

ϵ = porosity,

(0-) = $z = 0$, outside packed section,

(0+) = $z = 0$, inside packed section.

An exact solution for the diffusion equation, Eq. (1), applied to a column of finite length, has been given by Yagi and Miyauchi.[33] Brenner[1] has shown that the general equation and the boundary conditions are similar to those governing heat loss to "sinks" at the ends of a slab, for which Carslaw and Jaeger[6] have given the general solution.

The variables in Eq. (1) will be made dimensionless by introducing the relations $N = h/\ell = hU_0/E$, $X = c/c_0$, $T = U_0 t/\ell\epsilon$, and $Z = z/h$.

Here N is a "column Péclet number," or total number of "dispersion units." Thus we have

$$\frac{\partial^2 X}{\partial Z^2} - N\frac{\partial X}{\partial Z} = N^2\frac{\partial X}{\partial T} . \tag{2}$$

The solution to this equation, at the exit of the column, has the form

$$X = \frac{c}{c_0} = \sum_{n=1}^{n=\infty} \exp\left\{\frac{N}{2}\left[1 - \frac{T}{2N}\left(1 + \frac{4\mu_n^2}{N^2}\right)\right]\right\}$$

$$\cdot \frac{N\mu_n (N \sin\mu_n + 2\mu_n \cos\mu_n)}{\left[(N/2)^2 + N + \mu_n^2\right]\left[(N/2)^2 + \mu_n^2\right]}, \tag{3}$$

where μ is given by the transcendental equation

$$\mu_n = \cot^{-1}\left(\frac{\mu_n}{N} - \frac{N}{4\mu_n}\right) . \tag{4}$$

Hennico, Jacques, and Vermeulen[16] made calculations of outlet concentrations for a large number of N and Θ values, using the exact expression [Eq. (3)] with consecutive roots of μ. The breakthrough values are presented graphically in Fig. I-2. Theoretical slopes of breakthrough curves for different values of N were also obtained; these dimensionless midpoint slopes were plotted against number of mixing lengths in Fig. I-3.

An empirical algebraic correlation between column Péclet numbers and midpoint slopes was obtained in this study. The dimensionless slope s' can be converted to a column Péclet number by the relation

$$N = 4\pi s'^2 - 1.45 \tag{5}$$

2. Random-Walk Model

The random-walk model[3, 12, 17] is characterized by packets of fluid moving through the packing in a series of discreet jumps corresponding to a certain mean free path ℓ, with a mean linear velocity

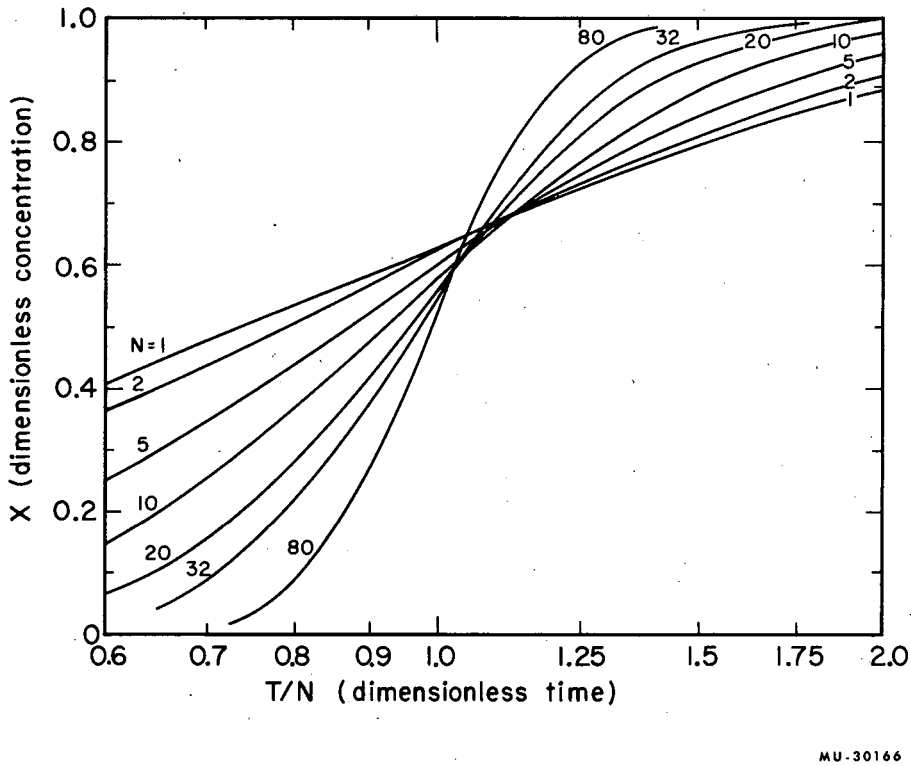

Fig. I-2. Breakthrough curves for bounded diffusion model.

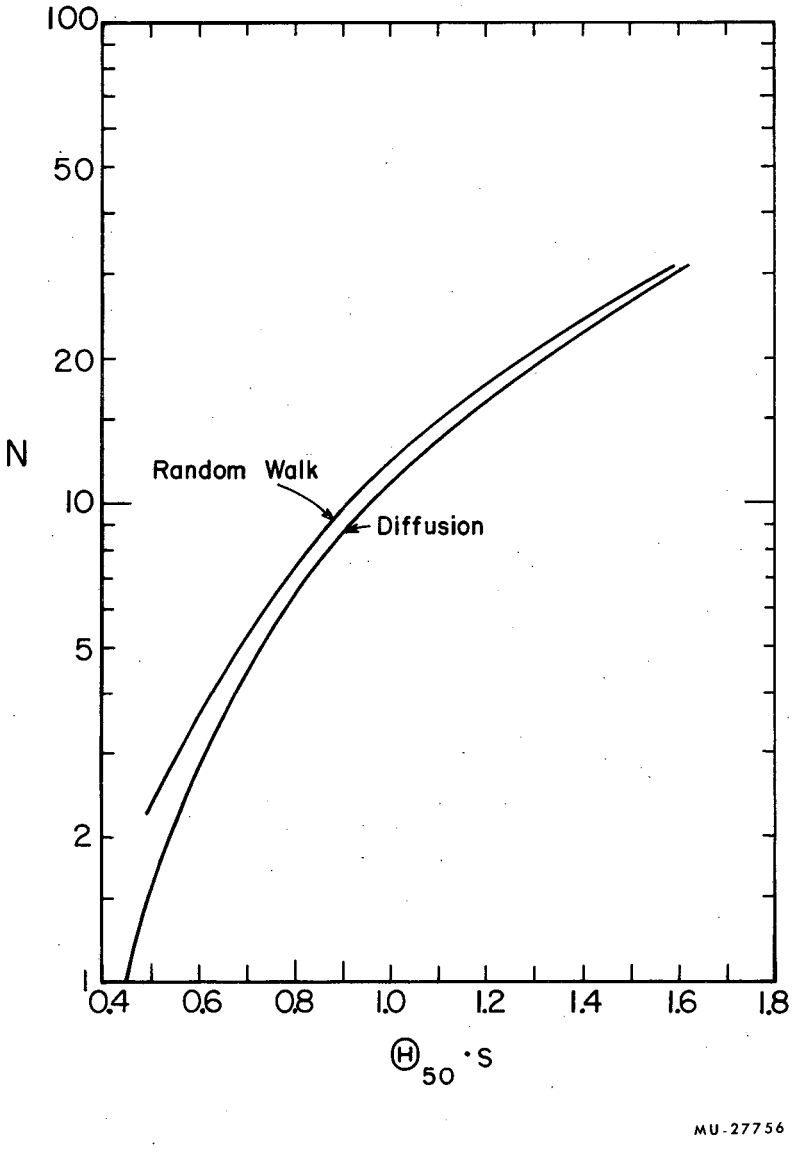

Fig. I-3. Midpoint slopes.

U ($= U_0/\epsilon$). If the total bed length is h, and the time that a packet of fluid has been in the bed is t, then the number of mixing lengths N (or column Péclet number) is defined as h/ℓ; and the dimensionless time scale, T, as Ut/ℓ. If a step input of tracer with magnitude c_0 has taken place at $N = 0$ and $T = 0$, the dimensionless concentration at the outflow is

$$X = \frac{c}{c_0} = \int_0^{T'} \exp(-N-\tau)\, I_0(2\sqrt{N\tau})d\tau \ , \qquad (6)$$

where τ is the dummy variable for another dimensionless time, T', with $T' = T(N+1)/N$. The solution of this integral is shown graphically in Fig. I-4, as a plot of dimensionless concentration against dimensionless time (the latter on a logarithmic scale) for several values of column Péclet number N. Here the time scale has been normalized about the stoichiometric time (the time required to replace one column-holdup of the phase of interest), at which $T = N$. Hennico, Jacques, and Vermeulen[16] made calculations of outlet concentrations for a large number of N and Θ values.

To compare these results with experimental curves, it was expedient to compute the midpoint slopes s relative to a time scale based on the time when X reaches 0.5; that is,

$$s' = (dX)/(dT) \cdot T_{(X=0.5)} \ . \qquad (7)$$

A numerical approximation to Eqs. (6) and (7), solved for N, was found to be

$$N = 4\pi s'^2 - 0.80 \ . \qquad (8)$$

Because the column Péclet number approaches the bounded-diffusion result at large values, it can again be used to define a packing Péclet number, $P = Nd_p/h = d_p/\ell$ and an effective dispersion coefficient, $E = U_0\ell$.

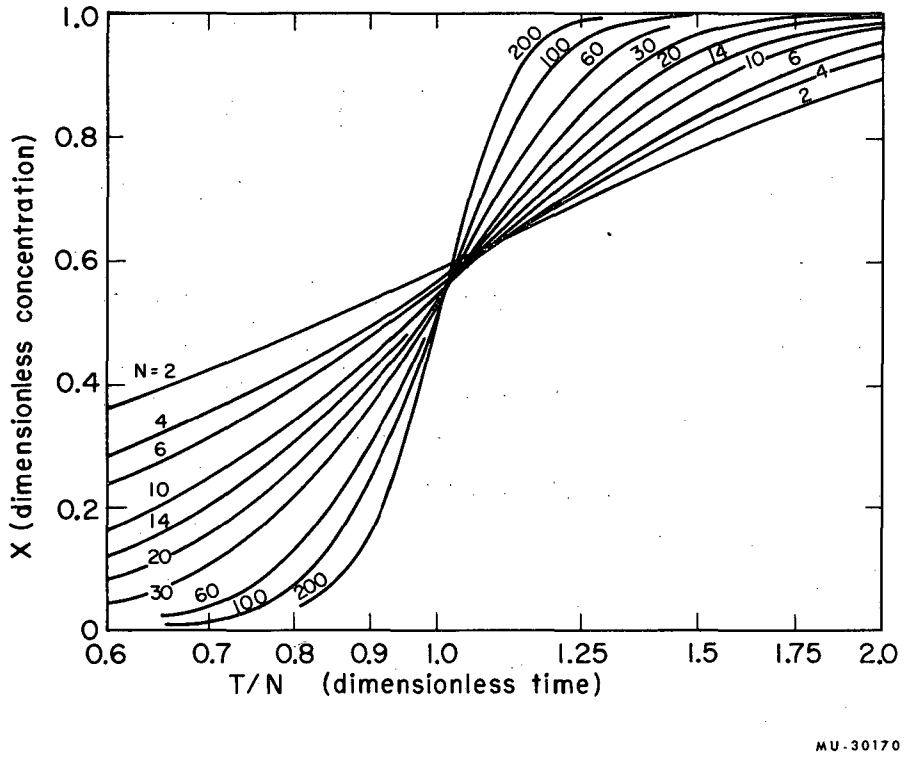

Fig. I-4. Breakthrough curves for random-walk model.

3. Interpretation of Experimental Data

Column Péclet numbers can be determined from experimental breakthrough curves by three different methods:

(a) The experimental breakthrough curve is compared with theoretical breakthrough curves predicted by the model. This graphical method has the advantage of utilizing the entire experimental curve, and thus shows whether or not the theoretical model is applicable.

(b) The midpoint slope obtained from the experimental curve can be used to determine the column Péclet number, utilizing Fig. I-4.

(c) Analytic relations can be employed for calculating column Péclet numbers from midpoint slopes. The random-walk model is used for this purpose in our investigation. In the low-Péclet-number range, where the difference between models is greatest, use of the diffusion model would give an ϵ_P 5% lower for the unpulsed column, or 15% lower for the pulsed column; the relative behavior would remain unchanged.

The method of data analysis is discussed in detail in Appendix I-2.

C. Apparatus

1. Column Assembly

Four different columns were used for the investigation, one with an ordered packing in an octagonal cross section, and three with random packings in circular or octagonal cross sections. The columns, for which overall dimensions are given in Table I-1, have been described in more detail by Jacques and Vermeulen[17] and Hennico, Jacques, and Vermeulen.[16] The relation of the central packed section to other elements of the column assembly is shown in Fig. I-5.

2. Column Packing

The ordered arrangements of uniformly sized spheres correspond to known types of crystallographic lattices. For such arrangements in packed columns, one must select two parallel planes through

Table I-1. Dimensions and packing of experimental columns.

Column no.	Packing	Effective diam (in.)	$(d_p)_v$ (in.)	$(d_p)_n$ (in.)	$(d_p)_a$ (in.)	a_p (ft^2/ft^3)	p (ft/ft^2)	ψ	Arrangement	Distance between layers (in.)	Fraction of voids (%)	Useful column height (in.)	Cross-sectional area ($in.^2$)
1	Spheres	0.75	0.75	0.75	0.75	65	22.2	1.0	Tetragonal	0.53	32.0	23.6	30.3
5	Spheres	0.75	0.75	0.75	0.75	56	28.2	1.0	Random	0.71	41.2	25.0	30.7
7	Raschig rings	0.75	0.65	0.47	0.28	80	66.0	0.42	Random	0.88	64.8	23.6	30.7
9	Berl saddles	1.0	0.76	0.42	0.25	78	77.0	0.33	Random	-	68.6	25.0	30.7

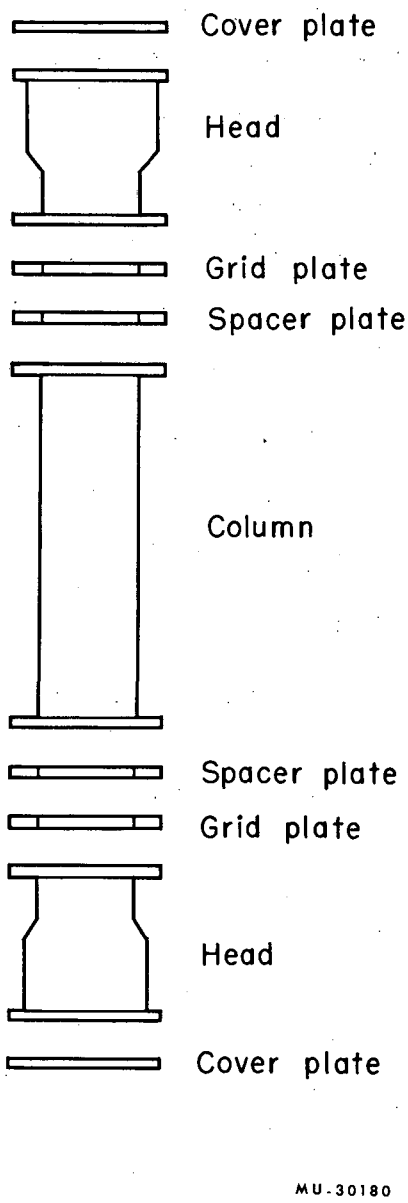

Fig. I-5. Exploded diagram of column assembly.

the lattice that will represent the ends of the column, and several planes each perpendicular to these that will constitute the column walls. The different lattice structures for spheres, each available for columns in one or more orientations, has been reported by Graton and Frazer[14] and Martin, McCabe, and Monrad.[23]

In our investigation one regular packing arrangement of spheres was used: tetragonal sphenoidal (Column 1), with a void-fraction of approximately 32%. Spheres 0.75 in. in diameter, obtained as oversized ceramic balls with rough surfaces, were wet-ground in a ball mill with granular alundum and classified between 0.74 and 0.76 inch. In the ordered packing, the lattice arrangement called for spheres adjacent to the wall, in alternate layers, to be either omitted or cut; this requirement was satisfied by insertion of spacers between the walls and the spheres, in these layers.

The randomly packed columns were stacked by pouring the packings into the column, with intermittent shaking of the bed, which was intended to avoid packing reorientation during pulsation. Table I-1 gives details on all the types and arrangements of packing used for the investigation.

The void-fraction ϵ was measured for all packings by measuring the amount of water necessary to fill a column of known volume.

For packings other than spheres, several different "equivalent" diameters can be defined. The most common one[2, 21] is the "equivalent spherical diameter," $(d_p)_v$, which corresponds to a sphere having the same volume as the packing unit. Pratt[26] introduced the "equivalent hydraulic diameter of void space," $(d_p)_h$, as

$$(d_p)_h = \frac{4 \cdot \text{free space}}{\text{periphery}} = \frac{4\epsilon}{p} \quad .$$

In the case of a stacked ring packing, the periphery (ft/ft^2) is identical with the superficial area (excluding edges) expressed as ft^2/ft^3. The determination of the periphery of random packing is much more difficult; thus, it has been convenient to adopt empirically the same definition for the periphery as that just stated for regular packings. A third measure

is the diameter of a sphere with the same surface-to-volume ratio as a packing particle.[25] From the properties of a sphere this diameter is defined as

$$(d_p)_a = \frac{6(1 - \epsilon)}{a_p} ,$$

where a_p is the surface area per unit volume.

Another property of packed beds is the sphericity ψ of the particle; this is defined as the area of a sphere having the same volume as the particle, divided by the area of the particle. We note that $(d_p)_a = \psi (d_p)_v$.

The values used for the above-mentioned parameters in this study are given in Table I-1. Where d_p is shown without a subscript, elsewhere in this report, $(d_p)_v$ is intended.

3. Conductivity Probes

The tracer used was sodium nitrate solution, with tap water for the main stream; the detection method was that of electrical conductivity. In the concentration range used, the electrical conductance of the aqueous "salt" solution was proportional to the concentration of $NaNO_3$. Thus, knowledge of the conductance of the mixed stream containing salt tracer allows a direct determination of the concentration.

The probes used to measure conductivity were constructed of two spherical sectors of 0.75-in. bakelite balls, connected by a pair of rhodium-plated pins. This probe design was chosen to avoid disturbing the packing arrangements in ordered sphere-packed columns. They were installed at different heights in the column, (nominally 0, 3, 6, 12, 18 and 24 in.), the plane of each probe being perpendicular to the main direction of the fluid flow, and the probes used being all located on the axis of the column.

4. Injection Nozzles

The injection unit was installed at the 0-in. nominal level, about 2 in. into the column. It consisted of several injection tubes connected to a manifold, the arrangement and number of tubes,

(normally 8) depending on the form of the cross section. Each injection tube was made of annealed type-302 stainless steel tubing (0.065 in. o.d., 0.031 in. i.d.), and had an aluminum sphere 0.75 in. in diameter affixed to its end.

To obtain as flat a salt distribution as possible, the central injection tube in each column had a 0.75-in. aluminum sphere with six radial holes (each 0.059 in. in i.d.) drilled 60 deg apart into the terminal aluminum ball, perpendicular to the axis of the column and to the injection supply tube for this outlet. In Column 7 all the injection tubes were provided with their terminal spheres similarly drilled, giving a total of 42 outlets.

In injecting a step flow of tracer, it was desired to avoid a large initial pulse of the tracer solution that would result from a momentary pressure surge in the injection line. A static build-up of pressure on the upstream side of the injection-control valve was prevented by having the tracer fluid circulate continuously past this point with the local pressure controlled at the needed level by a needle valve in the return line. When injection was to start, a three-way solenoid valve was used to transfer the salt flow-path with minimum time delay; the valve was actuated by an electrical switch, which also marked the recording chart at the time the valve was switched on.

5. Column Heads

Expanded end sections, nearly identical in construction, were connected above and below the particular packed section in use (see Fig. I-6). As the columns were designed to operate in upward as well as in downward flow, the same accessories were adopted for both upper and lower end sections: two windows for visual observation; a 6-in.-diameter inlet nozzle with interchangeable orifice plates, designed to give a velocity profile as flat as possible; and two symmetrically placed outlets. Pulsing was applied through the lower end section, using a distributor (1.5 in above the feed inlet nozzle) designed to provide as even a pulsing effect as possible across the entire column cross section.

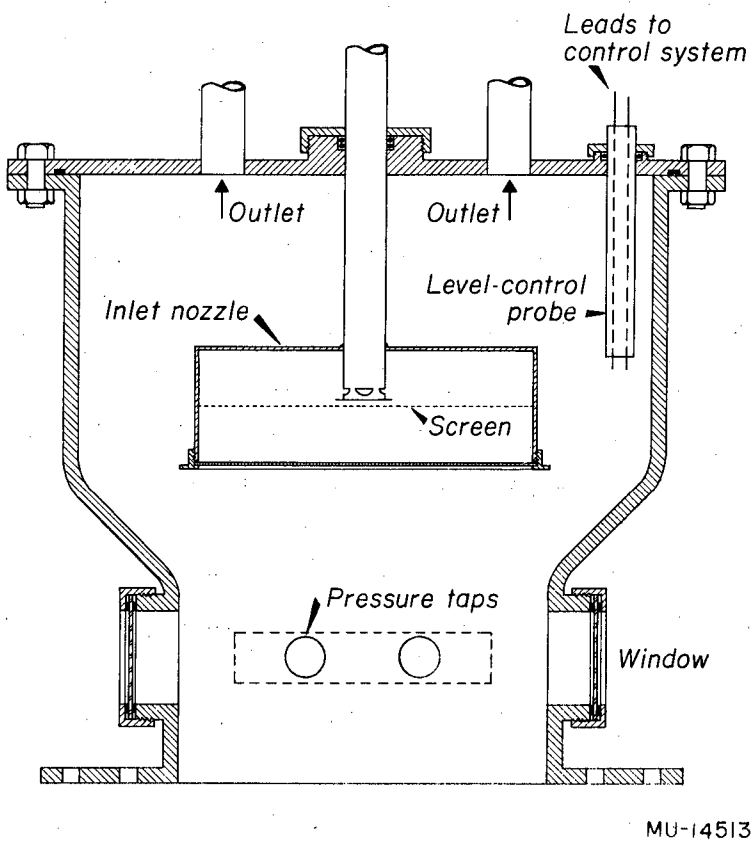

Fig. I-6. Diagram of column head.

6. Pulsing Unit

Pulsation was provided by a proportioning pump (Hills-McCanna K2R-F, 1.88 in. diameter, 2 in. stroke, rotary drive) from which the check valves had been removed, driven by a 3/4-hp single-phase 116/230-V ac motor through a chain and sprockets. This unit is shown in Fig. I-7. Frequencies could be varied from 20 to 250 cycles/min, by combining different sizes of sprockets, without putting severe strain on the pump. The amplitude was controlled by adjusting the length of the piston stroke, even without stopping the pump; the capacity per cycle could be varied from zero to 5.52 $in.^3$. The average amplitude in the column is defined as follows:

$$\text{amplitude} = \frac{\text{volume of fluid per stroke}}{(\text{area of column}) \cdot (\text{void fraction})} .$$

To minimize the loss of pulsing effect to the fluid inlet lines and to eliminate the rotameter fluctuations due to pulsing, throttle valves were inserted in these lines, adjacent to the column heads.

The pulse frequency was measured by a 1.00-min event-counter, with a contact switch at the pump shaft to provide a unit signal to the event-counter for each revolution of the pump shaft. A wiring diagram of the automatic 1.00-min event-counter is given in Fig. I-8.

The pulse line from the pulse generator to the packed column was 0.625-in.-i.d. copper tubing, 90 in. in effective length. The pulse line was designed so that cavitation-free operation could be maintained throughout the selected range of frequencies and amplitudes. Jealous and Johnson[18] have given an equation for the power required in pulsing, which was modified by Christensen[8] for calculating the point at which cavitation begins. By using this equation, we estimated that cavitation-free operation could be maintained up to the range of 0.7 in. in amplitude (the maximum used in this study) and 260 cycles/min in frequency (which is well above the maximum used).

To obtain even pulsing across the entire cross section of the columns, a pulse distributor was designed and installed. For this purpose an 0.75-in.-o.d. 5.5-in.-long aluminum tube, with six 0.375-in.-diameter holes drilled on each side, was installed in the bottom column-head 1.5 in. above the feed nozzle.

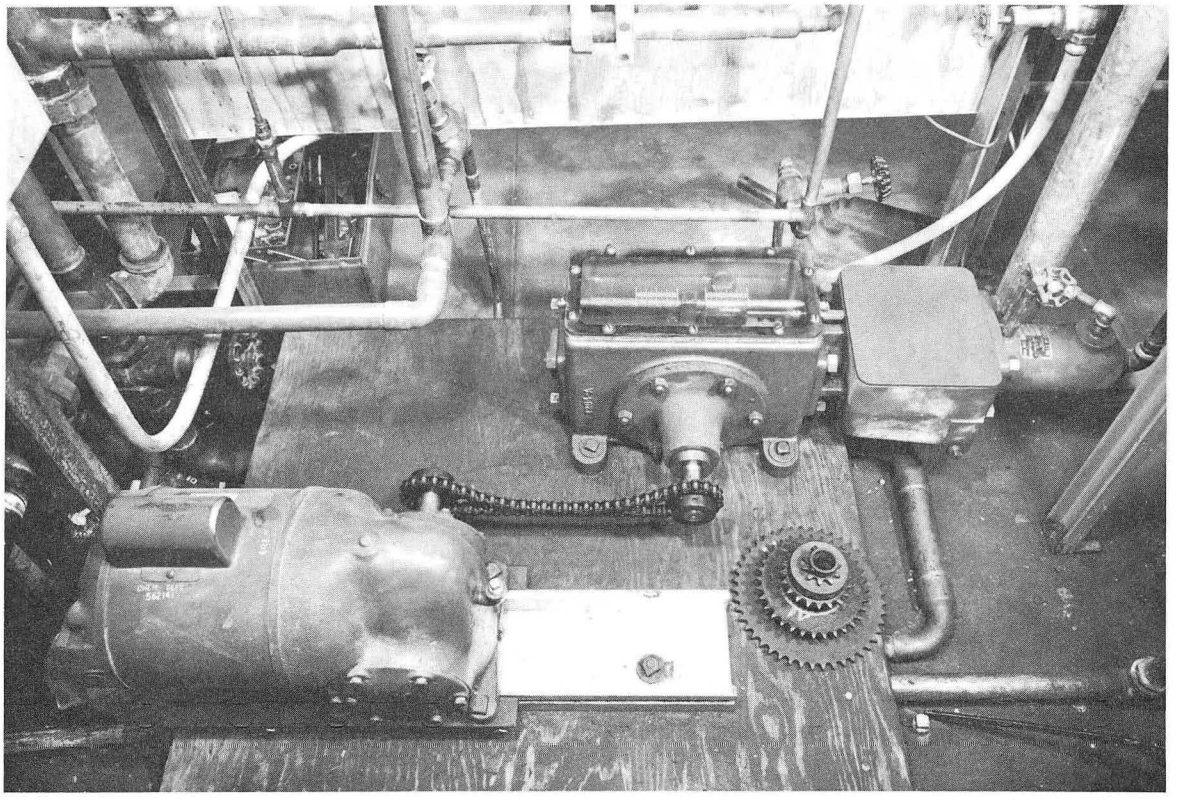

ZN-4057

Fig. I-7. Pulsing pump.

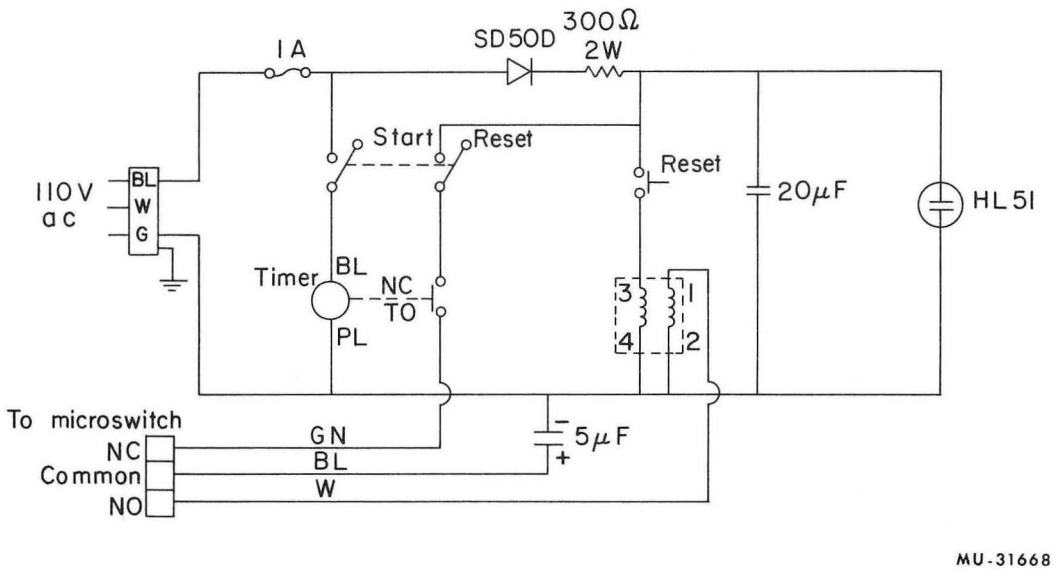

Fig. I-8. Wiring diagram of the event counter.

7. Circuitry

The basic electronic circuit used to measure the conductivity consists of four parts: an amplitude-stable oscillator, a low-impedance voltage source, an amplifier, and a self-balancing potentiometer which feeds the strip-chart recorder. These components have been described by Hennico, Jacques, and Vermeulen.[16]

A panel board for the wiring was attached to each column body. All the conductivity-cell leads of the column were connected to a rotary switch on the panel; six double-pole double-throw switches on the column panel allowed the selection of any cell for measurement. Finally, an eight-wire-cable plug on the panel board provided a separable connection to the electronic measuring and recording system.

8. Layout and Accessories

As noted in the specifications, the design and construction of a complete pilot-plant unit with extensive manifolding was needed. The flow arrangement is shown in Fig. I-9. A set of six pumps, six tanks, and seven rotameters made it possible to feed and meter three different types of liquids at the same time for a range of 0.005 to 40 gal/min.

Water for the experiments was provided from a 150-gal constant-head tank mounted on the roof of the building, about 25 ft above the column.

The rotameters were each calibrated by weight flow of water. Flow rates for fluids other than water were corrected by assuming that equal weight-flows give equal readings, using standard correction charts supplied by the Fischer-Porter Company. The working ranges of water flow through the six rotameters were 0 to 40, 0 to 6, (2) 0 to 0.8, (2) 0 to 0.3, and 0 to 0.005 gal/min.

Dial thermometers were inserted in the flow inlet and outlet. Temperature was not controlled, but stayed fairly constant; all runs were made at an ambient temperature of 23±2°C. The effect of temperature variation was neglected.

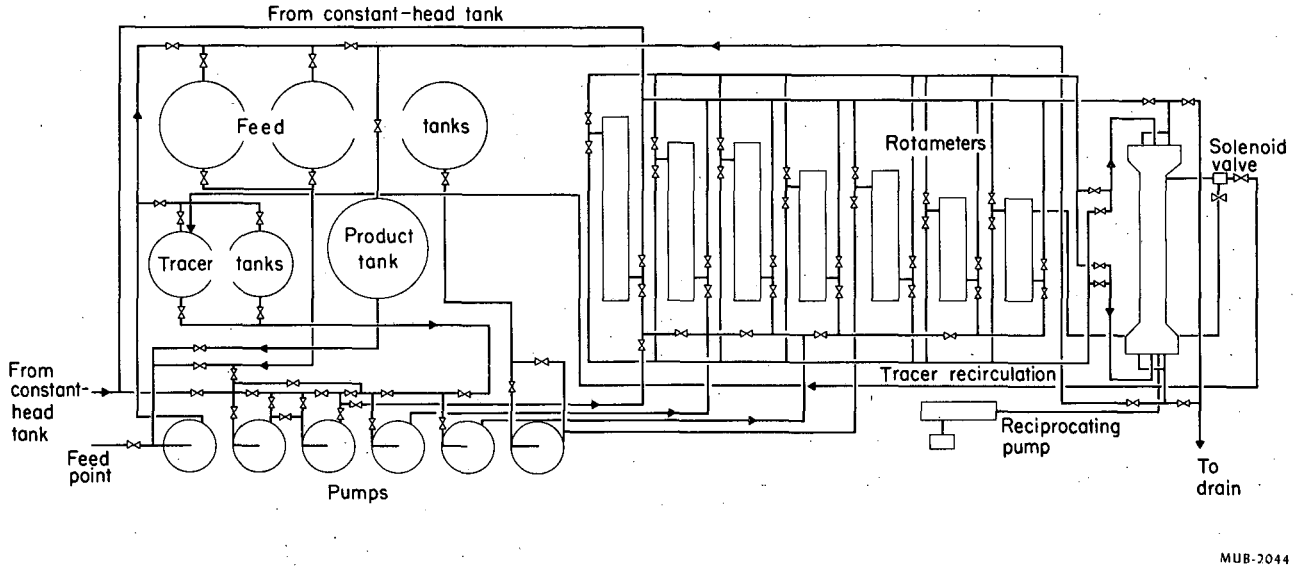

Fig. I-9. Layout of flow system.

D. Procedure

The equipment as designed allowed the injection of tracer solution at the top or bottom of the column. Theoretically the same breakthrough result should be obtained for either injection or shutoff of the tracer for either end of the column. Experimentally, it was found that for low flow rates large differences in behavior could occur due apparently to the density difference between the main stream and the tracer solution, which may cause a preferential irregular flow.[9, 15, 28, 31] It thus became necessary to find the operating conditions that would minimize the breakthrough differences.

The smoothness of the breakthrough curve, and the proper correspondence between the calculated and measured stoichiometric times determined in two different ways (that is, by dividing the measured flowrate into the column void volume, and by integrating the experimental breakthrough curve) were used as criteria for satisfactory operation. In our experiments we found that by reducing the salt concentration from 1 N to 0.05 N, the shape of the curves was improved, the two stoichiometric times showed better agreement, and a good match was obtained between equivalent tracer-in and tracer-out runs except at flow rates smaller than 0.3 gal/min. As a result, the following experimental conditions were adopted: For flow rates smaller than 0.5 gal/min, 0.05 N $NaNO_3$ solution was injected at a rate corresponding in all cases to less than 5% in volume (in most cases around 1 or 2%). For higher flow rates, the amount of tracer injected was less than 1% in volume, but the salt concentration was increased to 0.1 N. The injection was made at the top of the column for nearly all experiments. Both injection and purge breakthrough curves were recorded; in the low-flow-rate region, when the two curves did not agree fully, data were taken from the tracer-out or purging curves.

The experimental procedure for typical runs was as follows: Before each set of runs the electrical recording unit was tested for linearity by replacing the conductivity probe by a potentiometer; for

all the runs this error was within 1%. The actual run was started by using tap water from a constant-head tank flowing through the column at a chosen flow rate. The desired combination of frequency and amplitude was then applied to the column. Tracer ($NaNO_3$) solution was started through the recirculation line, and the pressure drops in the injection line and the recirculation line were equalized by means of two manual valves adjoining the solenoid valve.

After a final check of the flow rates, tracer injection into the column was started by opening the solenoid valve, with the starting time for injection marked electrically on the recorder chart. The voltages recorded during each run were proportional to the conductance of the main stream, and thus to the tracer concentration. Tracer injection was stopped after a constant reading was reached on the chart; the conductivity was again followed as a function of time to give the purge breakthrough curve.

E. Results and Discussion

The variables affecting axial dispersion that were investigated were viscosity, packing characteristics, and pulsing frequencies and amplitudes. As indicated above, the experimental breakthrough curve can be analyzed either by curve-matching or by taking midpoint slopes of the breakthrough curve as plotted on linear t/t_{50} coordinates. The method of data analysis is discussed in detail in Appendix I-2.

Full results as obtained from the run conditions are tabulated in Appendix I-1. A separate table is given for each column; within each table, for the different flow rates used, values are listed for superficial velocity, pulsing frequency and amplitude, midpoint slope, number of mixing units N, Péclet number P, modified Péclet number ϵP, modified Reynolds number $d_p U_0/\nu(1-\epsilon)$, and combined Reynolds number $d_p(U_0 + 2\omega A)/\nu(1-\epsilon)$.

1. Effects of Viscosity and Velocity

The effect of viscosity was studied by use of Column 5. Water and glycerol were blended to give a kinematic viscosity of 6.0 centistokes at 23°C. Experimental runs with this mixture are compared with results on tap water, in Fig. I-10.

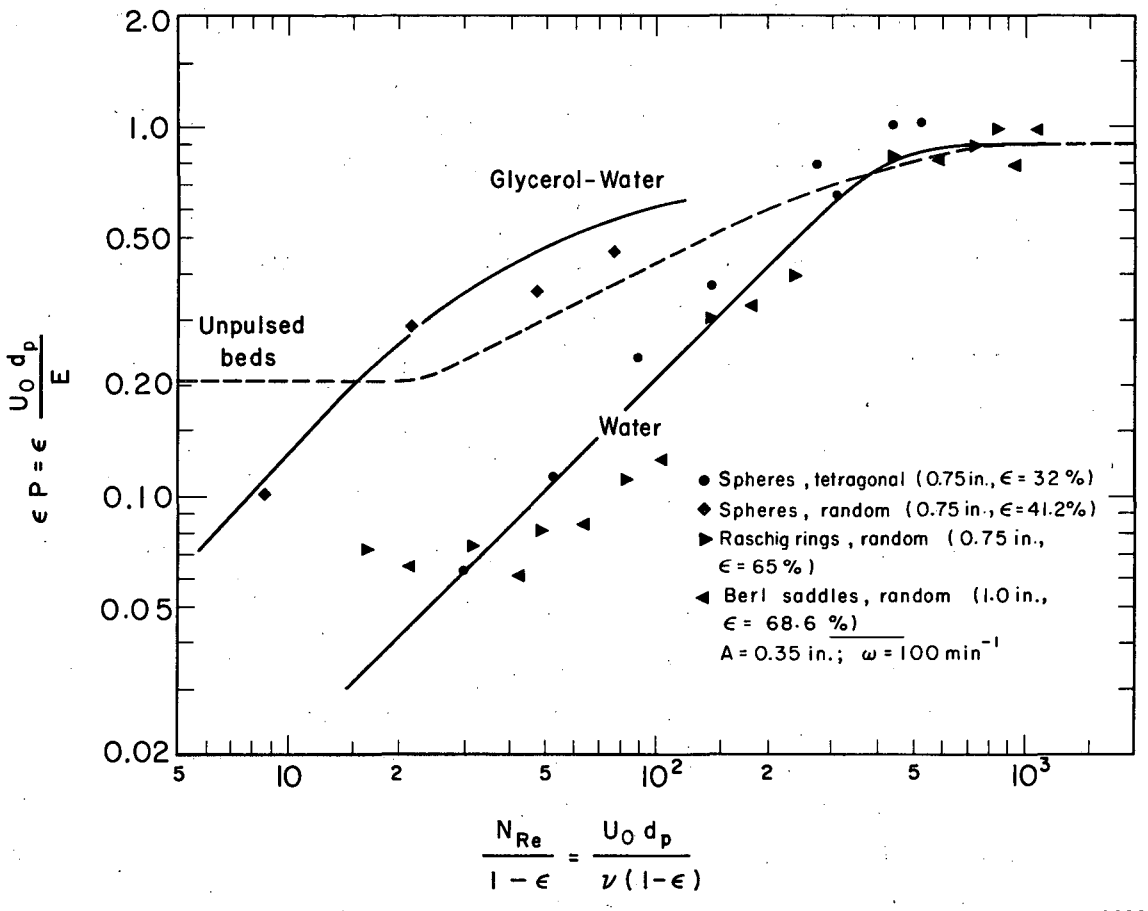

Fig. I-10. Experimental results at constant amplitude and frequency.

Péclet numbers of water - glycerol mixture are different from those of tap water under the same pulsing conditions and Reynolds numbers. For an unpulsed column, the Péclet numbers were found to be equal for the same Reynolds numbers, regardless of viscosity, by Hennico, Jacques, and Vermeulen.[16] However, in the pulsed column, Péclet numbers depend upon the viscosity even at the same Reynolds number, as shown in Fig. I-10. Thus the effect of pulsation on longitudinal dispersion depends upon viscosity as well as upon velocity. The probable explanation rests on two factors: the size of the eddies caused by pulsing, and the distance traveled by fluid "packets" due to acceleration by pulsation. Accordingly, it is necessary to consider the degree of turbulence caused by pulsing in order to interpret the dependence of Péclet numbers on viscosity. This will be done later in this study.

The solid curves shown in Fig. I-10 have been calculated from the correlation that will be presented. The dashed curve, for unpulsed columns, is from Hennico, Jacques, and Vermeulen.[16]

2. Effects of Packing-Particle Characteristics

Various types of packing were investigated to determine the effects of particle shape and packing arrangement, as listed in Table I-1. Experimental values of modifed Péclet number ϵP (based on the equivalent diameter of the packing material) at a fixed combination of frequency and amplitude, for different kinds of packings, were plotted in Fig. I-10 against the modified Reynolds number $N'_{Re} = U_0 d_p/\nu(1-\epsilon)$ used previously by Hennico, Jacques, and Vermeulen (with ν the kinematic viscosity of the fluid). It is seen that the experimental points do not fall into a single curve except at high Reynolds numbers. Hence the effect of pulsing also depends upon the packing characteristics, but the exact nature of the dependence is not yet known.

3. Effects of Pulse Frequency and Amplitude

To investigate the effect of pulse frequency on axial dispersion in packed columns, runs were made with various frequencies at fixed

amplitude, with given packing and flow rates. Several different flow rates were used for this investigation.

The results for modified Péclet number ϵP are plotted against frequency, at constant Reynolds numbers, in Fig. I-11. Higher frequency gives a lower Péclet number, and the effect is greater for low flow rate. The effect diminishes as the flow rates increase, and gradually disappears around a Reynolds number of 100. Also, at a fixed flow rate, the effect is greater in low ranges of frequency and disappears gradually.

This behavior can be explained in terms of the degree of turbulence in the packed bed. At a high flow rate, turbulence caused by pulsation is small compared with the turbulence caused by rapid flow, and the effect of pulsing is small. At low flow rate a contrary effect is observed: intense pulsation makes a large difference in the axial mixing. At a fixed flow rate, the degree of turbulence caused by pulsation has an effect on axial mixing up to a certain frequency, but additional pulsation does not give any greater effect, apparently indicating that the amount of turbulence does not increase further.

The effect of pulse amplitude at a fixed pulse frequency was also studied, with results as shown in Fig. I-12, for modified Péclet number vs pulse amplitude; again Reynolds number is a contour parameter. As in the case of frequency, Péclet number decreases as pulse amplitude increases with a greater effect at low flow rates.

These Péclet numbers were compared with the Péclet numbers without pulsing, and steps were taken to obtain an empirical correlation between these variables. The flow pattern in a pulsed column is dependent upon two factors: the bulk-flow Reynolds number, $U_0 d_p/\nu$, and a "pulsation Reynolds number," $2\omega A d_p/\nu$. When pulsed-column data are compared with data from an nonpulsed column, this must be done at corresponding flow conditions. In our investigation, the nonpulsed-column Péclet numbers at any given bulk-flow Reynolds numbers were compared with the pulsed-column Péclet numbers at a combined Reynolds number for pulsing, $d_p(U_0 + 2\omega A)/\nu$. The direct addition of U_0 and $2\omega A$ gives a very satisfactory empirical fit, better

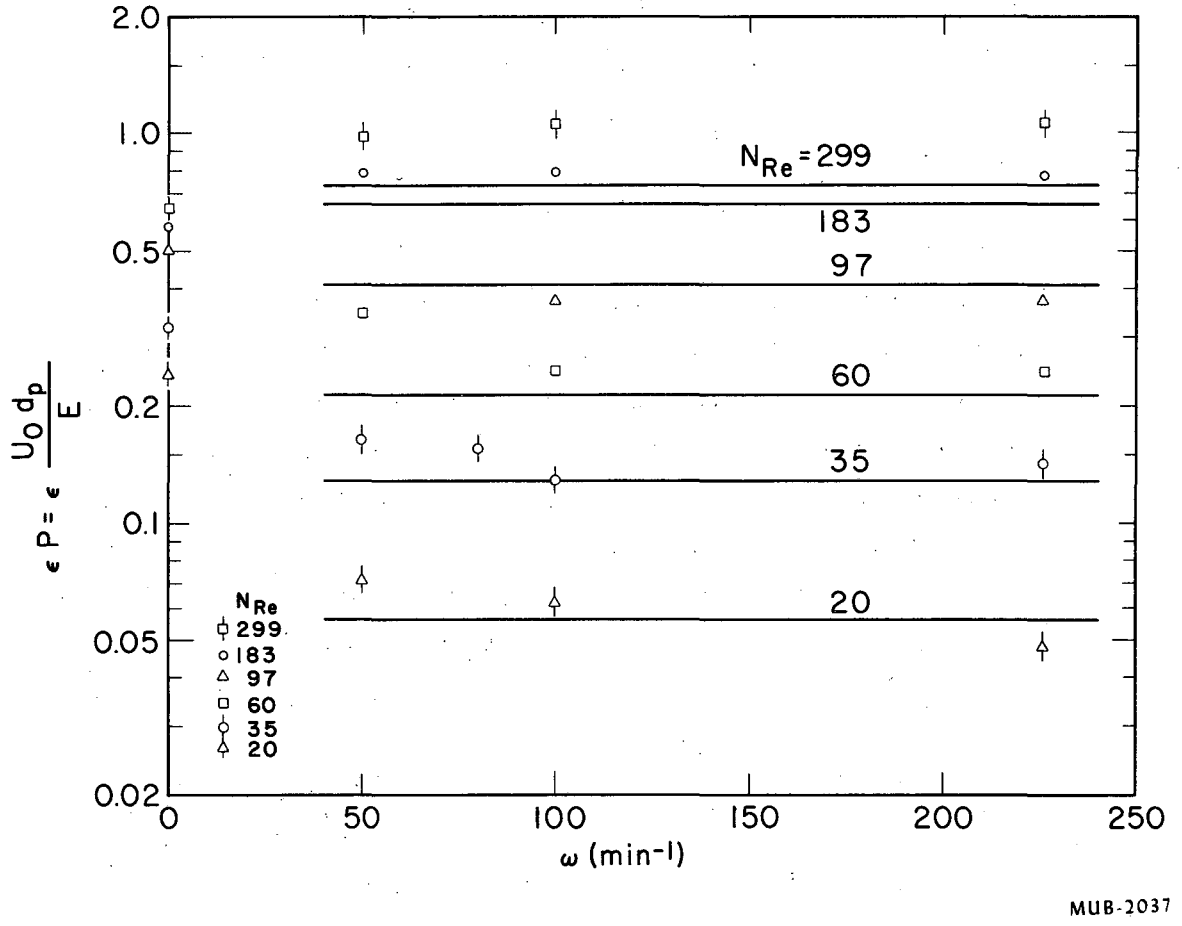

Fig. I-11. Effect of frequency.

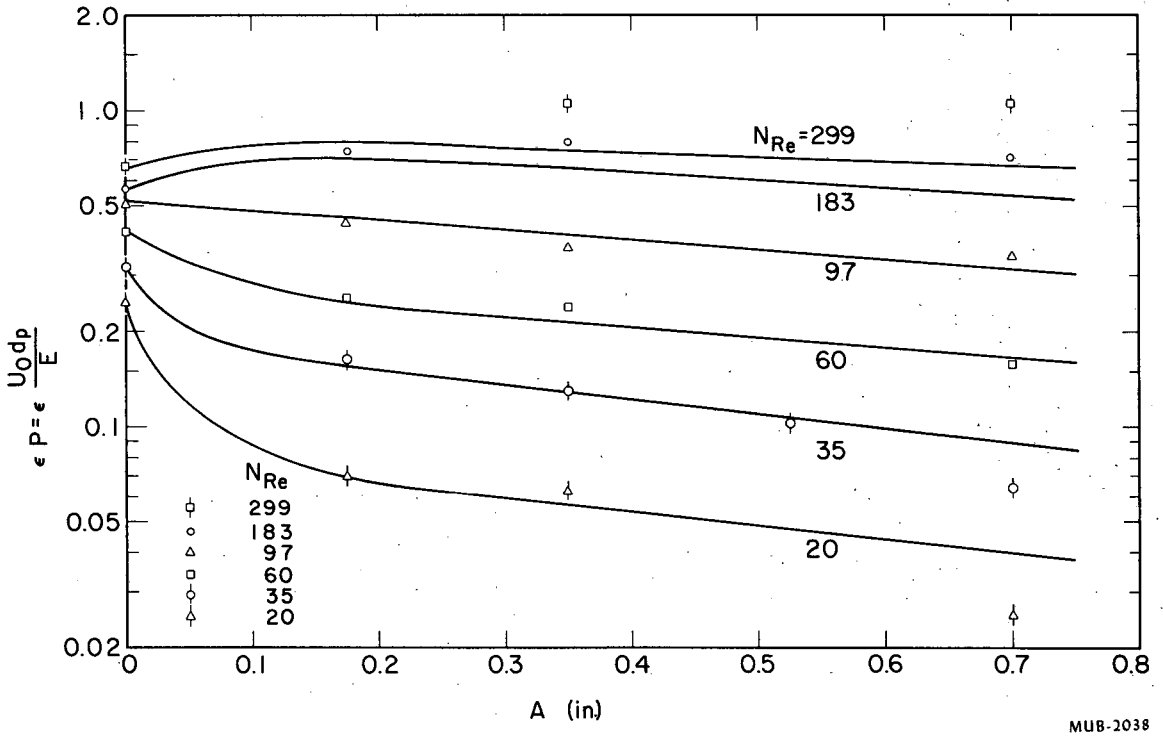

Fig. I-12. Effect of amplitude.

than for a lower or higher coefficient on ωA. In Fig. I-13, modified-Péclet-number values with and without pulsation are plotted against this combined Reynolds number. The Péclet numbers with pulsation are now seen to be always lower than those without pulsation. This appears to leave a single type of mixing effect to be accounted for in the rest of the correlation.

The additional dispersion due to pulsing can be expressed by the dimensionless parameter $(1/\epsilon P) - (1/\epsilon P_0)$, where ϵP_0 is the modified Péclet number without pulsation. Since the effect of pulsing is dependent upon packing characteristics such as the effective diameter, a dimensionless amplitude A/d_p was employed as a second parameter. After several trials to test for the effect of different exponents for the variables, the following correlation was adopted:

$$\frac{1}{\epsilon}\left(\frac{1}{P} - \frac{1}{P_0}\right)\left(\frac{d_p}{A}\right)^{1/2} = fn[U_0] \quad .$$

The correlation term $(1/\epsilon)(1/P - 1/P_0)(d_p/A)^{0.5}$ might also contain the group $(U_0/A\omega)$ raised to a low power (e.g., 0.1), in order to be continuous into zero frequency. The independent variable U_0 could be made dimensionless, if a theoretical basis were found to bring in the velocity of sound in the fluid, or some other nearly constant term with dimensions of velocity. Figure I-14, a plot of the present correlation, shows that the correction factor varies with the (-5/3) power of U_0 at high velocities. While some spread is observed on the correction factor, the effect of amplitude on the mixing is better correlated by a 0.5 power of (d_p/A) than by a higher or lower power.

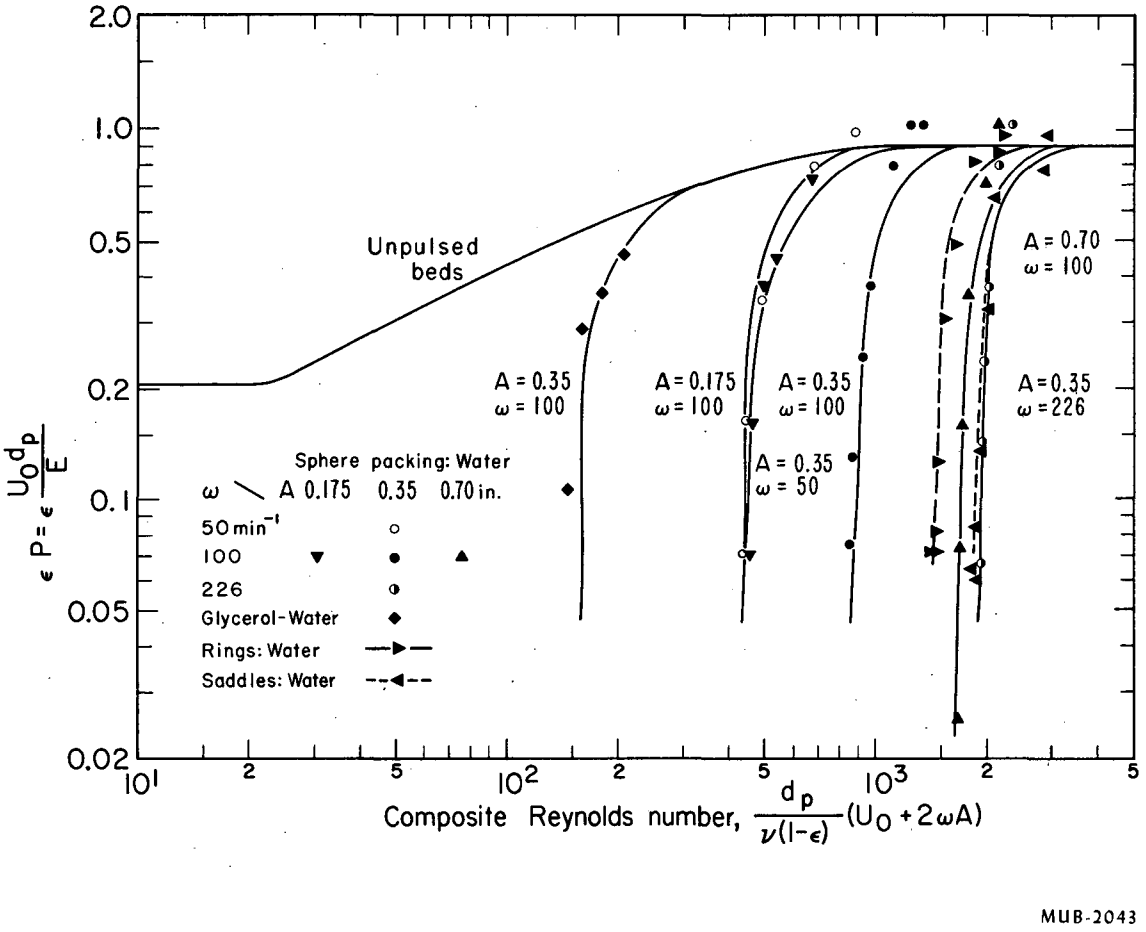

Fig. I-13. Péclet number vs composite Reynolds number.

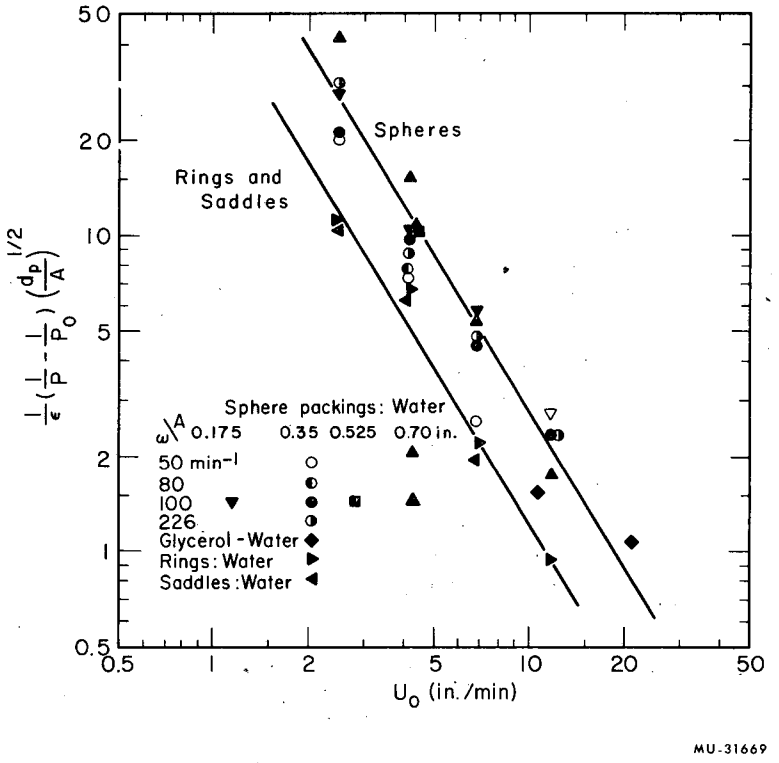

Fig. I-14. Correlation plot for pulsing effect.

F. Conclusion

For single-phase flow the use of pulsation serves to decrease the Péclet numbers as the amplitude increases, and to a lesser extent as the frequency increases. The effect is somewhat more pronounced in beds of Raschig rings and Berl saddles than in beds of uniform spheres. The Péclet-number decrease diminishes with increasing fluid viscosity and also with increasing flow rate. Extrapolation of our results predicts a rise in Péclet number for a relatively viscous fluid under certain conditions. Pulsation is expected to produce an increase in the mass-transfer rate; and this increase must outweigh the extra mixing produced, in order for pulsation of a packed-bed column to be of practical interest.

G. Notation for Part I

A	Pulse amplitude, in.
a_p	Surface area per unit volume, ft^2/ft^3
c	Concentration, gram-moles/cm^3
c_0	Feed concentration, gram-moles/cm^3
d_p	Particle diameter, in.
$(d_p)_a$	Equivalent diameter, in.
$(d_p)_h$	Equivalent hydraulic diameter, in.
$(d_p)_v$	Equivalent spherical diameter, in.
E	Superficial dispersion coefficient, cm^2/sec
h	Height of bed, ft
l	Mixing length, ft
N	Column Péclet number (h/l), dimensionless
N_{Re}	Reynolds number, dimensionless
N'_{Re}	Modified Reynolds number $[N_{Re}/(1-\epsilon)]$, dimensionless
p	Periphery of packing, ft/ft^2
P	Packing Péclet number (d_p/l), dimensionless
s	Midpoint slope (based on Θ scale), dimensioness
s'	Midpoint slope of breakthrough curve (based t/t_{50} scale), dimensionless
t	Time, sec
t_{50}	Time corresponding to X equals 0.5, sec
T	Dimensionless time
U	Intersticial velocity or mean linear velocity, ft/hr
U_0	Superficial velocity, equals $U\epsilon$, ft/hr
X	Dimensionless concentration (c/c_0)
z	Axial distance, ft
Z	Dimensionless axial distance (z/h)
ϵ	Bed void fraction, dimensionless
Θ	Dimensionless time T/N
ν	Kinematic viscosity, $(cm^2/sec.)$
ψ	Sphericity, dimensionless
ω	Pulse frequency, min^{-1}

REFERENCES FOR PART I

1. H. Brenner, Chem. Eng. Sci. 17, 229 (1962).
2. G. G. Brown and associates, Unit Operations (John Wiley & Sons, Inc., New York, 1950), p. 216.
3. E. J. Cairns and J. M. Prausnitz, Chem. Eng. Sci. 12, 20 (1960).
4. J. J. Carberry, Am. Inst. Chem. Engrs. J. 4, 13M (1958).
5. J. J. Carberry and R. H. Bretton, Am. Inst. Chem. Engrs. J. 4, 367 (1958).
6. H. S. Carslaw and J. C. Jaeger, Conduction of Heat in Solids (Oxford University Press, New York, 1959), 2nd ed., pp. 114-119.
7. W. A. Chantry, R. L. Von Berg, and H. F. Wiegandt, Ind. Eng. Chem. 47, 1155 (1955).
8. C. M. Christensen, Liquid-Liquid Extraction Efficiencies of a Pulsed Packed Column and a Pulsed Sieve-Plate Column of Four Inch Diameter (Ph. D. Thesis), Cornell University, 1961.
9. R. L. Chuoke, P. Van Meurs, and C. van der Pool, J. Petrol. Technol., Petroleum Trans. A. I. M. E. 216, 188 (1959).
10. P. V. Danckwerts, Chem. Eng. Sci. 2, 1 (1953).
11. E. A. Ebach and R. R. White, Am. Inst. Chem. Engrs. J. 4, 161 (1958).
12. H. A. Einstein, Ph. D. Thesis, Eidg. Techn. Hochschule, Zürich, 1937.
13. G. Feick and H. M. Anderson, Ind. Eng. Chem. 44, 405 (1952).
14. L. C. Graton and H. J. Frazer, J. Geol. 43, 785, 910 (1935).
15. F. Helfferich, Chem.-Ing. Tech. 34, 275 (1962).
16. A. Hennico, G. Jacques, and T. Vermeulen, Lawrence Radiation Laboratory Report UCRL-10696, March 1963.
17. G. L. Jacques and T. Vermeulen, University of California Radiation Laboratory Report UCRL-8029, November 1957.
18. A. C. Jealous and H. F. Johnson, Ind. Eng. Chem. 47, 1159 (1955).
19. G. de Josselin de Jong, Trans. Amer. Geophys. Union 39, 67 (1958).
20. H. Kramers and G. Alberta, Chem. Eng. Sci. 2, 173 (1953).

21. M. Leva, Tower Packing and Packed Tower Design (United States Stoneware Co., Akron, Ohio, 1951).
22. B. W. Mar and A. L. Babb, Ind. Eng. Chem. 51, 1011 (1959).
23. J. J. Martin, W. W. McCabe, and C. C. Monrad, Chem. Eng. Progr. 47, 91 (1951).
24. K. W. McHenry and R. H. Wilhelm, Am. Inst. Chem. Engrs. J. 3, 83 (1957).
25. J. M. Perry, Chemical Engineer's Handbook (McGraw-Hill Book Company, Inc., New York, 1950) 3rd. ed., pp. 394.
26. H. R. C. Pratt, Trans. Inst. Chem. Engrs. (London) 29, 195 (1951).
27. P. G. Saffman, J. Fluid Mech. 6, 321 (1959); Chem. Eng. Sci. 11, 125 (1959); J. Fluid Mech. 7, 194 (1960).
28. P. G. Saffman and G. I. Taylor, Proc. Roy. Soc. (London) A245, 312 (1959).
29. L. D. Smoot and A. L. Babb, Ind. Eng. Chem. Fundamentals 1, 93 (1962).
30. D. A. Strang and C. J. Geankoplis, Ind. Eng. Chem. 50, 1305 (1958).
31. G. I. Taylor, Proc. Roy. Soc. (London) A201, 192 (1950).
32. R. L. Von Berg and H. F. Wiegandt, Chem. Eng. 59, 189 (1952).
33. S. Yagi and T. Miyauchi, Kagaku Kogaku (Chem. Eng., Japan) 17, 382 (1953).

APPENDIX I-1

Table I-2. Péclet numbers from tracer breakthrough in single-phase flow.

Flow rate (gal/min)	U_0 (ft/hr)	A (in.)	ω (min^{-1})	Midpoint slope	N	P	ϵP	$\frac{d_p U_0}{\nu(1-\epsilon)}$	$\frac{d_p(U_0 + 2\omega A)}{\nu(1-\epsilon)}$
A. Column 1: 0.75-in. spheres, tetragonal arrangement (ϵ = 0.32); water									
0.327	12.30	0.35	50	0.785	7.0	0.223	0.071	30.0	444
		0.35	100	0.746	6.2	0.197	0.063	30.0	858
		0.35	226	0.662	4.7	0.149	0.048	30.0	1900
		0.175	100	0.781	6.9	0.219	0.070	30.0	444
		0.70	100	0.515	2.5	0.080	0.025	30.0	1685
0.560	21.07	0.35	50	1.160	16.1	0.512	0.164	51.5	466
		0.35	80	1.130	15.3	0.488	0.156	51.5	712
		0.35	100	1.042	12.8	0.407	0.130	51.5	880
		0.35	226	1.080	14.1	0.448	0.143	51.5	1921
		0.175	100	1.160	16.1	0.512	0.164	51.5	466
		0.525	100	0.926	10.0	0.319	0.102	51.5	1292
		0.70	100	0.752	6.3	0.200	0.064	51.5	1707
0.918	34.54	0.35	50	1.67	34.2	1.080	0.345	84.5	498
		0.35	100	1.39	23.5	0.747	0.239	84.5	913
		0.35	226	1.38	23.1	0.735	0.235	84.5	1954
		0.175	100	1.49	27.2	0.865	0.277	84.5	498
		0.70	100	1.134	15.4	0.487	0.156	84.5	1740
1.57	59.08	0.35	100	1.72	36.3	1.16	0.371	144	972
		0.35	226	1.72	36.3	1.16	0.371	144	2010
		0.175	100	1.89	44.1	1.40	0.448	144	558
		0.70	100	1.69	35.1	1.11	0.355	144	1799
2.98	112.13	0.35	50	2.5	77.7	2.47	0.79	274	688
		0.35	100	2.5	77.7	2.47	0.79	274	1102
		0.35	226	2.5	77.7	2.47	0.79	274	2144
		0.175	100	2.44	74.0	2.35	0.752	274	688
		0.700	100	2.38	70.3	2.23	0.714	274	1929
4.86	182.87	0.35	50	2.78	96.3	3.06	0.979	448	862
		0.35	100	2.89	104.1	3.30	1.056	448	1276
		0.35	226	2.89	104.1	3.30	1.056	448	2318
		0.70	100	2.89	104.1	3.30	1.056	448	2103
5.62	211.0	0.35	100	2.89	104.1	3.30	1.056	516	1344
B. Column 5: 0.75-in. spheres, random arrangement (ϵ = 0.41); water-glycerol (ν = 6.0 cs)									
0.567	21.34	0.35	100	0.893	9.3	0.255	0.1045	8.8	147
1.440	54.19	0.35	100	1.47	26.3	0.726	0.291	22.0	160
2.810	105.74	0.35	100	1.61	31.8	0.878	0.360	43.0	181
4.570	171.96	0.35	100	1.79	39.6	1.088	0.455	70.0	208
C. Column 7: 0.75-in. Raschig rings (d_p = 0.65 in., ϵ = 0.65); water									
0.109	4.10	0.35	100	0.616	3.9	0.111	0.072	16.9	1407
0.218	8.20	0.35	100	0.618	4.0	0.111	0.072	33.8	1424
0.326	12.30	0.35	100	0.656	4.6	0.127	0.082	50.5	1441
0.560	21.07	0.35	100	0.787	7.0	0.194	0.126	86.6	1477
0.918	34.54	0.35	100	1.190	16.9	0.468	0.303	142.0	1532
1.570	59.08	0.35	100	1.497	27.4	0.758	0.491	243	1633
2.980	112.13	0.35	100	1.930	46.0	1.274	0.825	461	1851
4.86	182.87	0.35	100	2.00	49.4	1.368	0.886	755	2145
5.62	211.47	0.35	100	2.09	54.0	1.50	0.971	870	2260
D. Column 9: 1-in. Berl saddles (d_p = 0.76 in; ϵ = 0.69); water									
0.109	4.1	0.35	100	0.56	3.1	0.094	0.065	22.2	1862.2
0.218	8.2	0.35	100	0.541	2.9	0.088	0.060	44.4	1884.4
0.326	12.3	0.35	100	0.616	4.0	0.122	0.084	66.5	1906.5
0.560	21.07	0.35	100	0.769	6.6	0.201	0.138	114.0	1954.0
0.918	34.54	0.35	100	1.150	15.8	0.480	0.329	187.0	2027.0
1.570	59.08	0.35	100	1.61	31.7	0.960	0.659	320.0	2160.0
2.980	112.13	0.35	100	1.77	38.5	1.170	0.803	610.0	2450.0
4.860	182.87	0.35	100	1.75	37.7	1.146	0.786	994.0	2834.0
5.62	211.47	0.35	100	1.96	47.4	1.441	0.989	1150.0	2990.0

APPENDIX I-2: SAMPLE CALCULATION

The calculation method used will be demonstrated with the data from a run (20710-3) in Column 1 (0.75-in. spheres in tetragonal arrangement, $\epsilon = 0.32$; flow rate 0.918 gal/min, A = 0.175 in., $\omega = 100$ cycles/min). The data from the recorder chart, and the calculations made on the breakthrough curve, are given in Table I-2. The calculations are made for both "salt-in" and "salt-out" breakthrough curves. A plot of the concentration (in percent) vs the ratio of the elapsed time to the time at the 50% concentration point is shown and compared with a theoretical breakthrough curve in Fig. I-15. From the slope (s'), taken at $t/t_{50}=1$, the Péclet number is calculated by the relation

$$N = 4\pi s'^{2} - 0.80$$

and

$$P = \frac{d_p}{h} N ,$$

where d_p is the packing diameter and h is the height of the bed (distance between the injection plane and the plane of measurement). For the represented run $s' = 1.49$, $N = 27.2$, and $P = 0.865$.

The experimental breakthrough curve is plotted on a t/t_{50} scale, and thus the theoretical stoichiometric point and the experimental stoichiometric points for the model occur beyond $t/t_{50} = 1$. For this column the theoretical stoichiometric point, equal to the ratio of column void-volume (cross section × height × porosity = 0.99 gal) to volumetric flow rate (0.918 gal/min), is 1.08 min.

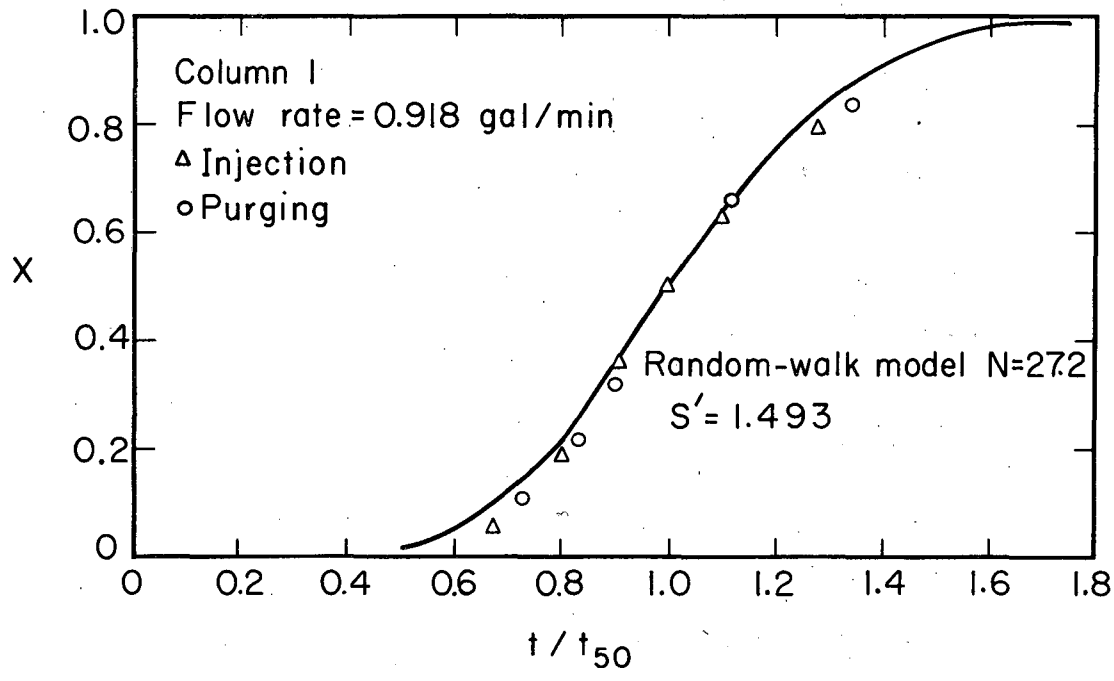

Fig. I-15. Experimental breakthrough curve vs theoretical breakthrough curve.

Table I-3. Sample calculation of an experimental breakthrough curve.[a]

Tracer in				Tracer out			
Recorder		Breakthrough c		Recorder		Breakthrough c	
c[b]	t[c]	c/c_0 (%)	t/t_{50}	c_0-c	t	$\frac{c_0-c}{c_0}$ (%)	t/t_{50}
0		0	0	0	0		
1.2	9.7	5.3	0.674	2.3	10.5	10.3	0.731
4.2	11.6	18.3	0.806	4.9	12.0	21.2	0.834
8.2	13.15	35.8	0.913	7.3	13.0	32.0	0.902
14.2	15.8	62.0	1.097	15.1	16.1	66.1	1.115
18.2	18.4	79.5	1.278	18.9	19.3	82.7	1.34
22.9	∞	100.0	∞	22.9	∞	100.0	∞

[a]Conditions: Column 1, tetragonal, $\epsilon = 0.32$; flow rate = 0.918 gal/min ($N_{Re} = 60.3$) A = 0.175 in.; ω = 100 cycles/min; injection at top of column; concentration of tracer = 0.05 N Na NO_3; flow, 0.009 gal/min.

[b]Concentration given in recorder-chart units.

[c]Time given in recorder-chart units (chart speed = 15 chart units/min).

PART II. COUNTERCURRENT LIQUID FLOW THROUGH PULSED PACKED COLUMNS

A. Introduction

The packed column is a simple and economical type of equipment for performing a variety of mass-transfer operations in the chemical industry.

Packed columns used in liquid-liquid extraction may be divided into two basic categories, according to the energy source used to obtain contact of the two immiscible phases; the one most commonly employed obtains this energy solely from the force of gravity acting upon the density difference between the two liquids; the other receives the extra energy from outside, by pulsation. The energy obtained from density difference is usually not optimum for providing an effective interphase contact. With additional mechanical energy supplied to move the liquid up and down, the packing becomes a sort of stirrer, with the advantage that its energy of agitation is supplied uniformly over the entire volume, without interfering with the continuity of the countercurrent action.

Numerous investigators who have worked with packed-bed columns[3, 4, 9, 15, 19] and with sieve-plate columns[4, 7, 17, 18] have reported that the column efficiency may be improved up to a factor of three, by applying proper pulsation.

The usual method for designing a packed extraction column with or without pulsation, as introduced by Colburn,[5, 6] involves computing the number of transfer units (NTU) required to bring about a given extraction, and multiplying this number by a height factor (the HTU, or height of a transfer unit) determined from direct or indirect experience. For extraction columns the HTU values vary widely with the physical properties of the two phases, the nature and amount of solute, rates of flow, and pulse frequency and amplitude, making it necessary to obtain very specific data for the contemplated design.

The mathematical definition of HTU is based upon a piston-flow model for each of the two counterflowing phases. The actual

phases would appear to be far from homogeneous at any one cross section, and the complex flow behavior within the packing would seem to produce considerable back-mixing within each phase.

The phenomenon of axial mixing or longitudinal dispersion arises from the fact that a molecular-scale "packet" of fluid does not move through a bed at constant velocity, nor usually at the same local velocity as other packets passing a given point. These fluctuations appear to result from (a) separation of the flow into filaments taking different paths through the packing, (b) eddy motion of the fluid, (c) molecular diffusion, and (d) forced back-mixing due to pulsation. The first mechanism of axial dispersion appears to be more characteristic of a laminar-flow regime, and the second more of turbulent flow; but the possibility also exists of effects (a), (b), and (d) occurring together.

Longitudinal dispersion in an extraction column has the effect of reducing substantially, the driving potential for mass transfer as compared with piston flow through the apparatus. In pulsed columns, generally, this reduction is more than compensated for by the higher mean values of overall mass-transfer coefficient that are attained. It becomes evident that any design correlation of mass-transfer coefficients or HTU values, to be correct fundamentally, should account separately for longitudinal dispersion rather than submerge its effect into apparent mass-transfer behavior; and relations have been developed for this purpose.[13, 14, 16]

Our investigation was conducted to measure the longitudinal-dispersion coefficients in pulsed counterflowing liquid-liquid systems (in the absence of actual extraction), so as to provide the numerical parameters needed for both interpretation and design of steady-state extraction operations in pulsed packed beds. Measurements have been made for both the continuous and the dispersed phase, with separate results for the latter in the cases where it does or does not wet the packing material.

B. Interpretation of Experimental Results

The column Péclet number values (P_iB) for each phase can be determined, in the absence of any extraction operation, by use of tracer techniques for unsteady-state flow. A step-input of tracer solution, containing a salt which is soluble only in one phase, was used, and a breakthrough curve was obtained by conductivity measurements.

For the theoretical analysis of experimental breakthrough curves, the random-walk model developed by Einstein[8] and extended by Jacques and Vermeulen,[11] and Cairns and Prausnitz[1] was used. Based on this model, Péclet numbers were obtained by comparing the experimental curve with theoretical ones, or by applying the simple relation

$$N = 4\pi s'^2 - 0.80,$$

where s' is the midpoint slope measured on a t/t_{50} time scale (see Part I).

C. Apparatus and Procedure

1. Columns

Three different columns were used for the investigation: one with ceramic Berl saddles, one with ceramic Raschig rings, and one with carbon rings. The column dimensions are given in Table II-1; the columns are described in more detail in Part I.

2. Conductivity Cells

Conductivity was used to determine the breakthrough curve for the aqueous phase. The conductivity cells, the same as those used for single-phase experiments, were constructed of two spherical sections of 0.75-in. bakelite spheres, connected by a pair of rhodium-plated pins. Water was used for the continuous phase and later for the discontinuous phase, as a measuring medium. The cell readings fluctuated owing to interference of the organic phase in the conducting path; the signal was damped to a 0.5-sec response time, and the remaining fluctuations did not interfere with a straightforward drawing and interpretation of smooth average curves.

Table II-1. Discussions and packing of experimental columns.

Column no.	Packing	d_{eff}	$(d_p)_v$ (in.)	Arrangement	Fraction of voids (%)	Sphericity	Height for continuous-phase runs	Height for dispersed-phase runs	Cross-sectional area ($in.^2$)
7	Ceramic rings	0.75	0.65	Random	64.8	0.42	23.6	23.6	30.7
9	Berl saddles	1.0	0.76	Random	68.6	0.33	25.0	25.0	30.7
12	Carbon rings	0.75	0.72	Random	67.0	0.40	23.6	24.0	30.7

3. Feed Nozzle

Special consideration was given to the nozzle through which the discontinuous phase is introduced. Uniform drop size was desired, in order to achieve uniform drop rise or fall with minimum coalescence of the drops. According to Johnson and Bliss,[12] the injection velocity has to be maintained between 1000 and 1500 ft/hr, and an inlet-hole diameter of 0.10 in. seems to be the optimum. Consequently the distribution nozzle was designed with a set of six removable plates, varying in number of holes (from 37 to 169) to provide the wide range of flow rates required. Five of these had 0.10-in.-diameter holes; the sixth, for high flow-rates, had 0.15-in.-diameter holes to avoid too great a drop in pressure.

4. Liquid-Interface Level Control

Conductivity probes were installed in the lower head and the upper head of the column. Each of those probes operated a magnet-controlled take-off valve, through relay circuits. By use of a set of switches it was possible to maintain the interface at either the upper or the lower end of the column. The on-off magnetic valve was by-passed by a globe valve, which could be adjusted to assure smooth operation of the liquid-level-control system. During actual measurements, careful manual adjustment of the globe valve was usually used to maintain the liquid interface at the desired constant level, in order to avoid the large variation in flow caused by the controller.

5. Piping Arrangement

The organic phase (kerosene) and tracer solution were fed from the storage tanks by means of centrifugal pumps. Water was supplied from a constant-head tank, about 25 ft above the column, under gravity flow. The incoming flows were manifolded and valved so as to meter each of them through the appropriate unit in a bank of seven rotameters. The organic phase was returned to the supply tanks through an overhead line, and the water phase was drained to the sewer.

6. Conductivity Measurements

a. Water as the continuous phase. When steady-state flow was reached for both phases, a solution of sodium nitrate (0.1 N) was

injected in an amount from 0.25 to 2.0 volume-percent of the water stream. The starting time was noted by a pip on the strip-chart recorder. When the breakthrough curve leveled off to a steady-state value, injection was stopped, and a second strip-chart record was taken to measure the purging of the tracer solution. The breakthrough curves recorded were not as smooth as in single-phase experiments because of the interference of droplets of the discontinuous organic phase in the conductance path; these fluctuations were averaged out for the Péclet-number computation.

b. Water discontinuous. For water dispersed, the breakthrough curves were again measured by conductivity. The same steps already outlined were taken to establish steady-state flow in the column, to inject the tracer, and to record the breakthrough curves.

All runs were made at an ambient temperature of 23 ± 2°C. At this temperature, the kerosene used had a viscosity of 2.46 cP and a density of 0.820 g/cc.

7. Holdup Measurements

The holdup in the pulsed column was measured at a small number of discontinuous-phase flow rates, with zero continuous-flow rate. The column was first brought to a steady-flow condition. With the interface at a known level the inlet and outlet valves were closed. When the discontinuous-phase droplets had settled out of the packing, the change of the liquid level was measured. The volume of liquid calculated from this measurement represented the free holdup. The continuous phase was then subjected to gentle pulsation, and again the change of liquid level were measured for the restricted holdup. The sum of the free and restricted holdup was defined as the operational holdup. Permanent holdup was not measured here but should be the same as in unpulsed flow.

8. Flooding or Emulsification Limits

The maximum throughout obtainable in a column is determined by flooding of the column. Flooding occurs if the linear-velocity difference corresponding to the superficial flow rates is greater than the mean drop velocity that the column is capable of developing.

The effect of pulsing on flooding limits in packed columns has been reported on by Callihan.[18] More intense pulsing (higher ωA) will give a lower flooding limit at a low flow rate of the dispersed phase, compared with an unpulsed column, but will give a higher flooding limit at a high flow rate of dispersed phase.

Emulsification is another factor in the flooding behavior of pulsed columns. The liquids in the column assume a white milky appearance, and the two phases in one or both end sections fail to separate completely.

The occurrence of emulsification at high frequency and amplitude is an inherent result of the pulsing, which is designed to decrease the dispersed-phase drop size. The emulsification limit depends upon physical properties of the two phases, and rises with increasing interfacial tension. The highest separation efficiency can be obtained when the column is operated just inside the emulsification limit.

A systematic study of flooding and emulsification limits was not made in our investigation. Any flow rates appreciably above the maximum values reported would have led to flooding. Higher pulsing frequencies than those for which data are reported would generally have produced emulsification. The system water-diisobutyl ketone, having a low interfacial tension (about 23 dyne/cm), could not be operated at the standard frequency (100 min^{-1}) and amplitude (0.35 in.).

D. Results and Discussion

1. Continuous Phase

Experimental results for longitudinal dispersion in the continuous phase are shown in Appendix II-1. These tables report both the packing Péclet number P_c, and the modified Péclet number ϵP_c, which will be used to account for the effect of void space. In each system studied, the modified Péclet number for the continuous phase was found to increase with increasing superficial velocity of the continuous phase, and to decrease with increasing superficial velocity of the dispersed phase.

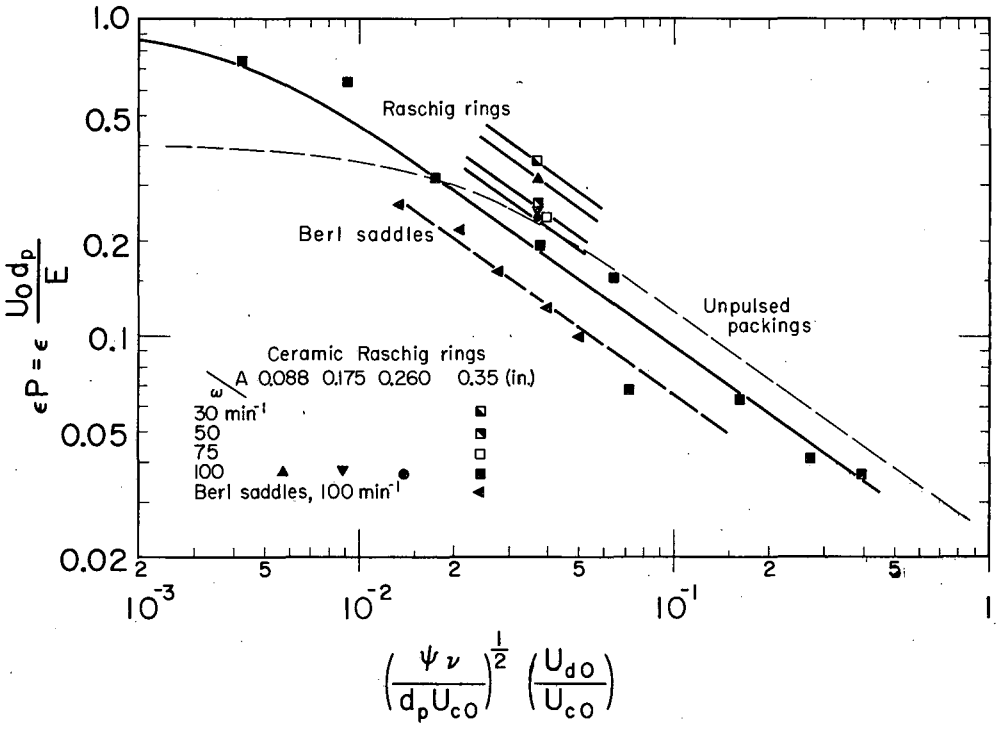

Fig. II-1. Dimensionless correlation for continuous-phase Péclet numbers.

One would also expect the Péclet number to be a function of the type of channels encountered by the flowing fluid. Some measurable variables that affect the channel shapes are the size (d_p), sphericity (ψ), and porosity (ϵ) of the packing material. (The particle sphericity is defined as the ratio A_s/A_p, where A_s is the surface area of a sphere having the same particle volume, and A_p is the surface area of the particle.) The experimental Péclet numbers have been plotted in terms of these variables, with the use of a velocity parameter, $(U_{c0}/U_{c0})\psi^{1/2}(\nu/d_p U_{c0})^{1/2}$, that has been found by Hennico, Jacques, and Vermeulen[10] to apply to unpulsed-column data. Figure II-1 shows ϵP for the continuous phase, plotted against a correlating group in which the ratio of superficial velocities (U_{d0}/U_{c0}) is multiplied by square root of sphericity and divided by square root of continuous-phase Reynolds number. The Péclet number ϵP decreases as the dispersed-phase flow rate increases, and increases as the continuous-phase flow rate increases.

As the product of ωA decreases, the Péclet number increases, so that with low extents of pulsing it becomes higher than the Péclet number without pulsation (shown as a light dotted curve); the value of ϵP is expected to fall back into the latter curve as the ωA product reaches values much smaller than those studied here. The difference between Berl saddles and Raschig rings at the (ω, A) combination studied is larger than the difference without pulsation.

2. Dispersed Phase

The results of a few dispersed-phase measurements are plotted on a semilogarithmic grid in Fig. II-2, as Péclet number vs U_{c0}/U_{d0}; the corresponding numerical values are given in Appendix II-2. Ceramic packings were used for the case where the dispersed phase wets the packing, and carbon Raschig rings were used for the case where the dispersed phase is nonwetting.

When $U_{c0} = 0$, the Péclet number is constant at 1.6 for these packings, unaffected by discontinuous-phase flow rates. However, the Péclet number decreases slightly as the continuous-phase flow

rate increases, possibly due to drag on the dispersed phase by the continuous phase. When the dispersed-phase flow rate is high, this effect becomes smaller, apparently because of frequent coalescence and redispersion of the discontinuous phase. The extent of axial dispersion is greater when the discontinuous phase wets the packing.

Within the range of pulsing conditions used, the Péclet number increases slightly (by an almost negligible amount) as the frequency and amplitude decrease. However, measurements by Hennico[16] in the same column and with the same liquid, without any pulsation, showed substantially lower Péclet-number values, as indicated in Fig. II-2. It was necessary to use different conductivity probes in the pulsed and unpulsed studies, and this may have led to errors in one type of measurement or the other. If the observed difference is real, it may be due to the following factors: (a) Frequent coalescence and redispersion of the discontinuous phase, due to pulsing, tend to reduce the probability of fluid "packets" becoming trapped in the packing voids, thus giving a more even velocity distribution; (b) the pulsing tends to make it easier for the dispersed phase to pass through the packings. At extremely low frequency or amplitude, the Péclet-number value could be expected to approach that for unpulsed columns.

3. Holdup

Direct experimental measurements of holdup in the dispersed phase are given in Appendix II-5. The effect of dispersed-phase flow rate on holdup was investigated only at zero continuous-phase flow, with a fixed pulsing condition. The holdup was found to increase as the discontinuous flow rate increased. The amount of operational holdup in the pulsed column was nearly the same as that of holdup in nonpulsed columns.

Shirotuka, Honda, and Yasumo[15] have measured holdup values in a pulsed column with Raschig-ring packing; they found that the holdup increases as the continuous- and dispersed-phase flow rates increase, and decreases as the pulsing intensity increases.

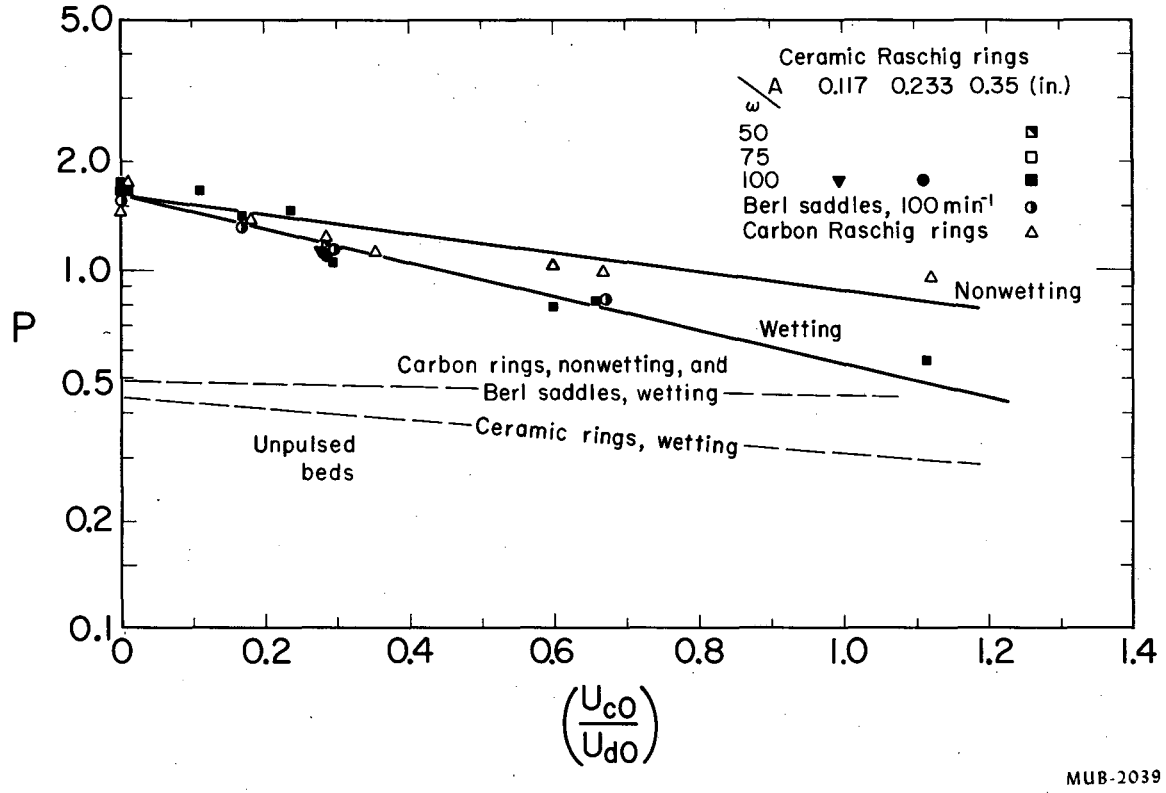

Fig. II-2. Dispersed-phase Péclet numbers.

E. Conclusions

Analysis of the results obtained in this study of two-phase countercurrent flow in pulsed-packed bed leads to the following conclusions:

(a) The axial Péclet number of the continuous phase increases with increasing continuous-phase flow rate, and decreases with increasing discontinuous-phase flow rate. The decrease relative to single-phase behavior may be caused by intermittent entrainment of the continuous phase by droplets of the dispersed phase. The modified Péclet number ϵP is believed to be a function (at given ω and A) of the dimensionless parameter suggested by Hennico, Jacques, and Vermeulen[16] for the nonpulsed column, involving the velocity ratio and the reciprocal square root of Reynolds number, but with the effect of viscosity not yet confirmed quantitatively. The causes of Péclet-number variation, with different packing types and properties, are not yet known.

(b) The axial Péclet number for the discontinuous phase decreases somewhat with decreasing continuous-phase flow rate and increasing discontinuous-phase flow rate. The extent of axial dispersion is greater when the discontinuous phase wets the packing. The Péclet number of the discontinuous phase is much greater than that of the continuous phase.

(c) The axial Péclet number, in the continuous phase, decreases as the degree of pulsing increases. The effect in the discontinuous phase is in the same direction, but almost negligible.

(d) The discontinuous-phase holdup increases with increasing flow rate of that phase, and is of the same range as that in the unpulsed column.

(e) Since the Péclet numbers of the discontinuous phase are much greater than those of the continuous phase, the phase which has greatest concentration change should be dispersed to achieve better efficiency, as a general rule. The viscosity of the dispersed phase remains to be investigated as a contributing variable.

F. Notation for Part II

A	Pulse amplitude, in.
A_s	Surface area of packing particle, ft^2
A_p	Surface area of packing particle, ft^2
B	Dimensionless height, h/d_p
d_p	Particle diameter, in.
F	Volumetric flow rate, gal/min
h	Total height of packed section of column, ft
N	Péclet number for the column, dimensionless
N_{Re}	Reynolds number; $d_p U_{c0}/\nu$, dimensionless
P	Péclet number for the packing, dimensionless
s'	Dimensionless midpoint slope of breakthrough curve (based on t/t_{50} scale)
t	Time, sec
U	Mean intersticial velocity, ft/hr
ϵ	Void fraction or porosity, dimensionless
ν	Kinematic viscosity, cm^2/sec
ψ	Sphericity of the packing (area of a sphere having the particle volume)/(actual area of particle), dimensionless
ω	Pulse frequency, min^{-1}

Subscripts

c	Continuous phase
d	Dispersed phase
i	For the "i" phase; as yet undesignated
0	Superficial

REFERENCES FOR PART II

1. E. J. Cairns and J. M. Prausnitz, Chem. Eng. Sci. 12, 20 (1960).
2. C. D. Calligan, Liquid-Liquid Extraction in a Pulsed Column (Ph. D. Dissertation), Michigan State University, 1957.
3. W. A. Chantry, R. L. Von Berg and H. F. Wiegandt, Ind. Eng. Chem. 47, 1155 (1955).
4. C. M. Christensen, Liquid-Liquid Extraction Efficiencies of a Pulsed Packed Column and a Pulsed Sieve-Plate Column of Four Inch Diameter (Ph. D. Thesis), Cornell University, 1961.
5. A. P. Colburn, Trans. Am. Inst. Chem. Engrs. 29, 174 (1939).
6. A. P. Colburn, Ind. Eng. Chem. 33, 459 (1941).
7. W. Eguchi and S. Nagata, Kagaku Kogaku (Chem. Eng. Japan) 23, 146 (1959).
8. H. A. Einstein, Ph. D. Thesis, Eidg. Techn. Hochschule, Zürich, 1937.
9. G. Feick and H. M. Anderson, Ind. Eng. Chem. 44, 405 (1952).
10. A. Hennico, G. Jacques, and T. Vermeulen, University of California Lawrence Radiation Laboratory Report UCRL-10696, March 1963.
11. G. L. Jacques and T. Vermeulen, University of California Radiation Laboratory Report UCRL-8029, November 1957.
12. H. F. Johnson and H. Bliss, Trans. Am. Inst. Chem. Engrs. 42, 331 (1946).
13. T. Miyauchi and T. Vermeulen, Ind. Eng. Chem. Fundamentals 2, 113 (1963).
14. T. Miyauchi, University of California Radiation Laboratory Report UCRL-3911, August 1957.
15. T. Shirotsuka, N. Honda, and T. Yasumo, Kagaku Kogaku (Chem. Eng., Japan) 21, 645 (1957).
16. C. A. Sleicher, Am. Inst. Chem. Engrs. J. 5, 145 (1959).
17. L. D. Smoot, B. W. Mar, and A. L. Babb, Ind. Eng. Chem. 51, 1005 (1959).
18. J. D. Thornton, Chem. Eng. Progr. Symp. Series 58, No. 13, 39 (1954).
19. R. L. Von Berg and H. F. Wiegandt, Chem. Eng. 59, 189 (1952).

Table II-3. Dispersed-phase Péclet numbers for water dispersed in kerosene.

F_d (gal/min)	U_{d0} (ft/hr)	F_c (gal/min)	U_{c0} (ft/hr)	U_{c0}/U_{d0}	ω (min^{-1})	A (in)	N	P
0.75-in. ceramic Raschig rings								
0.5	18.8	0	0	0	100	0.35	61.1	1.68
		0.15	5.4	0.287	100	0.35	42.2	1.16
		0.33	11.3	0.601	100	0.35	28.2	0.78
		0.562	21.0	1.117	100	0.35	20.4	0.56
0.85	32.0	0	0	0	100	0.35	61.1	1.68
		0.15	5.4	0.169	100	0.35	51.5	1.42
		0.33	11.3	0.292	100	0.35	39.0	1.07
		0.33	11.3	0.292	100	0.23	40.8	1.12
		0.33	11.3	0.292	100	0.12	42.2	1.16
		0.33	11.3	0.292	75	0.35	40.8	1.12
		0.33	11.3	0.292	50	0.35	42.2	1.16
		0.562	21.0	0.656	100	0.35	29.8	0.82
1.3	49.0	0	0	0	100	0.35	63.9	1.76
		0.15	5.4	0.110	100	0.35	60.0	1.65
		0.33	11.3	0.236	100	0.35	53.0	1.46
0.75-in. carbon Raschig rings								
0.5	18.8	0	0	0	100	0.35	53.8	1.64
		1.5	5.4	0.287	100	0.35	39.9	1.22
		0.33	11.3	0.601	100	0.35	34.2	1.04
		0.562	21.1	1.122	100	0.35	31.4	0.96

Table II-3. (Continued)

F_d (gal/min)	U_{d0} (ft/hr)	F_e (gal/min)	U_{c0} (ft/hr)	U_{c0}/U_{d0}	ω (min^{-1})	A (in.)	N	P
0.75-in. carbon Raschig rings								
0.85	32.0	0	0	0	100	0.35	48.4	1.48
		0.15	5.4	0.169	100	0.35	43.2	1.32
		0.33	11.3	0.352	100	0.35	36.4	1.11
		0.562	21.1	0.659	100	0.35	32.6	0.99
1-in. ceramic Berl saddles								
0.85	32	0	0	0	100	0.35	50.9	1.55
		0.15	5.4	0.169	100	0.35	43.8	1.33
		0.33	11.3	0.292	100	0.35	38.1	1.16
		0.561	21.1	0.656	100	0.35	27.1	0.83

Table II-4. Discontinuous-phase holdup: kerosene in water, 1-in. Berl saddles.

F_c (gal/min)	F_d (gal/min)	ω ($min.^{-1}$)	A (in.)	Free holdup (%)	Restricted holdup (%)	Operational holdup (%)
0.0	0.17	100	0.35	1.64	1.4	3.04
0.0	0.33	100	0.35	2.74	1.53	4.27
0.0	0.433	100	0.35	6.1	2.6	8.7
0.0	0.564	100	0.35	9.11	4.13	13.24

APPENDIX II-1

Table II-2. Continuous-phase Péclet numbers for kerosene in water.

F_c (gal/min)	U_{c0} (ft/hr)	F_d (gal/min)	U_{d0} (ft/hr)	U_{d0}/U_{c0}	$\left(\frac{\nu\psi}{d_p U_{c0}}\right)^{1/2}\left(\frac{U_{d0}}{U_{c0}}\right)$	ω (min^{-1})	A (in.)	N_c	P_c	ϵP_c
- - - - - - - - - - - - - - - - - -				0.75-in. Raschig rings						- - - - - - - - - - - - - - - - - -
0.326	12.0	0.150	5.4	0.460	0.073	100	0.35	3.9	1.07	0.07
		0.330	12.4	1.033	0.163	100	0.35	3.6	0.10	0.06
		0.562	21.1	1.730	0.273	100	0.35	2.3	0.06	0.04
		0.825	31.0	2.530	0.400	100	0.35	2.1	0.06	0.04
0.850	32.0	0.150	5.4	0.177	0.017	100	0.35	17.7	0.49	0.32
		0.330	12.4	0.388	0.038	100	0.35	11.0	0.30	0.20
		0.330	12.4	0.388	0.038	100	0.26	13.3	0.37	0.23
		0.330	12.4	0.388	0.038	100	0.18	13.8	0.38	0.25
		0.330	12.4	0.388	0.038	100	0.09	17.9	0.49	0.32
		0.330	12.4	0.388	0.038	75	0.35	13.2	0.36	0.24
		0.330	12.4	0.388	0.038	50	0.35	14.7	0.41	0.26
		0.330	12.4	0.388	0.038	30	0.35	20.1	0.55	0.36
		0.562	21.1	0.661	0.064	100	0.35	8.9	0.25	0.16
2.21	83.0	0.150	5.4	0.068	0.004	100	0.35	41.7	1.15	0.74
		0.330	12.4	0.149	0.009	100	0.35	36.4	1.00	0.65
0.85	32	0.150	5.4	0.169	0.014	100	0.35	12.4	0.38	0.26
		0.240	8.6	0.269	0.021	100	0.35	10.4	0.32	0.22
		0.330	11.3	0.353	0.028	100	0.35	7.6	0.23	0.16
		0.450	16.2	0.506	0.040	100	0.35	5.9	0.18	0.12
		0.562	21.1	0.659	0.053	100	0.35	4.8	0.15	0.10

PART III. CONCENTRATION-PROFILE MEASUREMENTS IN A PULSED PACKED EXTRACTION COLUMN

A. Introduction

In countercurrent solvent-extraction columns the effective coefficient of mass transfer is known to be reduced by longitudinal dispersion (axial mixing) in either liquid phase. Longitudinal dispersion may cause considerable distortion of the internal concentration profile from a piston-flow behavior, and hence reduce the concentration driving force. It is necessary, for reliable design of solvent-extraction columns, to be able to predict this profile and driving force.

An improved value for the mass-transfer coefficient is obtained by measuring the concentration distribution within an extractor, and applying the experimental concentration driving potential in the calculations.[8, 15] This approach should be more accurate than the alternative of using a logarithmic-mean driving force computed only from the end concentrations of the incoming and outgoing streams. But it is important to observe that this method retains the assumption of piston flow in both phases; if longitudinal mixing is extensive, even a graphical integration based on the actual concentration profile will not yield the "true" mass-transfer coefficients.

A diffusional model of the longitudinal-dispersion effect has been applied to two-phase countercurrent extraction by Miyauchi and Vermeulen,[10, 11] and Sleicher[14] as outlined previously in the General Introduction. This model shows a way of obtaining the true mass-transfer coefficient from experimental results. Miyauchi and Vermeulen[11] classified three different kinds of "transfer units," and gave the theoretical relations between them. The true number of transfer units is given as

$$N_{ox} = k_{ox}\, ah/F_x \,. \tag{1}$$

The "measured" number of transfer units has been defined as

$$N_{oxM} = \int_{C_{xo}}^{C_{x1}} \frac{dC_x}{C_x - m\,C_y} \,. \tag{2}$$

The number of transfer units for "piston flow" is defined in terms of the logarithmic-mean driving force:

$$N_{oxP} = \int_{1}^{C_{x1}} \frac{dC_x}{C_x - mC_y} , \qquad (3)$$

where, in this case, C_y is related to C_x by material balance. By use of the Miyauchi model and these definitions it is shown that $N_{ox} \geq N_{oxM} \geq N_{oxP}$.

"True" N_{ox} can be evaluated numerically by use of the relation (4):

$$N_{ox} = \int_{C_{xo}}^{C_{x1}} \frac{-dC_x + \frac{1}{P_x B}(d^2C_x/dz^2)dZ}{C_x - mC_y} , \qquad (4)$$

in which the first part of the integral corresponds to N_{oxM}. The accuracy of this calculation is limited by the difficulty in determining the second-derivative value.

Miyauchi and Vermeulen[11] suggested an approximate method of obtaining "true" N_{ox} from experimental values of N_{oxP} and known Péclet numbers for both phases. This approximation method is much faster than a complete analytical solution and is useful for calculating first trial values of true N_{ox}.

In our investigation, the applicability of this diffusional model to the pulsed packed bed is tested by measuring concentration profiles inside the extraction column and comparing them with the profiles calculated from the Péclet numbers obtained in Part II.

B. Previous Studies

Since 1950 several experimental investigations have been made to determine concentration profiles inside solvent-extraction columns, which provide evidence that longitudinal dispersion occurs.

Geankoplis and co-workers[6,7] did pioneering research in internally sampling the continuous phase in spray extraction columns. They report an end effect of considerable magnitude at the continouos-phase entrance. Later Newman[12] pointed out that this large end effect could be due to longitudinal dispersion.

Gier and Hougen[8] measured both dispersed- and continuous-phase concentration gradients in spray and packed extraction columns; diethyl ether - adipic acid - water was chosen as a system. Large end effects were observed in the experiment, particularly in the continuous phase. In their calculations, H_{oxP} was shown to be greater than H_{oxM}, within experimental accuracy. They suggested that the bulk-mixing effect is an important factor in the design of equipment for heat and mass transfer.

Kreager and Geankoplis,[9] using a spray column, reported that for tall columns $(HTU)_P$ approaches a constant value as the end effect becomes decreasingly important. Vogt and Geankoplis,[16] continuing this study, observed the end effect in a spray column by using a movable sampling tube; investigation of longitudinal dispersion was not their primary object.

Cavers and Ewanchyna[2] sampled both continuous and dispersed phases in a spray column, at several elevations between the spray nozzle at the bottom of the column and the interface at the top, to obtain concentration profiles for each phase. Discontinuity in the concentration profiles was noted at the interface. The discontinuity in the continuous-phase concentration profile was split into two parts, one representing the effect of drop agitation at the interface, and the other the effect of axial mixing in the continuous phase. From the results of runs, they concluded that there is virtually no back-mixing in the discontinuous phase in the spray columns; N_{oxM} was calculated by graphical integration and compared with N_{oxP}.

Eguchi and Nagata,[5] studying a pulsed sieve-plate column, observed large apparent end effects, and attributed these to longitudinal dispersion. The corrected capacity coefficient was therefore calculated on the assumption that longitudinal diffusivity was constant throughout the column.

Barlage[1] studied a pulsed sieve-plate column for liquid-liquid heat transfer. Measurement of the temperature differences at the ends of the column and at several points within the column led to the conclusion that rather large end effects existed.

Claybaugh[3] also investigated the effects of back-mixing on concentration profiles in a pulsed plate column. The experimental concentration profiles were compared with concentration profiles which were calculated from Miyauchi's diffusional model.

Smoot and Babb[14] also utilized a pulsed sieve-plate extraction column. The operation of the column was simulated with a digital computer, using the Miyauchi model for the effects of longitudinal mixing. From the experimental concentration profiles, the true transfer units were computed and compared with the apparent transfer units computed only from the concentrations of the entering and leaving phases. Dimensional analysis was applied to the variables affecting the height of a transfer unit, and an incomplete empirical correlation of HTU was obtained.

Besides the mentioned concentration-profile studies, which are of primary importance to chemical engineers, a few investigations[4, 13] have dealt with concentration profiles inside extraction columns, as a topic of general interest. Thus several previous investigations have provided fairly extensive data relative to spray columns and pulsed sieve-plate columns. However, investigation of packed columns has been very limited, and no study of concentration profiles for pulsed-packed columns has been found in the literature.

C. Experimental Objectives

The measurement of both dispersed- and continuous-phase concentration gradients for countercurrent extraction in a pulsed packed column was undertaken to determine the applicability of the Miyauchi model to steady-state mass transfer, using Péclet numbers obtained from unsteady-state conditions. The variables considered were the flow rates of both phases, the pulse frequency, the amplitude, and the direction of mass transfer.

D. Materials, Apparatus, and Procedure

1. Extraction System Studied

The ternary system selected for these experiments was water - crotonic acid - isododecane. Tap water was used as the aqueous feed. The "isododecane" (IDD) was a 350 to 400°F paraffinic distillate from sulfuric acid alkylate bottoms, supplied through the courtesy of California Research Corporation. Crotonic acid was Eastman Kodak practical grade, with water as the principal impurity. The distribution of crotonic acid between water and isododecane was measured and is shown in Fig. III-I and Table III-1.

2. Column

An aluminum-wall column with random packing and octagonal cross section was used for this investigation. The general specifications of the column, and of all auxiliary equipment, are the same as those in Parts I and II.

3. Sampling Probes

Six holes were drilled along the column wall to provide an entrance for the hypodermic needles (type 19BD) that were used to sample the continuous phase.

Another six holes were drilled along the column length to provide an entrance for the dispersed (organic) phase samplers. A special probe was used, initially designed by Norman Li, as shown in Fig. III-2. A 0.5-in. hole was drilled in a bakelite sphere of 0.75-in. diameter. The sampling tube (0.0625 in. o.d., 0.031 in. i.d.) was extended through the wall of the sphere, and the entire probe was pointed

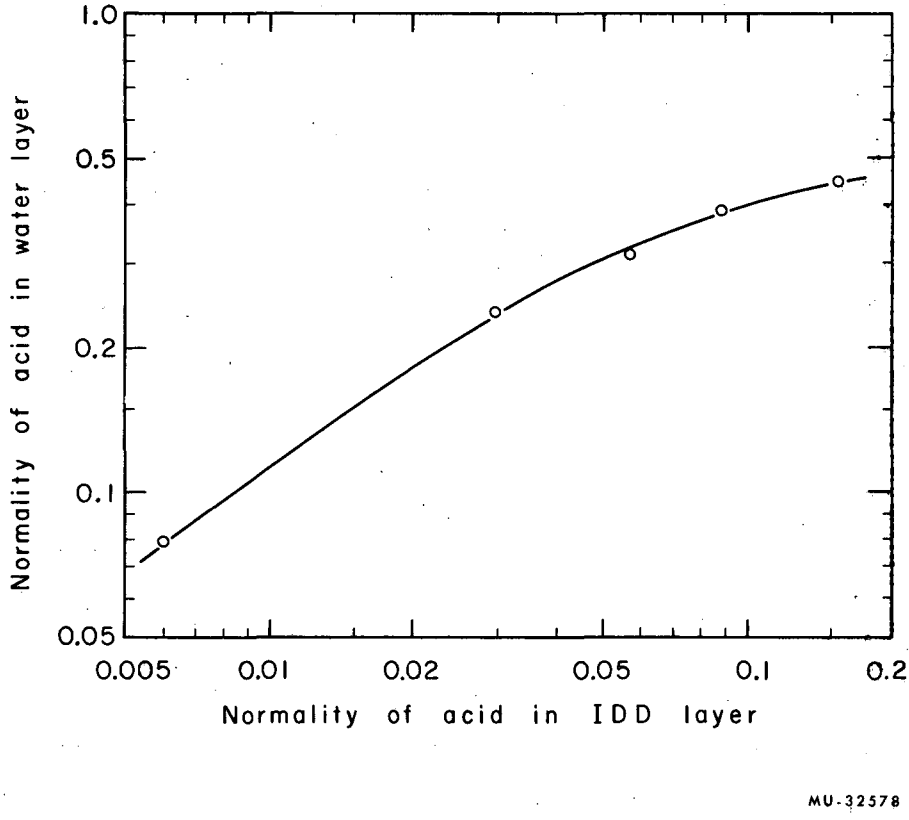

Fig. III-1. Distribution of crotonic acid between water and isododecane.

Table III-1. Distribution data for the system: water - crotonic acid - isododecane.

Normality of crotonic acid in:	
Water layer	Isododecane layer
0.079	0.006
0.240	0.030
0.314	0.057
0.397	0.088
0.441	0.154

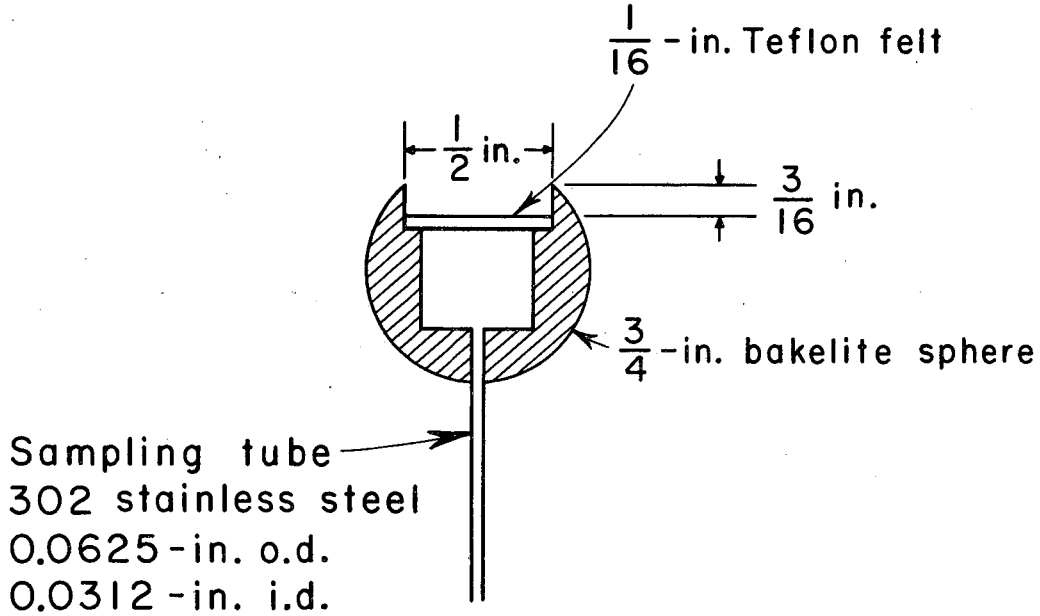

Fig. III-2. Organic-phase sampler.

in the direction that would trap the moving droplets. A disk of Teflon felt (supplied by American Felt Company) of 0.0625-in. thickness was cemented in the mouth of the cylindrical cavity in the sphere to give selective flow of organic phase.

Special care was taken to prevent unwanted blocking of the samplers by packing particles, especially for the dispersed-phase samplers. The intervals between the samplers were varied; those at the entrance of each phase were more closely spaced to give a more accurate observation of the expected concentration discontinuity. One hole was made in each column head, to obtain samples (one continuous-phase, one discontinuous-phase) outside the packed section. Locations of the probes are given in Table III-2, and shown diagrammatically in Fig. III-3; both types passed through the wall along the same vertical line, although for clarity they are shown on opposite sides of the column. The samplers were connected to individual collecting flasks by polyethylene tubes; flow was controlled by pinch clamps.

In a majority of the cases, the probes used gave 100% purity of the desired phase. Organic-phase samples with aqueous contamination were corrected according to the method of Gier and Hougen;[8] those of less than 70% purity were discarded. The purity of the dispersed-phase samples was somewhat dependent upon the dispersed-phase flow rate.

4. Start-Up

At the beginning of a run the continuous phase (water) was allowed to fill the column, and the desired amplitude and pulsing frequency were set. Then dispersed phase (organic phase, presaturated with water) was introduced. After column operation had reached steady state, samples of the two phases were collected in 50-ml Erlenmeyer flasks. It has been reported that steady state is reached in such columns after sufficient feed has been introduced to change the contents of the column two to three times.[7] For most of our runs, a still longer time was allowed to reach a steady state, as verified in several runs by repeated sampling.

Table III-2. Column details. (Wall material: aluminum alloy, type 6061-T4, 0.188-in. thickness; height: 26.75 in.; cross section: octagonal; cross-sectional area: 30.7 in.^{2}; packing: 0.75-in. ceramic Raschig rings.)[a]

Continuous-phase samplers			Dispersed-phase samplers		
No.	Height (in.)	Z[b] (%)	No.	Height (in.)	Z[b] (%)
1	0.5	1.9	1	1	3.7
2	6.75	25.3	2	4	15.0
3	14.75	54.8	3	7	26.2
4	18.75	70.1	4	13	48.6
5	21.75	81.3	5	19	71.0
6	24.25	90.7	6	23.5	87.9

[a]Sampler location measured from bottom of packed section.

[b]Fractional height.

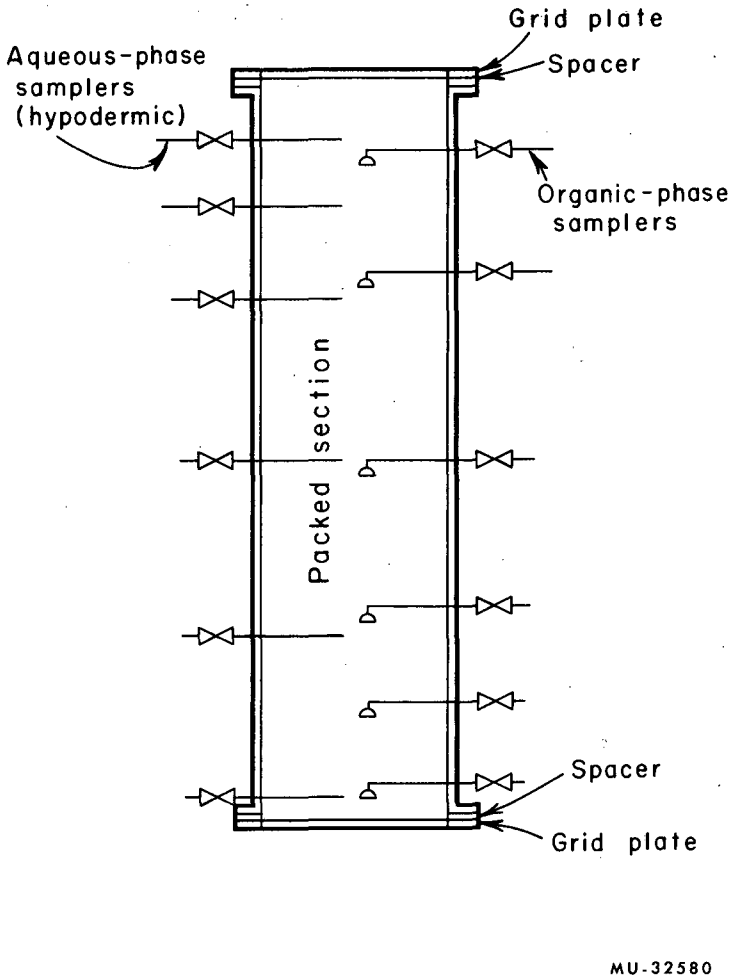

Fig. III-3. Column sampling locations.

The sampling rate was less than 1% of the total flow rate. Geankoplis[7] found this rate to have little effect on the column operation. The initial portion of each sample was discarded, owing to hold-up of the previous sample in the sampling tube; then the current sample was collected. Outlet-stream samples for both phases were also taken. Experimental measurements were made only at times when the interface was held constant, following close adjustment of the outlet flow rates.

5. Method of Analysis

The amount of acid in each of the samples, subsequent to addition of distilled water, was determined by titration with 0.1 N and 0.01 N standard sodium hydroxide solution, with 0.05% phenolphthalein as indicator.

6. Calculation of Data

The experimental concentration profiles were matched by theoretical profiles calculated on an IBM 7090 from the experimentally determined exit concentrations, using the Péclet numbers of the two phases as determined in Part II.

As a first-trial value, N_{ox} was estimated by the rapid-calculation method of Miyauchi and Vermeulen,[11] with $P_x B$, $P_y B$, Λ, and X_1 as input values, with the weighting factors initially estimated from N_{oxP}. Successive iterations on N_{ox} were used to bring the absolute value of $[(N_{ox})_j - (N_{ox})_{j+1}]/(N_{ox})_{j+1}$ to less than 0.02.

With the trial N_{ox} obtained in this way, X_1 was computed by the exact Miyauchi equation.[10,11] If $\left|(X_1)_{calc} - (X_1)_{exptl}\right| / (X_1)_{exptl}$ was greater than 0.01, a new N_{ox} was determined, utilizing the N_{oxP} value that corresponded to this trial:

$$(N_{oxP})_{trial} = \frac{1}{1 - \Lambda} \ln \left\{ \frac{\Lambda[(X_1)_{calc} - 1] + 1}{(X_1)_{calc}} \right\} . \qquad (5)$$

From this $(N_{oxP})_{trial}$ and $(N_{ox})_{trial}$, a new N_{ox} was estimated:

$$\frac{1}{(N_{ox})_{new}} = \frac{1}{(N_{ox})_{trial}} + \frac{1}{(N_{oxP})_{exptl}} - \frac{1}{(N_{oxP})_{trial}} . \qquad (6)$$

Then $(N_{ox})_{new}$ was used to compute X_1. This process was repeated until the $(X_1)_{calc}$ matched $(X_1)_{exptl}$ within 1%. The Fortran program for this entire calculation is given in Appendix III-1.

To obtain a value of $\left| (N_{ox})_j - (N_{ox})_{j+1} \right| / (N_{ox})_j$ less than 0.02, fewer than four iterations were needed in most cases. At no time in our investigation were more than eight iterations needed. To make $(X_1)_{calc}$ approach $(X_1)_{exptl}$, only one or two cycles were needed in all cases. The time required for the IBM 7090 to calculate a final concentration profile by this method was under 10 sec.

E. Results and Discussion

1. Experimental Results

The experimental conditions of five extraction runs are shown in Table III-3, which reports continuous- and dispersed-phase flow rates, extraction factors, pulse frequency and amplitude, and direction of mass transfer. The steady-state profiles for those runs are shown in Figs. III-4 to III-8, as dimensionless concentration X and Y vs Z (fractional height).

2. Comparison with Theoretical Profiles

The long-dash curves in Figs. III-4 to III-8 show the concentration profiles computed by the procedure just described, using experimental Péclet-number values from unsteady-state measurements. In all cases the experimental results for the continuous-phase concentration profiles fit these theoretical profiles relatively well. Near the entrance end for the continuous phase, the experimental concentrations tend to be slightly lower than the calculated ones; this tendency may be due to inadequency of the diffusion model but the disagreement is not serious.

The dispersed-phase concentrations determined experimentally do not coincide as well with the calculated (long-dash) curves as in the case of the continuous phase. The experimental values are generally higher than calculated values, especially at the inlet end for the dispersed phase.

Table III-3. Experimental conditions and results.

Run no.	1	2	3	4	5	6	7	8
F_c (gal/min)	0.244	0.244	0.244	0.244	0.244	0.244	0.244	0.261
U_{c0} (ft/hr)	9.18	9.18	9.18	9.18	9.18	9.18	9.18	9.84
F_d (gal/min)	0.580	0.580	1.100	0.580	0.580	0.58	0.58	1.71
U_{d0} (ft/hr)	21.8	21.8	41.4	21.8	21.8	21.8	21.8	64.4
Λ	1.35	0.58	1.10	0.58	0.58	1.35	0.705	0.49
ω (min^{-1})	100	100	100	50	100	0	0	0
A (in.)	0.35	0.35	0.35	0.35	0.175	0	0	0
Feed phase	Water	IDD[a]	IDD	IDD	IDD	Water	IDD	Water
P_x	0.047	1.15	1.25	1.23	1.23	0.064	0.50	0.025
P_y	1.15	0.047	0.044	0.067	0.061	0.50	0.064	0.50
N_{oxP}	0.91	1.41	0.63	0.80	1.19	0.35	0.47	1.02
N_{ox}	1.30	2.0	0.79	0.93	1.55	0.40	0.54	1.54
H_{oxP} (in.)[b]	34.0	21.6	48.90	38.40	25.80	76.50[c]	57.20[c]	26.50[c]
H_{ox} (in.)[b]	23.7	15.4	38.90	33.00	19.80	66.50[c]	50.75[c]	17.20[c]

[a] IDD = "isododecane"; this phase dispersed in all runs.

[b] Calculated for an effective height of 30.75 in. except where noted.

[c] Effective height is 26.75 in.

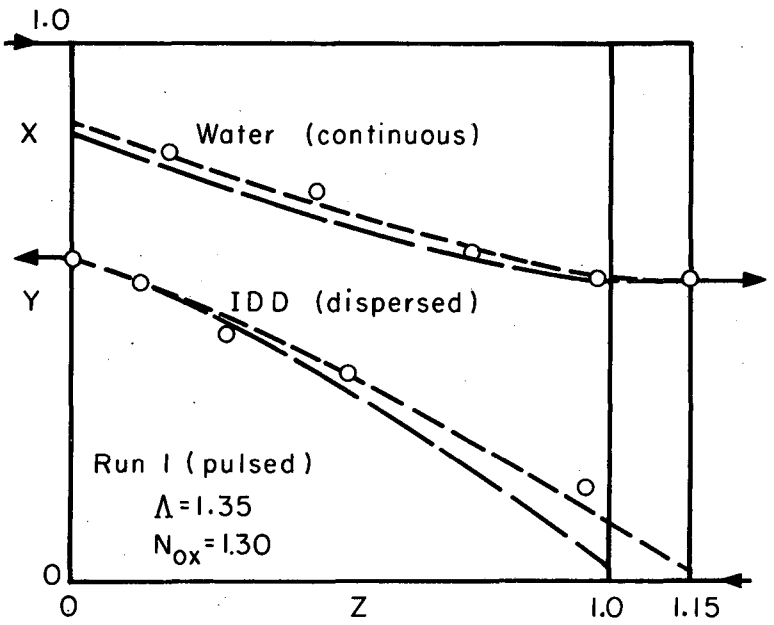

Fig. III-4. Experimental concentrations and theoretical concentration profile: Run 1.

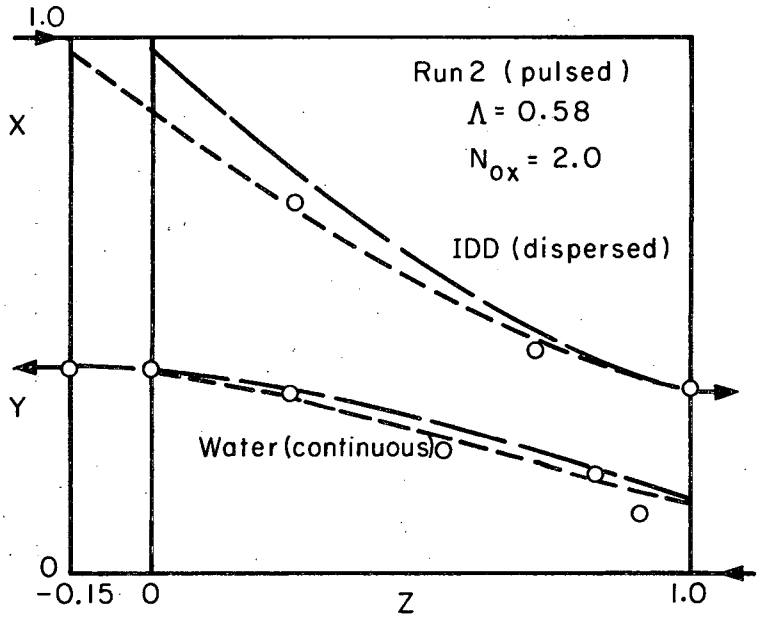

Fig. III-5. Experimental concentrations and theoretical concentration profile: Run 2.

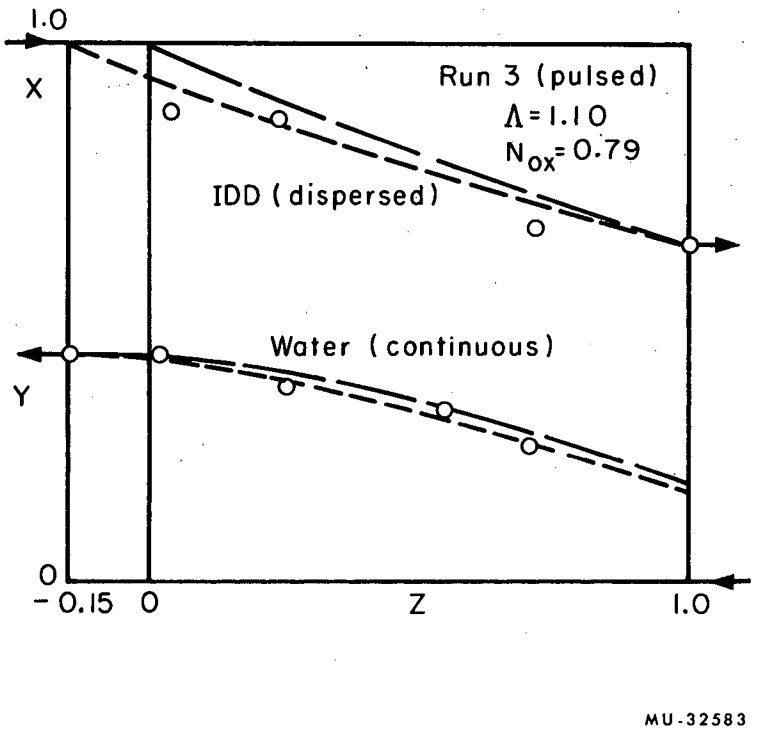

Fig. III-6. Experimental concentrations and theoretical concentration profile: Run 3.

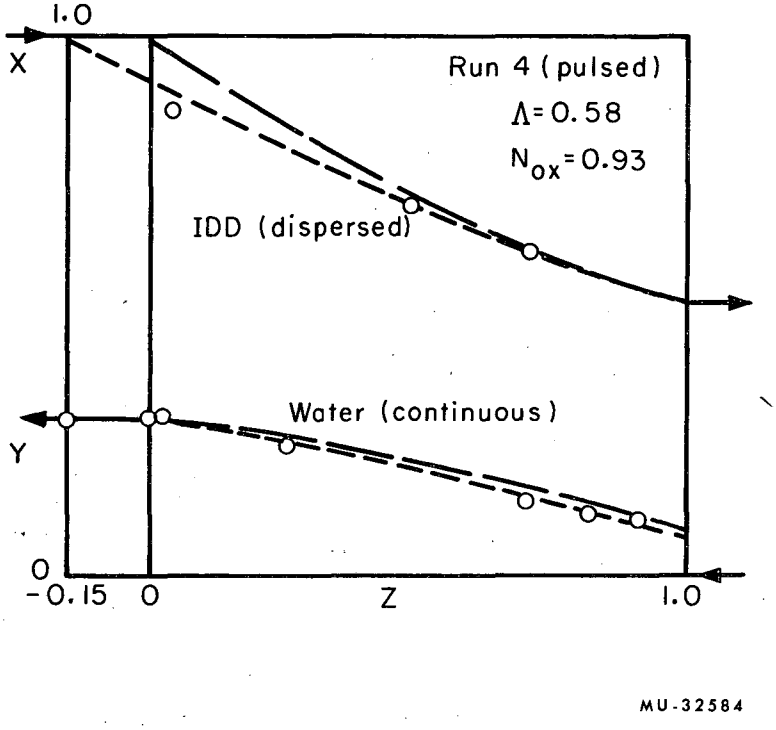

Fig. III-7. Experimental concentrations and theoretical concentration profile: Run 4.

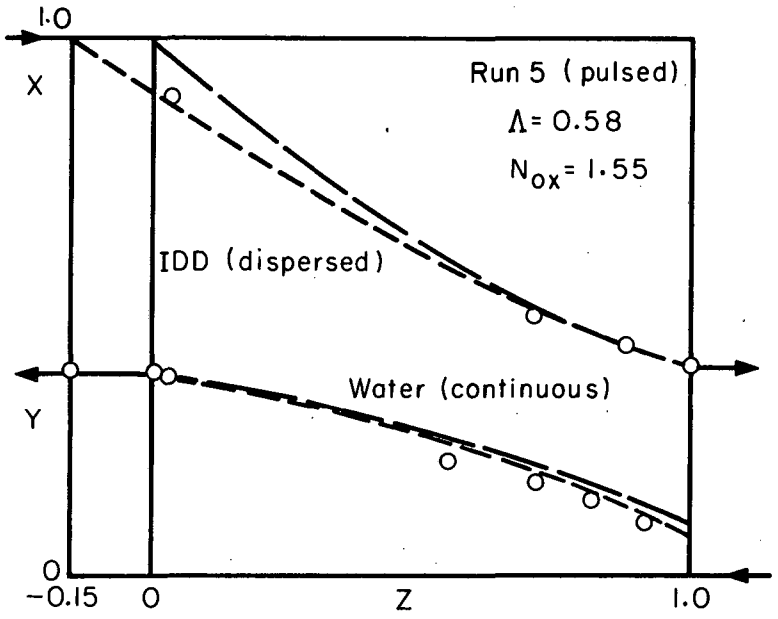

Fig. III-8. Experimental concentrations and theoretical concentration profile: Run 5.

A possible explanation of this behavior for the dispersed phase is as follows: The dispersed phase was fed in from the bottom, the pulse distribution being located 1.5-in. above the bottom feed nozzle. Hence the pulsation may have produced considerable mixing below the packed section, which would cause the observed end effect. It seems likely that a small amount of mass transfer also occurred outside of the packed section, due to this mixing.

Ideally the column should be calculated as two separate columns in series, one representing the dispersed-phase inlet-end section and the other the packing section. The extent of axial dispersion in the end section, for each phase, has not been measured by unsteady-state behavior; and the experimental concentration profiles do not give much information on the end section. Therefore the end section was treated as if it were an extension of the packings, with the assumption that N_{ox} and B would increase in the same proportion relative to the packed section. Trial calculations indicated that an increase in B of about 15% would provide a satisfactory fit for the end-section behavior. The profiles computed on this basis are shown as dotted-line curves in Figs. III-4 to III-8, and the corresponding values of N_{ox}, H_{ox}, and H_{oxP} (based on an effective packed height of $1.15 \times 26.75 = 30.76$ in.) are given in Table III-3.

3. Effect of Pulsing on H_{ox}

Runs 6 to 8, made without pulsing and reported in more detail in Part V, are included in Table III-3 for comparison.

As expected for both pulsed and unpulsed runs, the tabulated values of H_{oxP} are each greater than for H_{ox}. In the pulsed runs, for the same continuous and dispersed flow rates, the mass-transfer coefficient is greater when the acid is transferred from the dispersed phase to the continuous phase. For the same continuous-phase flow rate, H_{od} increases as U_d increases. Comparing Runs 2 and 4, a greater frequency gives a higher mass-transfer coefficient. In the case of Runs 2 and 5, a greater amplitude also gives lower H_{ox}.

With ωA constant, the increase in frequency gives a much higher mass-transfer coefficient than the increase in amplitude.

Comparison of Runs 6 to 8 with the rest of the runs shows that pulsing generally gives a higher mass-transfer coefficient. Run 1 gives about 2.8 times higher separation efficiency than Run 6; the separation efficiency of Run 2 is also 2.3 times higher than Run 7. These results are in general agreement with those reported for other types of pulse column. The increased efficiency is due to higher N_{ox}, and also, somewhat, to higher P_x and P_y.

F. Conclusions

Concentration profiles inside the pulsed packed bed during solvent extraction have been measured and compared with theoretical profiles. This work shows that:

(a) The one-dimensional diffusion model discussed in the General Introduction adequately represents the behavior of fluids in pulsed packed-bed extraction columns. With appropriate Péclet numbers for both phases, this model should be very useful for the more accurate and economical design of pulsed packed-bed solvent-extraction columns.

(b) The Péclet numbers determined by the unsteady-state tracer-injection method appear to represent closely the longitudinal-mixing behavior of two phases during countercurrent extraction in a pulsed packed bed.

(c) The rapid-calculation method and the iteration method used here have proved to be very useful for theoretical analysis of the experimental results.

(d) The true HTU (H_{ox}) decreases as the pulse frequency and amplitude increase. Doubling the frequency gives a greater reduction in H_{ox} than doubling the amplitude. Pulsed columns give uniformly higher mass-transfer coefficients than unpulsed columns. It is noteworthy that the Péclet numbers were also higher for pulsed columns, under the experimental conditions actually used.

G. Notation for Part III

a	Interfacial area per unit column volume, ft^2/ft^3
A	Pulse amplitude, in.
B	Dimensionless height, h/d_p
C	Dimensionless concentration, c/c_x^0
c	Concentration, gram-moles/cm^3
F	Volumetric flow rate, gal/min
H_{ox}	Overall height of transfer unit, relative to X phase, in.
h	Total height of packed section of column, in.
k_{ox}	Overall mass-transfer coefficient, relative to X phase, cm/sec
m	Partition ratio; c_x/c_y at equilibrium, dimensionless
N_{ox}	Overall number of transfer units, relative to X phase, dimensionless
P	Péclet number for the packing; N_{Pe}, dimensionless
q	Intercept on linear equilibrium plot of c_x vs c_y, when the equilibrium equation is $c_x = q + mc_y$; gram-moles/cm^3
Q	q/c_x^0, dimensionless
U	Mean intersticial velocity, ft/hr
X	Generalized solute concentration in X phase, $[C_x - (Q + mC_y^0)]/[1-(Q + mC_y^0]$, dimensionless
Y	Generalized solute concentration in Y phase, $m(C_y-C_y^0)/[1-(Q + mC_y^0]$, dimensionless
Z	Dimensionless height, z/h
z	Height within column, in.
Λ	Extraction factor; mU_{x0}/U_{y0}, dimensionless
ω	Pulse frequency, min^{-1}

Superscripts

0	Feed end of column, outside the column
1	Solvent-entering end of column, outside the column

Subscripts

c	Continuous phase
d	Dispersed phase
i	For the "i" phase; as yet undesignated
o	Overall
0	Superficial
P	Exterior apparent value, conforming to piston-flow model
x	For the X phase
y	For the Y phase
0	Feed end of column, inside the column
1	Solvent-entering end of column, inside the column

REFERENCES FOR PART III

1. W. B. Barlage, Jr., Dissertation Abstr. 20, 4353 (1960).
2. S. D. Cavers and J. E. Ewancyna, Can. J. Chem. Eng. 35, 113 (1957).
3. B. E. Claybaugh, Effects of Backmixing on Concentration Profiles in Pulsed Column (Ph. D. Thesis), Oklahoma State University, August 1961.
4. J. Durandet, D. Defives, and B. Choffé, in Proceedings of the Second United Nations International Conference on the Peaceful Uses of Atomic Energy (United Nations, Geneva, 1958), Vol. 17, p. 181.
5. W. Eguchi and S. Nagata, Kagaku Kogaku (Chem. Eng., Japan) 23, 146 (1959).
6. C. J. Geankoplis and A. W. Hixson, Ind. Eng. Chem. 42, 1141 (1950).
7. C. J. Geankoplis, P. J. Wells, and E. L. Hawks, Ind. Eng. Chem. 43, 1848 (1951).
8. T. E. Gier and J. O. Hougen, Ind. Eng. Chem. 45, 1362 (1953).
9. R. M. Kreager and C. J. Geankoplis, Ind. Chem. Eng. 45, 2156 (1953).
10. T. Miyauchi, University of California Radiation Laboratory Report UCRL-3911, August 1957.
11. T. Miyauchi and T. Vermeulen, Ind. Eng. Chem. Fundamentals 2, 113 (1963).
12. M. L. Newman, Ind. Eng. Chem. 44, 2457 (1952).
13. B. G. Ryle, Chem. Engr. Prog. 53, 551 (1957).
14. C. A. Sleicher, Am. Inst. Chem. Engrs. J. 5, 145 (1959).
15. L. D. Smoot and A. L. Babb, Ind. Eng. Chem. 1, 2 (1962).
16. H. J. Vogt and C. J. Geankoplis, Ind. Eng. Chem. 46, 1763 (1954).

APPENDIX III-I

```
      DIMENSION Z(7), X(7), Y(7)
      READ 200,(Z(I),I=1,7)
  200 FORMAT (7F5.4)
      PRINT 500
  500 FORMAT (1H1,19HPYB AND PXB FINITE.)
  400 READ 300,(FLAMDA,  XA,  PXB, PYB)
  300 FORMAT(4F10.5)
      FNOXP=(1.0/(1.0-FLAMDA))*LOGF((FLAMDA*(XA-1.0)+1.0)/XA)
      FNOX=FNOXP*1.05
      J=0
   24 FX=(FNOX+6.8/(FLAMDA**0.5))/(FNOX+6.8/(FLAMDA**1.5))
      J=J+1
      FY=(FNOX+6.8/(FLAMDA**0.5))/(FNOX+6.8*(FLAMDA**0.5))
      PBY=1.0/((FLAMDA/FX*PXB)+1.0/(FY*PYB))
      PHY=1.0-0.05/((FLAMDA**0.5)*(PBY**0.25)*(FNOX**0.5))
      FNOXD=(LOGF(FLAMDA)/(FLAMDA-1.0))*PHY+PBY
      FNOXA=(FNOXD*FNOXP)/(FNOXD-FNOXP)
      IF(ABSF((FNOXA-FNOX)/FNOXA)-0.02) 22,22,23
   23 FNOX=FNOXA
      IF (J-10) 24,400,400
   22 FNOX=FNOXA
      K=0
   44 ALF=(PXB-PYB)/3.0
      BET=(FNOX*PXB)+(PXB*PYB)+(FLAMDA*PYB*FNOX)
      GAM=(1.0-FLAMDA)*PYB*PXB*FNOX
      PEA=(ALF**2   )+(BET/3.0)
      QUE=(ALF**3   )+(ALF*BET/2.0)+(GAM/2.0)
      RAR=SQRTF(PEA)
      IF (QUE) 12,11,12
   11 UWE=1.5707963
      SES=0.
      GO TO 8
   12 SES=QUE/(RAR*PEA)
      TEA=(SQRTF(1.0-(SES**2   )))/SES
      UWE=ATANF(TEA)
      IF (SES) 31, 8, 8
   31 UWE=UWE+3.14159
   31 UWE=UWE+3.14159
    8 RARAR=RAR+RAR
      UA=UWE/3.0
      UB=UA+2.0943951
      UC=UB+2.0943951
      FLAMB=ALF+(RARAR*(COSF(UA)))
      FLAMC=ALF+(RARAR*(COSF(UB)))
      FLAMD=ALF+(RARAR*(COSF(UC)))
   13 AHB=(FLAMB/FNOX)*(1.0-(FLAMB/PXB))+1.0
      AHC=(FLAMC/FNOX)*(1.0-(FLAMC/PXB))+1.0
      AHD=(FLAMD/FNOX)*(1.0-(FLAMD/PXB))+1.0
      IF (ABSF(FLAMB)-70.0) 3, 400,400
    3 IF (ABSF(FLAMC)-70.0) 4, 400,400
    4 IF (ABSF(FLAMD)-70.0) 5, 400,400
    5 ELAMB=EXPF(FLAMB)
      ELAMC=EXPF(FLAMC)
      ELAMD=EXPF(FLAMD)
      AA=ELAMB*FLAMB*((((-FLAMC/PXB)+1.0)*FLAMD*AHD)+(((FLAMD/PXB)-1.0)*
     1FLAMC*AHC))
      AB=ELAMC*FLAMC*((((-FLAMD/PXB)+1.0)*FLAMB*AHB)+(((FLAMB/PXB)-1.0)*
     2FLAMD*AHD))
```

```
      AC=ELAMD*FLAMD*((((-FLAMB/PXB)+1.0)*FLAMC*AHC)+(((FLAMC/PXB)-1.0)*
     3FLAMB*AHB))
      DETO=AA+AB+AC
      BA=((((FLAMD/PYB)+1.0)*AHD*FLAMC)-(((FLAMC/PYB)+1.0)*AHC*FLAMD))*A
     1HB*FLAMB/ELAMB
      BB=((((FLAMB/PYB)+1.0)*AHB*FLAMD)-(((FLAMD/PYB)+1.0)*AHD*FLAMB))*A
     2HC*FLAMC/ELAMC
      BC=((((FLAMC/PYB)+1.0)*AHC*FLAMB)-(((FLAMB/PYB)+1.0)*AHB*FLAMC))*A
     3HD*FLAMD/ELAMD
      DETA=ELAMB*ELAMC*ELAMD*(BA+BB+BC)
      DETB=FLAMC*FLAMD*((AHD*ELAMC)-(AHC*ELAMD))
      DETC=FLAMB*FLAMD*((AHB*ELAMD)-(AHD*ELAMB))
      DETD=FLAMB*FLAMC*((AHC*ELAMB)-(AHB*ELAMC))
      DEN=DETA-DETO
      DO 100 I=1,7
      ZEE=Z(I)
      EFZB=EXPF(FLAMB*ZEE)
      EFZC=EXPF(FLAMC*ZEE)
      EFZD=EXPF(FLAMD*ZEE)
      X(I)=(DETA+(DETB*EFZB)+(DETC*EFZC)+(DETD*EFZD))/DEN
  100 Y(I)=(DETA+(AHB*DETB*EFZB)+(AHC*DETC*EFZC)+(AHD*DETD*EFZD))/DEN
      IF (ABSF((XA-X(7))/XA)-0.01) 41, 41, 43
   43 PRINT 301, (X(7))
  301 FORMAT (5H0X7 =F5.4)
      PRINT 302, (FNOX)
  302 FORMAT (6HONOX =F6.4)
      FNOXPA=(1.0/(1.0-FLAMDA))*LOGF((FLAMDA*(X(7)-1.0)+1.0)/X(7))
      FNOXD=(FNOX*FNOXPA)/(FNOX-FNOXPA)
      FNOX=(FNOXD*FNOXP)/(FNOXD-FNOXP)
      K=K+1
      PRINT 310, (K)
  310 FORMAT(4HOK =I3)
      IF (K-5) 44, 44, 41
   41 PRINT 501,((Z(I),I=1,7),(Z(I),I=1,7),FLAMDA,FNOX,PXB,PYB,(X(I),I=1
     1,7),(Y(I),I=1,7))
      PRINT 530, (J)
      PRINT 502,(FNOXP,FNOX)
      PRINT 540, (UWE)
      GO TO 400
  502 FORMAT (1H0,2F8.5)
  530 FORMAT(4H0J =I3)
  540 FORMAT (4H0U =F6.4)
  501 FORMAT(1H0,1X,6HLAMBDA,2X,3HNOX,4X,3HPXB,4X,3HPYB,1HX,1X,F4.2,6F6.
     12,1HY,1X,F4.2,6F6.2/1X,4F7.3,1X,F5.4,1X,F5.4,1X,F5.4,1X,F5.4,1X,F5
     1.4,1X,F5.4,1X,F5.4,1X,F5.4,1X,F5.4,1X,F5.4,1X,F5.4,1X,F5.4,1X,F5.4
     2,1X,F5.4)
      END
```

PART IV. LONGITUDINAL DISPERSION IN UNPULSED PACKED COLUMNS

A. Introduction

Recently many investigators have studied the nature and magnitude of longitudinal dispersion in packed beds, in both single-phase and two-phase flow. Studies reported in the literature include single-phase measurements;[1, 2, 4, 5, 6, 8, 11] gas-liquid two-phase;[3, 9, 10, 13] and liquid-liquid two-phase.[5, 6, 7]

This part of our investigation, dealing with unpulsed columns, is a continuation of work by Hennico, Jacques, and Vermeulen.[5]

1. Single-Phase Flow

Hennico, Jacques, and Vermeulen,[5] from a comparison of their data on the liquid phase with experimental results obtained by McHenry and Wilhelm[8] for the gas phase, proposed to explain the difference between gas and liquid Péclet numbers by transverse molecular diffusion in the packing void spaces. They suggested that at low Reynolds number, when "Taylor diffusion" controls the dispersion behavior, the Péclet number is inversely proportional to the Reynolds number:

$$\epsilon P = \frac{K_1}{N_{Sc}[N_{Re}/(1-\epsilon)]}$$

Also, at very low Reynolds number, when axial molecular diffusion is controlling, the Péclet number decreases proportionally to Reynolds number:

$$\epsilon P = K_2 N_{Sc}[N_{Re}/(1-\epsilon)] \ .$$

The K's are constants that depend on the porosity of the packing and on the velocity profile of the fluid.

Several investigators[4, 5, 8] have shown that constant Péclet numbers occur for both turbulent and laminar flow of liquids through packed beds, with the turbulent-flow value higher by a factor of about 4. To match liquid and gas behavior in the laminar region, it was expected that if the Reynolds number is decreased to a sufficiently low

value the Péclet number would begin to rise in the manner shown in Eq. (1). Also, upon further reduction, it was expected that Péclet number should level off at the void-cell-mixing value, and later fall again as shown in Eq. (2) as the Reynolds number decreased still further.

It was our purpose to obtain Péclet numbers at a low Reynolds number, to investigate the proposed theory and hence to find the Reynolds-number range (if any) in which radial molecular diffusion is predominant.

2. Two-Phase Flow

Few investigations have been made of Péclet numbers for immiscible fluids flowing countercurrently through a packed bed; as a result, in order to work toward a generalized correlation for Péclet numbers based on liquid properties, it was necessary to make measurements on liquid systems other than those already studied.

In our investigation, Péclet numbers for both phases were obtained for the diisobutyl ketone - water system; these Péclet numbers are used later (in Part V) to calculate theoretical concentration profiles from the Miyauchi model discussed in Part III.

B. Apparatus and Procedure

1. Columns

Two columns of the design shown in Fig. I-5 were used for our investigation: one for the low-Reynolds-number regime of single-phase flow, the other for two-phase flow.

To obtain low Reynolds number while maintaining relatively small liquid-phase Schmidt number, glass beads 0.0058 in. in diameter ("Superbrite," Minnesota Mining and Manufacturing Company) were packed in a cylindrical column 6.25 in. in diameter and 26.4 in. high, fitted with 200-mesh stainless steel screens at each end between the grid plate and the packing. The column body used was that of Column 7 in Table I-1, with a circular cross section. Water was used as the flowing liquid. Two conductivity probes were put in the column, one located 23.5 in. and the other 19 in. from the injection level.

The other column used for the two-phase investigation was packed with 0.75-in. ceramic Raschig rings. This was the same column body employed in measuring Péclet numbers of both phases in Part II (see Table II-1, Column 7).

2. Conductivity Cells

The conductivity of an aqueous phase, downstream from the point where a tracer solution was injected, was used to determine the breakthrough behavior for the aqueous phase.

For single-phase experiments and two-phase studies with water continuous, the conductivity cells were the same as those used in Parts I and II.

When the aqueous phase was dispersed, two different conductivity cells were used: the one just mentioned, and one used by Dunn[3] and by Hennico[5] in related studies. A cross-sectional drawing of the cell used is shown in Fig. IV-1. The conducting discontinuous phase enters the sampler through the funnel-shaped top, and leaves through the port in the side. In our runs the probe was installed immediately under the grid plate that supports the packing. The conductance of the solution between the pins was determined by the electronic equipment described in Part I.

3. System Studied

A water - diisobutyl ketone system was used for this investigation. Tap water was used as the aqueous phase. Diisobutyl ketone (DIBK) was of commercial U. S. P. grade supplied in 55-gal drums, and was saturated with water prior to use.

4. Procedure

For single-phase measurements, practically the same procedure as described in Part I was used. In this case the conductivity probe was less sensitive, due to the presence of glass beads between the two pins of the probe; a high recorder sensitivity was used to compensate for this effect. For the two-phase measurement, the procedure described in Part II was used. The random-walk model, explained in Part I, was used to interpret the breakthrough curves.

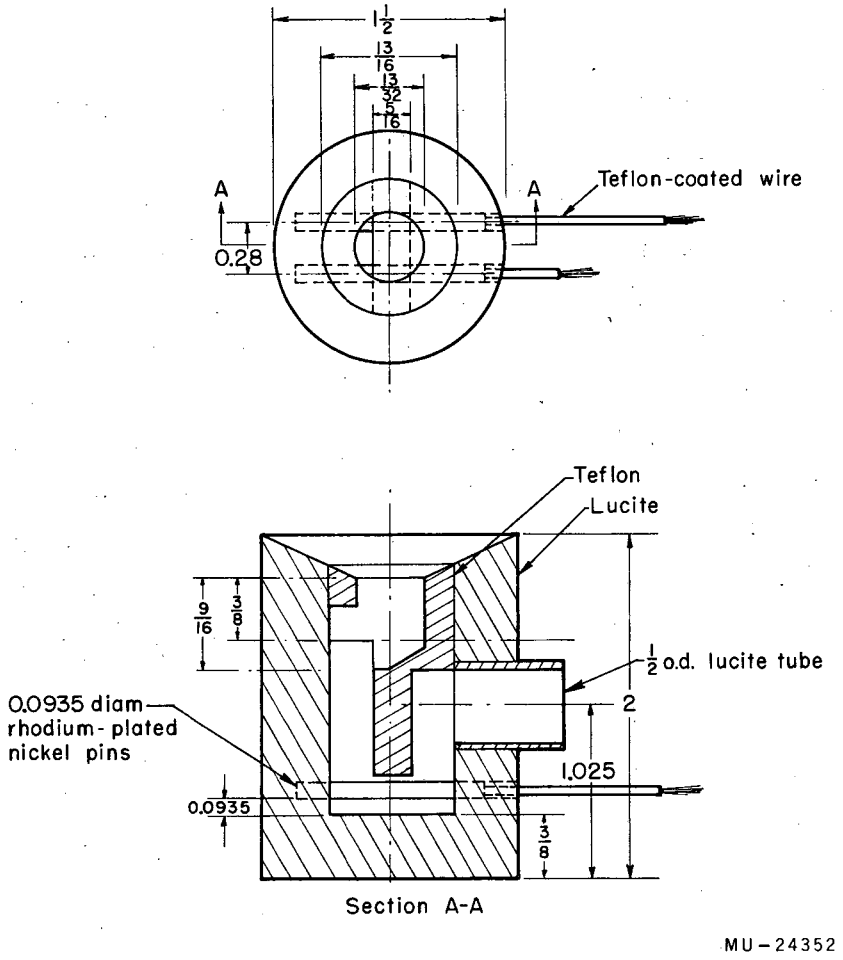

Fig. IV-1. Cross-sectional drawing of a liquid-conductivity cell.

C. Results and Discussion

1. Single-Phase Flow

The experimental results of this study are shown in Appendix IV-1. Data were obtained in the Reynolds-number range of 0.4 to 0.04. Results are shown in Fig. IV-2, along with the results obtained by Hennico.[5] In the range of Reynolds numbers investigated in this study, the modified Péclet numbers remained constant at 0.205 ± 0.020, and the predicted rise in Péclet numbers did not occur down to the lowest Reynolds number (0.04) studied in this investigation. The observed constancy of P for the liquid phase at low Reynolds number appears to indicate that the transverse (radial) contribution to Taylor diffusion is not as great for a liquid as for a gas, at comparable Schmidt numbers; this result may be due to channeling in the fine packing.

2. Continuous Phase in a Two-Phase System

The results of measurements on longitudinal dispersion in the continuous phase, for the system water (continuous) - diisobutyl ketone (dispersed) are shown in Appendix IV-2. The results were plotted on the coordinates used by Hennico, Jacques, and Vermeulen[5] in Fig. IV-3, and were found to agree well with the results of investigators using water - kerosene as the system for study. The physical properties of kerosene and diisobutyl ketone are shown in Appendix IV-4. From this comparison, we can assume tentatively that no physical properties of the dispersed phase, other than density, affect the continuous-phase Péclet number. The effect of density difference, which is directly responsible for the velocity of dispersed-phase droplets, could not be analyzed because of the similar densities of kerosene and diisobutyl ketone.

3. Dispersed Phase

In this study only the case where the dispersed phase wets the packing was studied. The results of this study are shown in Appendix IV-3. Péclet numbers were plotted against (U_{c0}/U_{d0}) on semilogarithmic scales in Fig. IV-4, for comparison with values reported by Hennico et al.

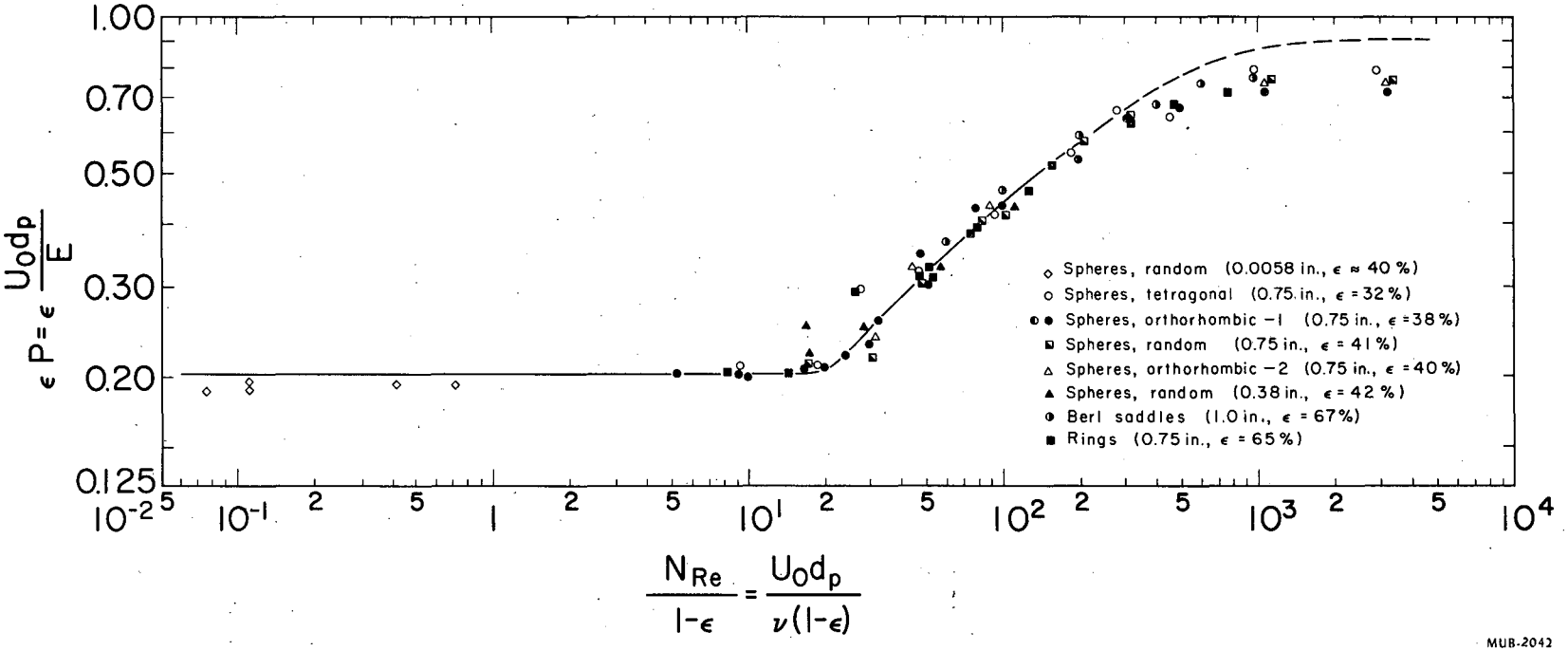

Fig. IV-2. Single-phase Péclet number.

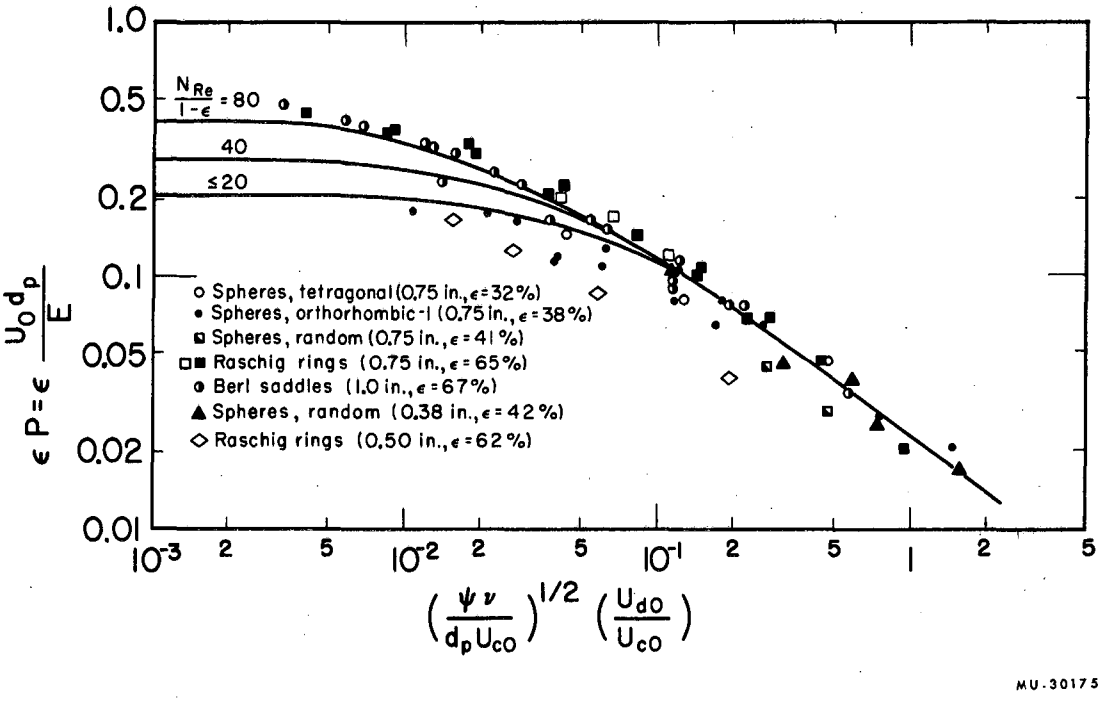

Fig. IV-3. Continuous-phase Péclet number.

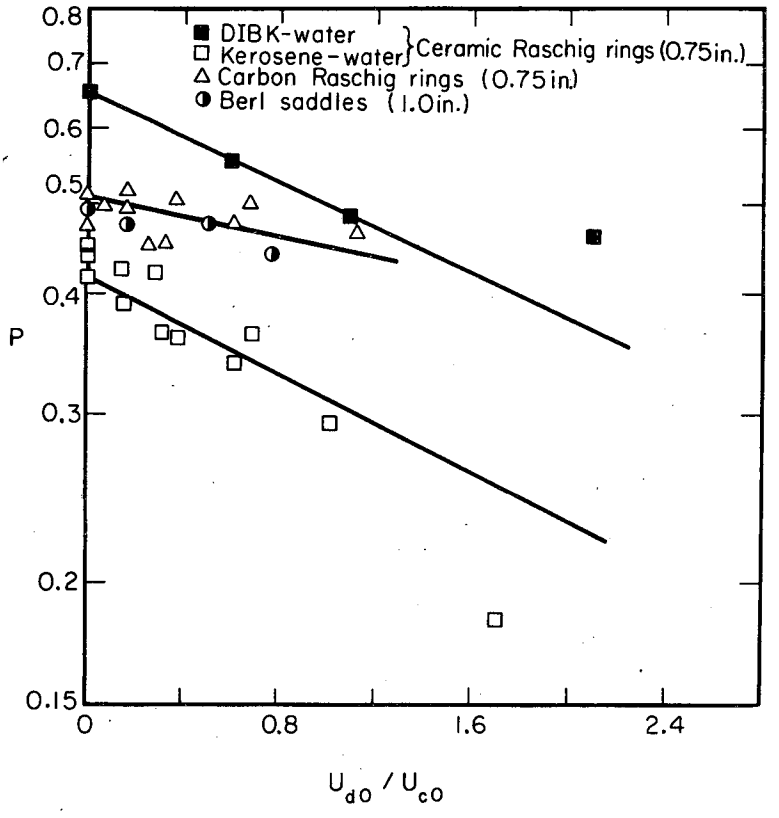

Fig. IV-4. Dispersed-phase Péclet number.

The system water - diisobutyl ketone gives higher Péclet numbers than water - kerosene at the same value of U_{d0}/U_{c0}. This may be due to a larger holdup of dispersed phase, resulting from a smaller drop size (proportional to the square root of the interfacial tension). The product of Péclet number with the square root of the dimensionless group $(\sigma/d_p^2 \Delta\rho g)$, which appears to be a measure of drop size, is plotted against U_{d0}/U_{c0} in Fig. IV-5, and is seen to bring the DIBK and kerosene curves together.

D. Conclusions

Analysis of the results obtained in this study leads to the following conclusions:

(a) The rise in Péclet number at low Reynolds numbers, anticipated by Hennico et al., does not occur, down to Reynolds numbers as low as 0.04.

(b) The continuous-phase Péclet number is not affected by changes in physical properties of the dispersed phase; however, the effect of dispersed-phase density and viscosity changes was not studied.

(c) The Péclet number of the dispersed phase decreases as the continuous-phase flow rate increases, at constant dispersed-phase flow rate.

(d) Higher dispersed-phase Péclet numbers were obtained for the system diisobutyl ketone - water than for kerosene - water. This result is believed due to a decreased average size of the dispersed-phase drops.

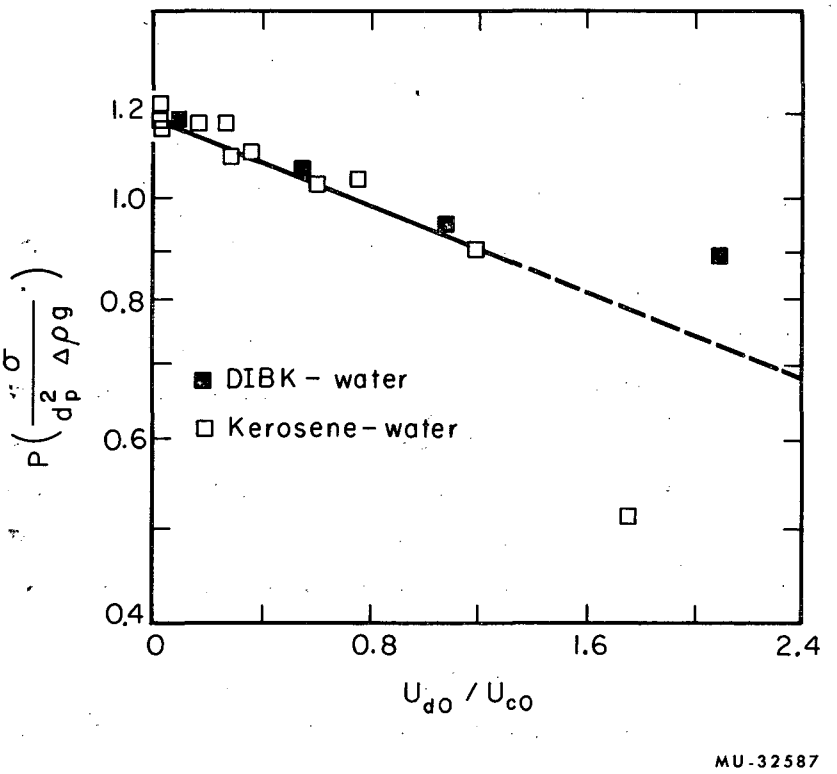

Fig. IV-5. Dispersed-phase Péclet number for ceramic Raschig rings.

E. Notation for Part IV

D	Molecular diffusivity, cm^2/sec
N_{Re}	Reynold number, dimensionless
N_{Sc}	Schmidt number, ν/D, dimensionless
P	Péclet number for packing, dimensionless
U	Mean interstitial velocity, ft/hr
ϵ	Porosity, dimensionless
ν	Kinematic viscosity, cm^2/sec
ψ	Sphericity, dimensionless
σ	Interfacial tension, dyne/cm
ρ	Density, g/cm^3
g	Gravitational acceleration, cm/sec^2

Subscripts

c	Continuous phase
d	Dispersed phase
0	Superficial

REFERENCES FOR PART IV

1. E. J. Cairns and J. M. Prausnitz, Chem. Eng. Sci. 12, 20 (1960).
2. J. J. Carberry and R. H. Bretton, Am. Inst. Chem. Engrs. J. 4, 367 (1958).
3. W. E. Dunn, T. Vermeulen, C. R. Wilke, and T. T. Word, Lawrence Radiation Laboratory Report UCRL-10394, August 1962.
4. E. A. Ebach and R. R. White, Am. Inst. Chem. Engrs. J. 4, 161 (1958).
5. A. Hennico, G. Jacques, and T. Vermeulen, Lawrence Radiation Laboratory Report UCRL-10696, March 1963.
6. G. L. Jacques, and T. Vermeulen, University of California Radiation Laboratory Report UCRL-8029, November 1957.
7. G. L. Jacques, J. E. Cotter, and T. Vermeulen, Lawrence Radiation Laboratory Report UCRL-8658, April 1959.
8. K. W. McHenry and R. H. Wilhelm, Am. Inst. Chem. Engrs. J. 3, 83 (1957).
9. T. Otake and E. Kunugita, Kagaku Kogaku (Chem. Eng., Japan) 22, 144 (1958).
10. A. Stemerding, in Proceedings of the Second European Symposium on Chemical Reaction Engineering, Chem. Eng. Sci. 14, 209 (1961).
11. D. A. Strang and C. J. Geankoplis, Ind. Eng. Chem. 50, 1305 (1958).
12. T. Vermeulen, N. N. Li, J. S. Moon, and T. Miyauchi, paper presented at A. I. Ch. E. Meeting, New Orleans, March 1961.
13. Tracy T. Word, Longitudinal Dispersion in Packed Gas-Absorption Columns, Lawrence Radiation Laboratory Report UCRL-9844, September 1961.

APPENDIX IV-1

Table IV-1. Single-phase Péclet numbers. (0.0058-in. spheres; random arrangement; porosity 40%; single phase, water.)

Flow rate (gal/min)	N_{Re}	$N_{Re}/1-\epsilon$	Slope	N	P	P'
0.65	0.408	0.680	12.5	1961.7	0.485	0.194[a]
0.45	0.233	0.388	12.5	1961.7	0.485	0.194[a]
0.15	0.111	0.185	11.1	1546.7	0.472	0.189[b]
0.15	0.111	0.185	12.5	1961.7	0.485	0.194[a]
0.075	0.0406	0.0679	11.1	1546.7	0.472	0.189[b]

[a] Probe position = 23.5 in.

[b] Probe position = 19.0 in.

Table IV-2. Continuous-phase Péclet numbers for diisobutyl ketone in water (0.75-in. Raschig rings).

F_c (gal/min)	U_{c0} (ft/hr)	F_d (gal/min)	U_{d0} (ft/hr)	$U_{d0}/U_{c0}\left(\frac{\nu\psi}{d_p U_{c0}}\right)^{1/2}\frac{U_{d0}}{U_{c0}}$	N_c	P_c	ϵP_c
0.84	31.6	0.95	35.7	1.13	0.1092	7.3	0.200	0.130
		0.56	21.1	0.668	0.0645	10.6	0.287	0.187
		0.30	14.6	0.462	0.0446	11.3	0.311	0.202

Table IV-3. Dispersed-phase Péclet numbers for water dispersed in diisobutyl ketone.

F_d (gal/min)	U_{d0} (ft/hr)	F_c (gal/min)	U_{c0} (ft/hr)	$\frac{U_{c0}}{U_{d0}}$	N	P	$P\left(\frac{\sigma}{d_p^2 \Delta \rho g}\right)^{1/2}$
0.515	19.4	1.077	40.5	2.09	17.0	0.461	0.0896
		0.557	20.9	1.08	18.0	0.488	0.0946
		0.296	11.1	0.572	20.4	0.553	0.1072
		0.0	0.0	0.0	24.1	0.653	0.127

Table IV-4. Physical properties of kerosene and diisobutyl ketone.

	Density at 20°C (g/cc)	Viscosity at 20°C (cP)	Interfacial tension with water (dynes /cm)
Diisobutyl ketone	0.806	0.93	23.0
Kerosene	0.802	2.4	43.6

PART V. CONCENTRATION-PROFILE MEASUREMENTS IN AN UNPULSED PACKED EXTRACTION COLUMN

A. Introduction

The applicability of the diffusion model to packed beds in liquid-liquid extraction is tested in this study by measuring the concentration profiles inside a Raschig-ring-packed extraction column, and comparing them to the concentration profiles calculated from the Péclet numbers obtained in Part IV.

B. Materials, Apparatus, and Procedure

1. Extraction Systems Studied

The ternary systems studied in this experiment were water - acetic acid - diisobutylketone and water - crotonic acid - isododecane. Tap water was used for the aqueous phase. The diisobutyl ketone (DIBK) used in this experiment was of commercial U. S. P. grade, supplied in 55-gal drums. The "isododecane" used was a 350 to 400° F distillate fraction from alkylation bottoms, supplied for research use by California Research Corporation.

Acetic acid (glacial) of U. S. P. quality was obtained from General Chemical Division. The crotonic acid was practical grade, from Eastman Kodak Company.

The distribution of acetic acid between water and DIBK is shown in Fig. V-1. A distribution curve for the other system (water - crotonic acid - isododecane) has been given in Part III.

2. Apparatus and Procedure

The equipment employed was as described in Part III, but with the pulsing system not in operation. Both continuous- and dispersed-phase concentration profiles were measured.

C. Experimental Results

The conditions used for eight experimental runs, on the two systems just described, are shown in Table V-1. These extraction runs were made for both directions of solute transfer. The experimental concentration profiles are compared with calculated profiles

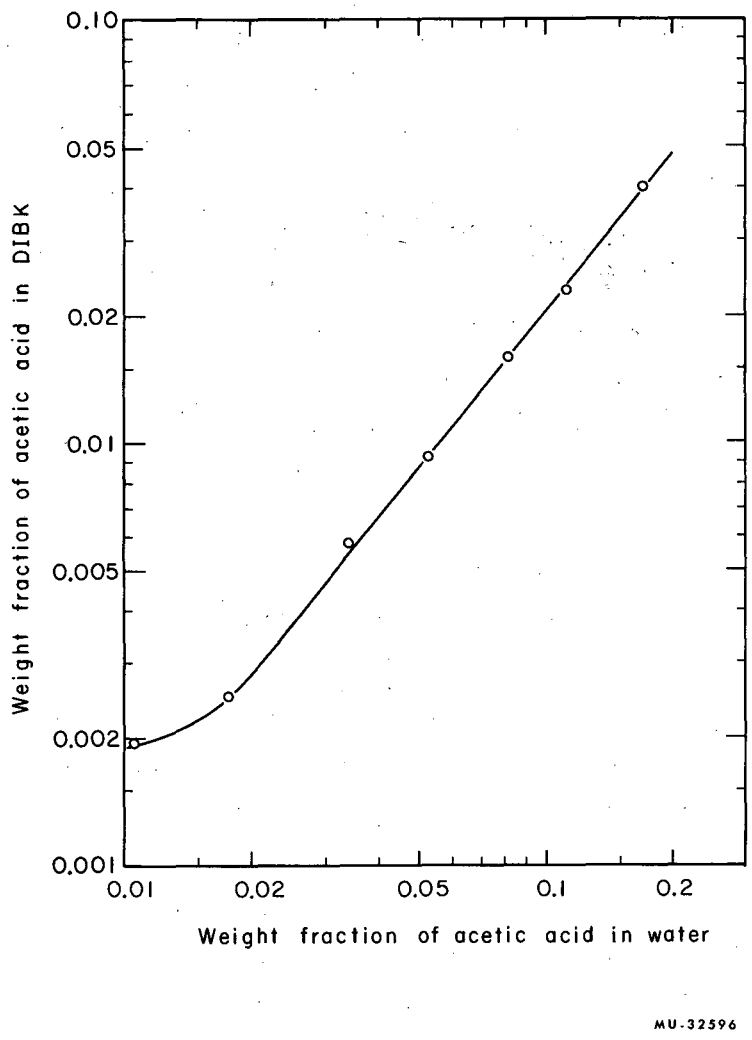

Fig. V-1. Distribution of acetic acid between water and diisobutyl ketone.

in Figs. V-2 through V-9; the theoretical profiles were calculated on an IBM 7090, using the Fortran program given in Part III.

1. Mass Transfer from Aqueous to Organic Phase

Runs were made with the solute transferring away from the aqueous phase. The experimental concentration profiles were found to agree reasonably well with the theoretical ones. The relatively small disagreement may be due to limitations in the theoretical model, or to inaccuracies in sampling.

2. Mass Transfer from Organic to Aqueous Phase

Runs 7, 9, 10, and 11 were made with the solute transferring away from the organic phase. Here the experimental results do not coincide so well with the calculated values (shown as solid curves in Figs. V-6 through V-9). The calculated values are always below the experimental curves for the dispersed phase, and always above for the continuous phase. Since the experimental outlet-end concentrations for the continuous phase do not lie on a continuation of the concentration profiles inside the packed section, it appears that mass transfer is occurring in the end section of the column (possibly at the dispersed-phase inlet nozzle). Thus it becomes necessary to interpret the experimental results as a combination of mass transfer in one end region (or both) and in the main column, where longitudinal dispersion also occurs.

In our study, a graphical extrapolation of the concentration profiles to the ends of the packed section was found to yield an adjusted continuous-phase inlet concentration and a consistent dispersed-phase outlet concentration for the packing. These extrapolated values defined the extent of the end effect, which was assumed to occur under piston-flow conditions. New theoretical concentration profiles were then calculated, which fit closely to the experimental profiles, as indicated by the dashed curve in Figs. V-6 to V-9. The values of N_{ox} calculated without, and with, allowance for end effect are given in Table V-1, along with values of N_e (end-section NTU), H_{oxP}, and H_{ox} for the end-effect basis. The average amount of mass transfer taking place

Table V-1. Experimental conditions and results.

Run no.	6	7	8	9	10	11	12	13
Solute acid	Crotonic	Crotonic	Crotonic	Acetic	Acetic	Acetic	Acetic	Acetic
F_c(gal/min)	0.244	0.244	0.261	0.263	0.310	0.244	0.244	0.244
U_{c0}(ft/hr)	9.2	9.2	9.8	9.9	11.7	9.2	9.2	9.2
F_d(gal/min)	0.58	0.58	1.71	2.03	0.85	1.24	1.46	9.80
U_{d0}(ft/hr)	21.8	21.8	64.4	76.5	31.9	46.7	55.1	37.0
Λ	1.35	0.71	0.49	1.20	1.42	0.78	1.08	0.68
Feed phase	Water	IDD	Water	DIBK	DIBK	DIBK	Water	Water
Solvent	IDD	Water	IDD	Water	Water	Water	DIBK	DIBK
P_xB	2.67	20.6	1.11	26.8	26.8	26.8	1.27	1.79
P_yB	20.6	2.67	20.6	1.15	3.05	1.59	26.8	26.8
N_{oxP}[a]	—	0.61	—	0.91	1.26	0.846	—	—
N_{ox}[a]	—	0.71	—	1.62	1.55	1.15	—	—
N_e	—	0.14	—	0.154	0.13	0.06	—	—
N_{oxP}	0.35	0.47	1.02	0.76	1.13	0.75	0.62	0.54
N_{ox}	0.40	0.54	1.54	1.22	1.35	1.00	0.84	0.70
H_{oxP}(in.)	76.5	57.2	26.5	35.2	23.7	35.5	42.6	49.2
H_{ox}(in.)	66.5	50.8	17.2	21.9	19.7	26.8	31.7	38.3

[a] Without allowing for end effect.

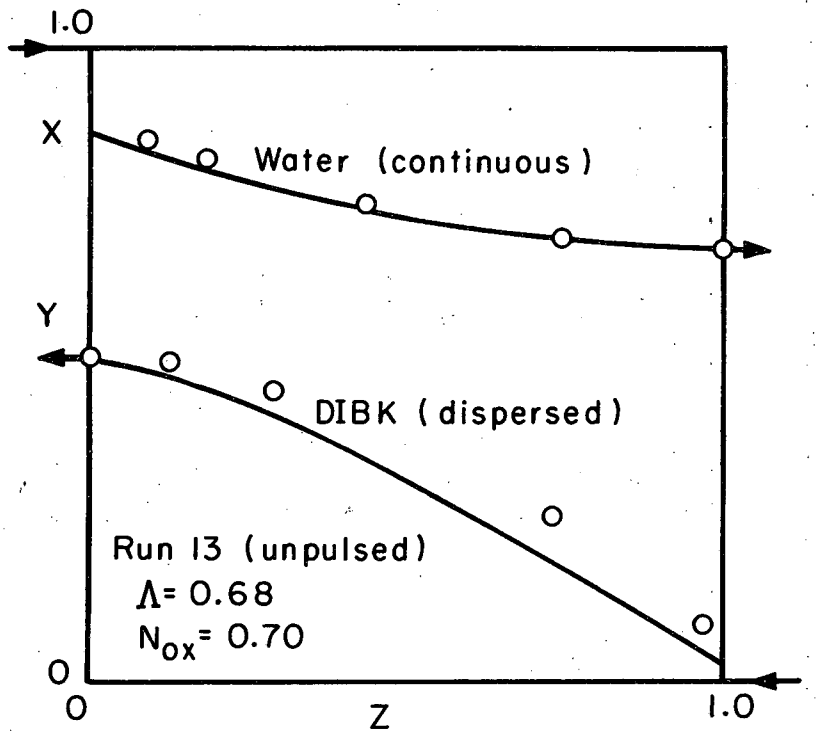

Fig. V-2. Experimental concentrations vs theoretical concentration profile: Run 13.

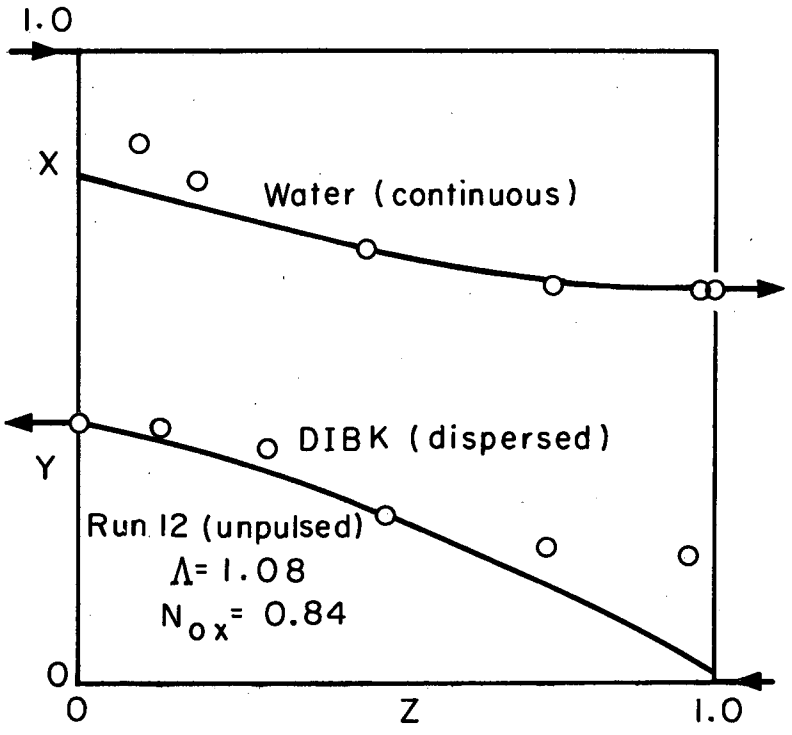

Fig. V-3. Experimental concentrations vs theoretical concentration profile: Run 12.

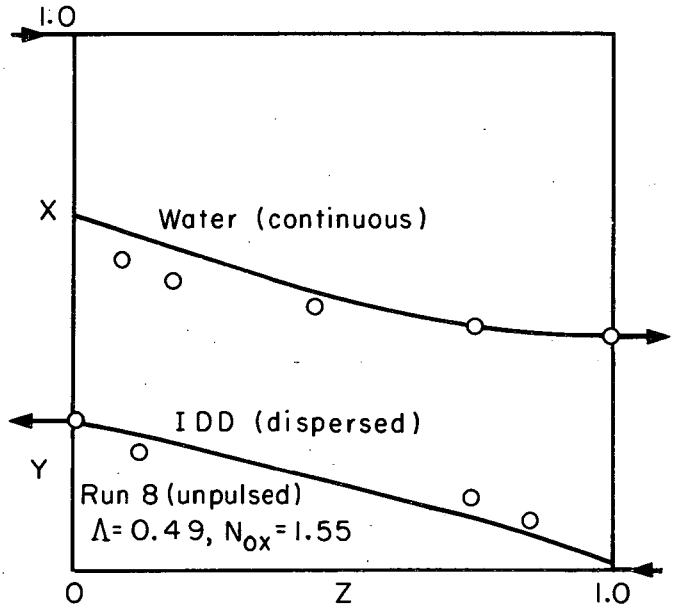

Fig. V-4. Experimental concentrations vs theoretical concentration profile: Run 8.

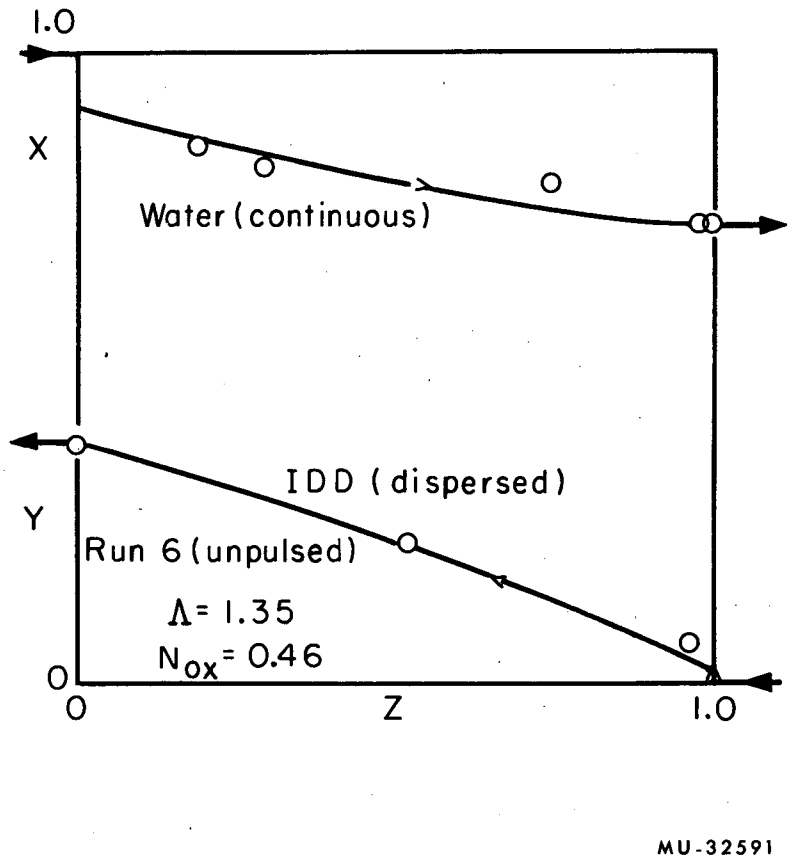

Fig. V-5. Experimental concentrations vs theoretical concentration profile: Run 6.

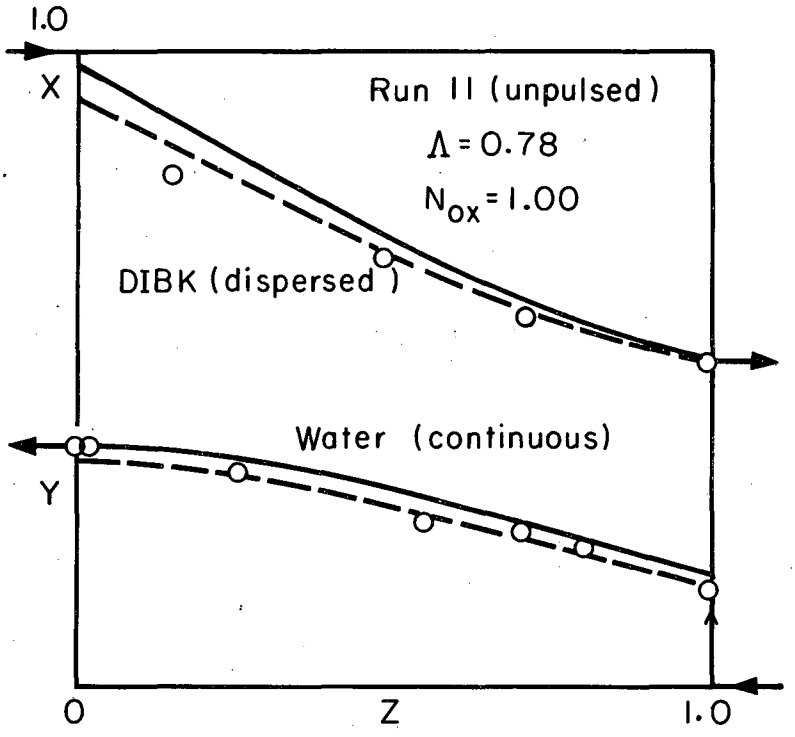

Fig. V-6. Experimental concentrations vs theoretical concentration profile: Run 11.

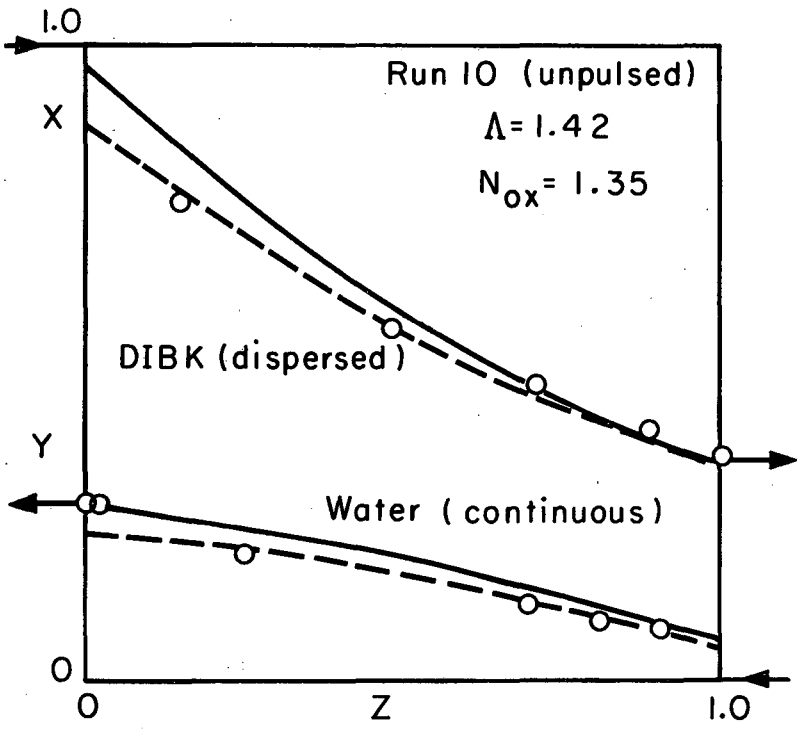

Fig. V-7. Experimental concentrations vs theoretical concentration profile: Run 10.

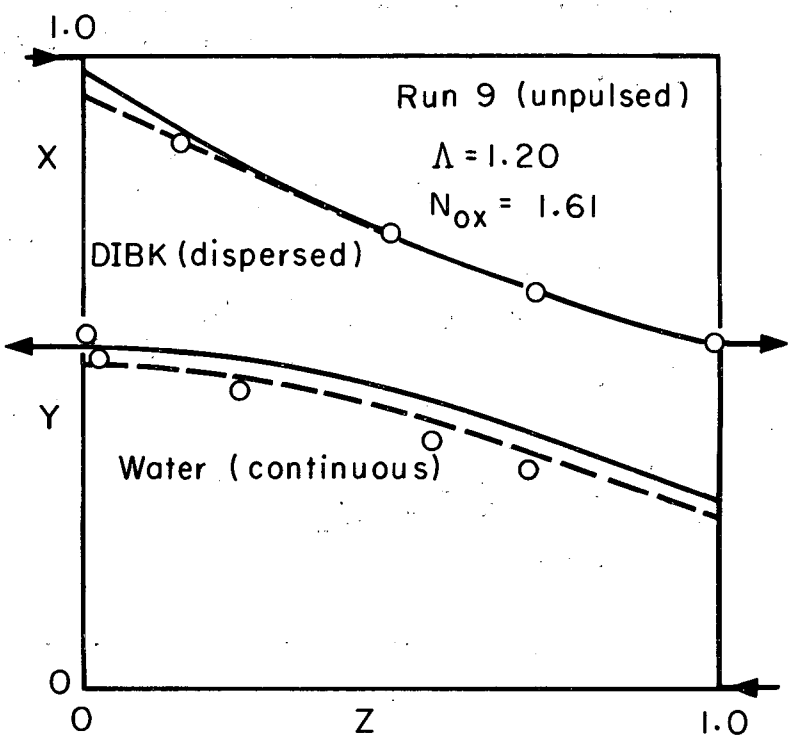

Fig. V-8. Experimental concentrations vs theoretical concentration profile: Run 9.

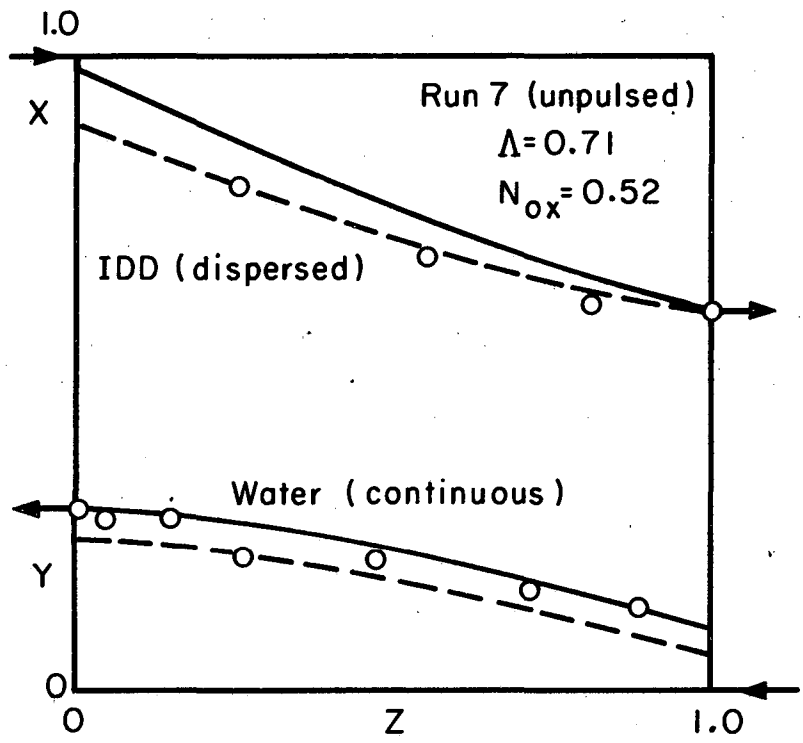

Fig. V-9. Experimental concentrations vs theoretical concentration profile: Run 7.

in the end section was about 8%. Comparison of Runs 7 and 6 (at the same flow rates for the two phases) shows that the true mass-transfer coefficient ($k_{ox}a = F_x/H_{ox}$) is greater when solute is transferred from the dispersed to the continuous phase, as is also found in pulsed packed beds (Part III). For a constant continuous-phase flow rate, H_{od} increases as U_d increases, as found by many other investigators.

D. Conclusions

Experimental concentration profiles inside the column were obtained and compared with theoretical profiles calculated from the model discussed in the General Introduction. This two-phase one-dimensional diffusional model adequately represents the fluid behavior in packed extraction columns for both systems employed in this study, and appears to provide an accurate and efficient design procedure for packed columns in general. For the proper use of this model, mass transfer in the end sections must be accounted for where necessary.

The Péclet numbers determined by the unsteady-state tracer-injection method for countercurrent flow appear to represent quite closely the longitudinal-dispersion behavior during steady-state extraction.

ACKNOWLEDGMENTS

The authors wish to express their appreciation to C. J. King and D. R. Olander for helpful discussions; to F. T. Upham and J. Orsino for design and installation of the electronic instrumentation; to Donald Coleman for his part in construction of the experimental equipment; and to E. M. Blue and A. H. Batchelder of California Research Corporation for providing the isododecane supply.

The work reported was done in the Lawrence Radiation Laboratory under the auspices of the U. S. Atomic Energy Commission.